Power HIL Simulation of an Electric Minibus Powertrain

by

Pitchapa Lotrakul

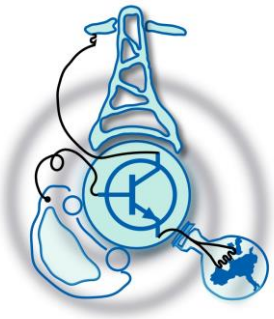

Submitted to the Department of Electrical Engineering, Electronics, Computers and Systems
in partial fulfillment of the requirements for the degree of Erasmus Mundus Master Course in Sustainable Transportation and Electrical Power Systems
at the
UNIVERSIDAD DE OVIEDO
September 2017

Author .....
Pitchapa Lotrakul

Certified by.....
Professor Paulo Pereirinha
Polytechnic Institute of Coimbra (ISEC-IPC), Coimbra, Portugal
Thesis Supervisor

Professor Alain Bouscayrol
University of Lille1, Lille, France
Thesis Supervisor

Power HIL Simulation of an Electric Minibus Powertrain

by

Pitchapa Lotrakul

Submitted to the Department of Electrical Engineering, Electronics, Computers and Systems
on September 1, 2017, in partial fulfillment of
the requirements for the degree of
Erasmus Mundus Master Course in Sustainable Transportation and
Electrical Power Systems

Abstract

The objective of this project is to utilize the test bench at the Coimbra Institute of Engineering – Polytechnic Institute of Coimbra (ISEC-IPC, Instituto Superior de Engenharia de Coimbra – Instituto Politécnico de Coimbra), Coimbra, Portugal, to perform a Hardware-In-the-Loop (HIL) simulation. This involved, first, to take contact and study different components of the test bench and consequently improving the charging procedure to allow charging in a safe environment. Then, Energetic Macroscopic Representation (EMR) graphical formalism technique was employed to organize the simulation. In particular, such technique was employed to ease the integration between the controls of the traction drive and the load drive through a dSPACE platform. This involved an intermediate stay of about one month at University of Lille 1 at Lille, France, to learn and improve the EMR technique and to take contact with other HIL platforms and dSPACE system. Finally, the test bench was used to emulate the electric minibus of Coimbra (in reduced-scale) with a real driving profile reference to study the system.

Thesis Supervisor: Paulo Pereirinha

Title: Professor Coordenador

Thesis Supervisor: Alain Bouscayrol

Title: Full Professor

Acknowledgments

First of all, I would like to acknowledge Professor Paulo Pereirinha and Professor Alain Bouscayrol for the supervision and support throughout this project. This project comprises of many aspects and implementation. Your advices have been very helpful. I am also grateful for all professors throughout the EMMC STEPS program. This journey has been full of experience. I am very grateful for the opportunity.

I would like to thank my family for being wonderful supporters. I could not have been here without you. Thanks to STEPS friends who go through this experience together. Two years is not very long but we are bound. Being away from home would be much harder without you.

This accomplishment would not have been possible without all the supports. Thank you.

Pitchapa Lotrakul

Contents

List of Figures

List of Tables

List of abbreviations and symbols

Abbreviations

ADC	Analog-to-Digital Converter
COB-ID	Communication Object Identifier
DAC	Digital-to-Analog Converter
ECU	Electronic Control Unit
EMR	Energetic Macroscopic Representation
HIL	Hardware-In-the-Loop
I/O	Input/Output
IS	Interface System
MCS	Maximal Control Structure
NEDC	New European Driving Cycle
OD	Object Dictionary
PD	Process Data
PDO	Process Data Object
P-HIL	Power Hardware-In-the-Loop
PMSM	Permanent Magnet Synchronous Machine
RPDO	Receive Process Data Object
SDO	Service Data Object
S-HIL	Signal Hardware-In-the-Loop
SoC	State-of-Charge
TPDO	Transmit Process Data Object

Symbols

Symbol	Unit	Property
A_f	m^2	Vehicle front area
C_D	-	Aerodynamic drag coefficient
C		Closed-loop controller
e	V	Back-emf of the machine
F	N	Force
f	Nm/(rad/s), N	Friction coefficient, friction
g	m/s^2	Gravitational acceleration
i	A	Current imposed by a component
J	$kg \cdot m^2$	Moment of inertia

Symbol	Unit	Property
K_D	-	Distribution criterion
k	-	Coefficient, Reduction ratio
L	H	Inductance
M	kg	Mass
m	-	Modulation ratio
P	W	Instantaneous power
R	Ω	Resistance
R_{wh}	m	Wheels radius
SoC	%	State of Charge
T	Nm	Torque
u, V	V	Voltage
v	m/s	Velocity
α	rad	Road angle
η	%	Efficiency
μ_{rr}	-	Rolling resistance coefficient
ρ	kg/m^3	Air density
φ	Wb	Machine flux
Ω	rad/s	Rotational speed

Subscripts

Subscripts	Property
a	Aerodynamic
b	Bearing
bat	Battery
br	Braking
ch	Chopper
d	Drive
dcm	DC Machine
em	Electric Machine
eq	Equivalent
g	Gearbox
L	Load
-meas	Measured
oc	Open-Circuit
P	Power
-ref	Reference

Subscripts	Property
res	Resistive
stat	Static
T	Torque
tot	Total
tr	Transmission
ve	Vehicle
w	Wind
wh	Wheel
Ω	Speed

Chapter 1 Introduction

1.1 Background

Verification processes are important steps in product designing as they ensure that product functionalities meet all the requirements. It is also beneficial in studies to improve existing systems. In such process, simulations are employed. In addition to software simulation, there could be an intermediate step of Hardware-In-the-Loop (HIL) simulation before going to test the whole real system. In this type of simulation, some parts of the simulation are replaced by real components [1]. This eliminates the problem of accuracy in modeling. The cost of testing is also lower than the test of the complete system and it avoids the risk of damage related to the real system. In addition, before performing a full-scale HIL simulation, a reduced-scale simulation can be employed as an intermediate step[2][3][4]. Nonetheless, since real components are implemented, this simulation requires a real-time hardware simulation. It also requires controls over, both, the system under test and the emulation system. Therefore, the HIL simulation is quite complex.

The Energetic Macroscopic Representation (EMR) graphical formalism is an organization method which respects the principle of causality and the principle of action-reaction [5]. It is a very useful tool to organize complex systems and to deduce systematically their control organization. It has shown its ability in many fields of application such as hybrid-electric vehicles and wind turbine generation systems. Therefore, it is chosen as a tool to organize this HIL simulation.

The case study of this thesis is the electric minibus of Coimbra. Electric buses are potential alternatives to reduce CO_2 emission. They also provide quiet operation and no energy losses during idle operation [6]. In Coimbra, there is one line of electric minibuses which has been providing a mean of transportation in the historical center for tourists and inhabitants. Nonetheless, some improvements are being considered and this HIL setup could provide a mean of studying the system.

1.2 Objectives

The main objective of the present work is to develop a HIL setup to emulate the electrical minibus of Coimbra. In order to reach this objective, other objectives of the learning process are the following:

1) To understand and be able to use previous setup,
2) To learn and gain more experience with the Battery Management System (BMS) and to improve the charging process by employing the BMS to the charging process,
3) To learn about EMR and apply such formalism to study the electric minibus of Coimbra, and
4) To learn how to use dSPACE platform to control both drives at the same time to allow HIL simulation.

1.3 Procedures

The procedures defined to reach the objectives were to:

1) Study previous works on the test bench and familiarize with the setup
2) Study related literature and manuals
3) Identify the connections and wiring, solve the problems with BMS, and operate the machines using manufacturer's software
4) Develop control of the system using EMR
5) Implement the control using dSPACE platform
6) Perform experiments
7) Conclude the results

1.4 Thesis structure

The structure of the following chapters in this thesis is:

Chapter 2: Literature Review

Essential background knowledge in order to complete this study is explained in this chapter. In section 2.1, the importance of Hardware-In-the-Loop (HIL) and the organization of different types of HIL are explained. Then, in section 2.2, the HIL test bench in ISEC-IPC is introduced. After that, the method of EMR formalism is explained in section 2.3. Finally, section 2.4 provides background information about the electric minibus of Coimbra which is the case study of this thesis.

Chapter 3: Improvement of Charging Procedure

The first part of the process to improve the test bench is to work with the charging facilities. The issue of inaccuracy current measurement of the BMS is solved in section 3.1. Then, a safe charging procedure is developed in section 3.2.

Chapter 4: Developing of the EMR of the Electric Minibus of Coimbra

Knowledge about EMR and the electric minibus are combined together in this chapter in order to develop the EMR. First, the electric minibus is modelled and represented by its EMR in section 4.1. Then, the inversion-based control is deduced in section 4.2. The control strategy for such system is explained in section 4.3. However, the model which is employed in the simulation is a quasi-static model. Such model is explained in section 4.4. After that, MatLab Simulink program of the EMR is developed in section 4.5. Finally, the program is tested in real-time simulation and Signal HIL simulation in section 4.6.

Chapter 5: Power HIL Simulation Implementation through dSPACE

In this chapter, the software simulation from previous chapter is extended to a power HIL simulation. In section 5.1, the EMR of P-HIL simulation is explained. This starts in full-scale and finishes with reduced-scale HIL simulation. Then, the configuration in order to prepare the test bench for such simulation is explained in section 5.2. Finally, the setup and results of the reduced-scale P-HIL simulation of the electric minibus are shown in section 5.3.

Chapter 6: Conclusion and Future work

The thesis is summarized in this chapter. The conclusion of the work is drawn in section 6.1 and the future works are discussed in section 6.2.

Chapter 2 Literature Review

2.1 Hardware-In-the-Loop simulation

In designing a system, one of the popularly used design workflows is the V-cycle model-based design method [7]. This method includes analysis activities on the left side of the cycle. The user requirements are decomposed into design of small units. Then, the right side of the V-cycle shows the corresponding testing activities to assure that the system meets the requirements. It starts from the widest point of view down to single element of the system then verifies from each element back to the whole system. Decomposing the systems makes it easier to design and troubleshoot the system. A traditional single V-cycle work flow is shown in Figure 2.1.

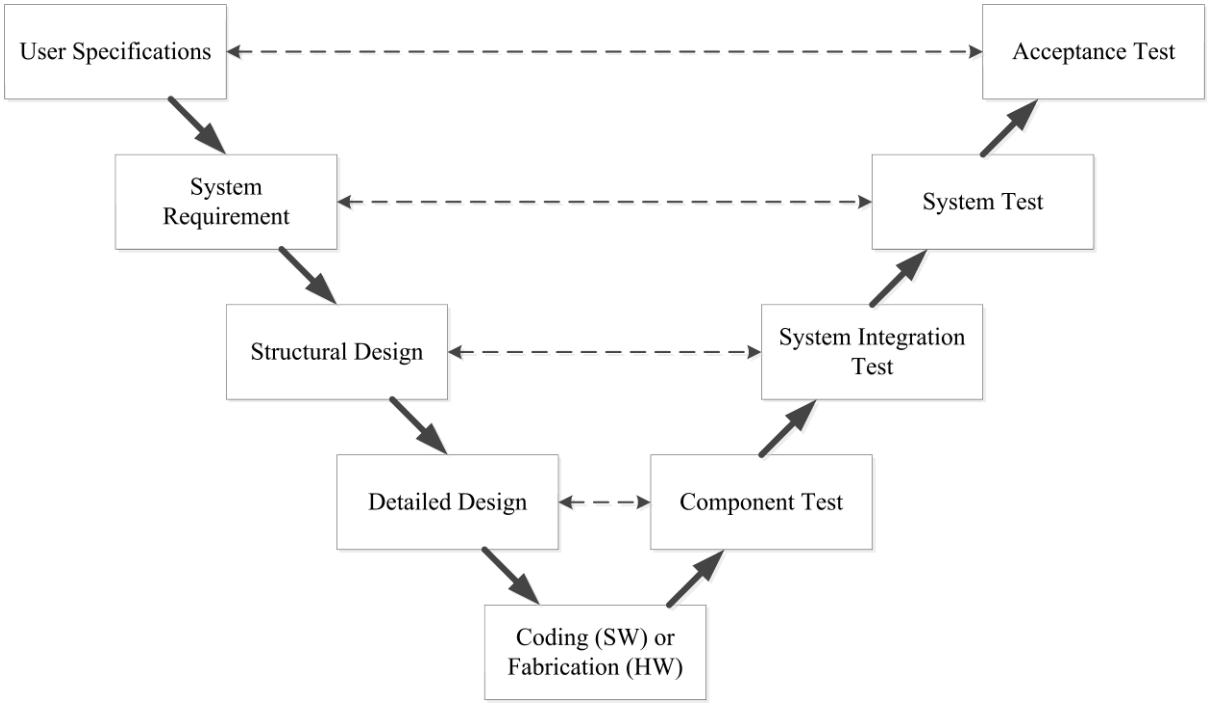

Figure 2.1 Traditional V-cycle of system designing (modified from [7])

The work flow in V-cycle comprises of:

1) User requirements engineering

2) System requirements engineering

3) Architecture engineering

4) Designing

5) Coding of software and fabrication of hardware

Then, the work flow continues on the right side with verification processes which correspond to the designing process in the same level:

6) Component testing

7) System integration testing

8) System testing

9) Acceptance testing

In this process (the V-cycle), simulation is a valuable tool for verification and testing. Conventional method of simulation is software simulation in which a component or a system is modeled in computer software. However, there is a limitation of accuracy of the result which depends on the ability to model the component or the system. Therefore, in the recent years, there has been increasing interest in a technique called Hardware-in-the-Loop (HIL) simulation in which real components are implemented in the simulation loop [1].

In an energy conversion system, there could be 2 directions of energy flows. If energy is converted from a generator to a load, it is referred to as a unidirectional energy flow. However, it is possible to have energy flow back from the load to the generator e.g. in regenerative braking in electric vehicle. A system in which both directions are possible is referred to as a bi-directional energy flow system. The system can be decomposed into several subsystems which are connected by action and reaction variables [8] as shown in Figure 2.2. The product of these variables is the exchanged power which is differential of energy [5]. Moreover, the conversion or the system is controlled by an ECU (Electronic Control Unit).

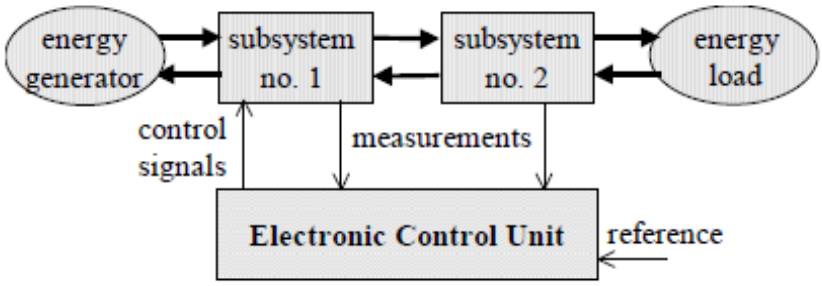

Figure 2.2 Control of an energy conversion system [9]

In order to study such system, the first step is to derive a model of the system. Then, tests are performed according to the objective of each study. For instance, to develop a control of a system, a control scheme is proposed. Then, the control parameters are tuned in order to fulfil the requirements. There may be several intermediate steps to test and retune the parameters. Finally, the control is implemented to the real system.

The studying process is usually done by simulation. It allows testing without the risk of costly and damaging failures to the actual system. This leads to reduction in cost and developing time. Two main types of simulation which will be discussed in this thesis are software simulation and Hardware-In-the-Loop simulation.

In software simulation, the whole system is replaced by its model. The performance of the simulation depends on the accuracy of the model. Usually, there are tradeoffs between the accuracy of the model and the computation power and time required. In addition, some variations such as effect of temperature on parameters are hard to take into account. The effects of implementation such as the sensor accuracy are also usually neglected [9].

On the contrary, in Hardware-In-the-Loop simulation, one or several actual components are utilized instead of their simulation models. Other parts are simulated into a controller board or in parallel computer [1]. It allows validation of the embedded systems before implementing into real system. This gives more accuracy in testing equipment which is hard to model such as an Internal Combustion Engine. It also eases verification of specific conditions such as fault conditions. In addition, implementation constraints such as sensor accuracy are taken into account. Being able to test each part before implementing to the whole system also simplifies the verification process since it avoids complex integration. For instance, HIL has been applied in aerospace industry to verify flight control systems which are critical for safety of operation. It has also been applied to automotive industry to verify the performances of embedded ECU. Moreover, new applications include HIL of powertrain of Electric Vehicles (EVs) and Hybrid Electric Vehicle (HEVs) where actual drives (power electronics and electrical machines) can be tested.

However, since actual parts need to communicate with the simulation parts, it is important to have an Interface System (IS) to link actual parts to simulation parts [2]. Its inputs and outputs must be the same as the actual system. Selection of the IS is, thus, very important since it has to generate different kinds of variables to connect both parts. It should represent the behavior of the real system. For instance, it must not induce time delay which would affect the behavior of the closed-loop system. As additional elements are required in the simulation, HIL has higher cost than software simulation. Moreover, higher power computer or controller board is required to enable real-time operation. Figure 2.3 shows the organization of HIL simulation of an energy conversion system. The system is split into subsystems under test and subsystems in simulation environment as indicated by dash lines. The IS is the connection between both parts.

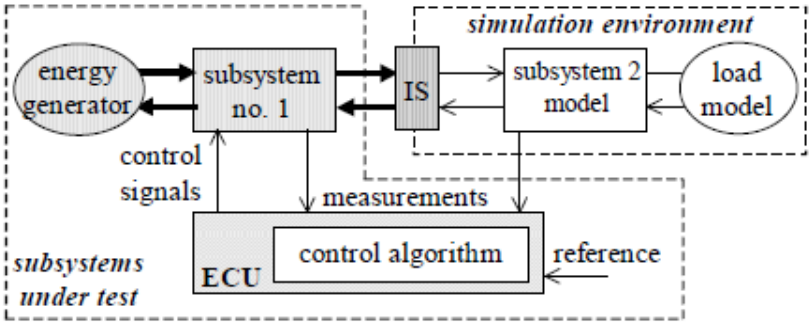

Figure 2.3 An organization of a HIL simulation of an energy conversion system [2]

There are two types of HIL simulations, depending on the objective of the simulation [9]:

1) Signal HIL simulation (S-HIL)

Signal HIL simulation is used to test control algorithms and ECUs. It is widely used in industry to test ECUs under different operation condition, especially in fault conditions. It allows several test repetitions without impact on the real system. For instance, it was applied to agricultural self-propelled machines. It increases test coverage and reduce required time. Particularly, in this case, testing with real system is limited to short period of time by the harvesting season. HIL eases the test of Functional Safety requirements [10].

In this type of HIL simulation, the entire system is simulated in a real-time simulation environment and the IS links only signal variables. The ECU is usually connected to the second ECU, called the emulation ECU. Real-time simulation of the energy conversion system is performed through this ECU i.e. this ECU is the IS. The sampling period of the emulation ECU must be adapted according to the system to provide the same measurements as in the real processes and it must be synchronized to the tested ECU to avoid undesirable effects. Figure 2.4 (a) shows the organization of a signal HIL simulation while Figure 2.4 (b) shows the practical implementation of such simulation. The entire system is implemented (using their simulation models) to the emulation ECU which is the IS. The only real part or the subsystem under test is the actual ECU. These two parts are connected together through the control signals and the measurements which are also signals.

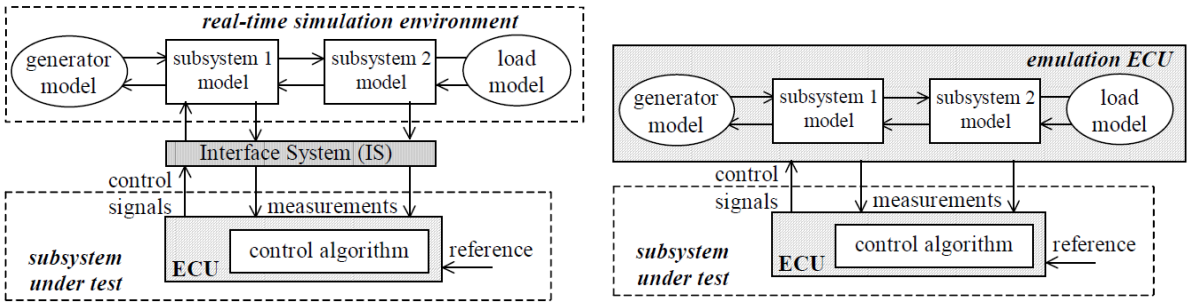

(a) (b)

Figure 2.4 (a) An organization of a signal HIL simulation and (b) its implementation [9]

2) Power HIL simulation (P-HIL)

Power HIL simulation is used to test ECUs and parts of the energy conversion system. It is useful in testing subsystems and their control. Due to its advantages of safety and flexibility, it is widely used to test a new traction system before implementation to moving vehicle.

In this type of HIL simulation, the power parts of the system are split into the parts to be tested and the parts to be emulated, similar to Figure 2.3. As opposed to S-HIL, the IS in P-HIL links both, power and signal variables between the tested and the simulated parts. The power is simulated in real-time using the subsystem models while the control algorithm is implemented through ECU. Since power is required in the connection, an emulation device is required as the IS. This device must deliver the same power variables as the real subsystem would deliver to the subsystem under test. In addition, in order to deliver such power, an emulation power source is required. Moreover, an emulation ECU is required to control the emulation device to provide desired behavior i.e. the same behavior as the real subsystem. The practical implementation of such HIL is shown in Figure 2.5. The dash lines show the boundary between both parts of the system. Moreover, the sampling period and dynamics of the system must be taken care of as in the case of signal HIL simulation. In addition, there is a requirement in term of power in which the power of the emulation device must be higher than the actual system. This is in order to be able to simulate the whole range of power. Otherwise, such power HIL is referred to as a reduced-scale power HIL simulation.

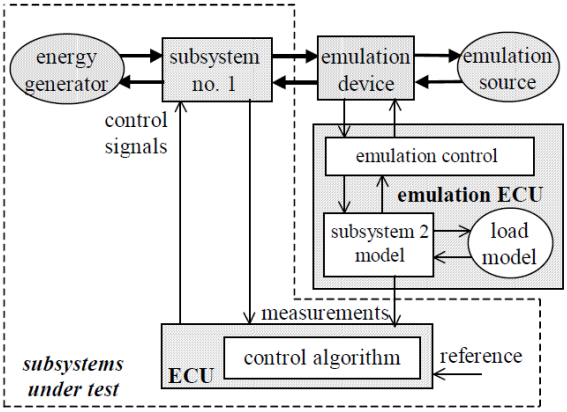

Figure 2.5 An implementation of a P-HIL simulation of an energy conversion system [2]

In reduced-scale power HIL simulation, an equivalent subsystem with lower power is tested. It is beneficial in simulating systems with high power. It allows initial test to be performed without issue associating with high power.

In order to develop a reduced-power HIL simulation, several steps can be followed:

1) Developing of a full-power simulation,

2) Splitting the systems into full-power and reduced-power parts,

3) Inserting an Interface System (IS), and

4) Implementing real devices to the loop [1].

The organization of such simulation is shown in Figure 2.6. It is adapted from the

full-power HIL simulation by adding power adaptations. The first power adaption is added between the emulation control and the subsystem model. It involves a linear power amplification which allows maintaining the non-linear characteristics of the simulated subsystem. Another power adaptation is added between the controls of the tested and simulated parts. These define the boundary between the reduced-scale and full scale parts.

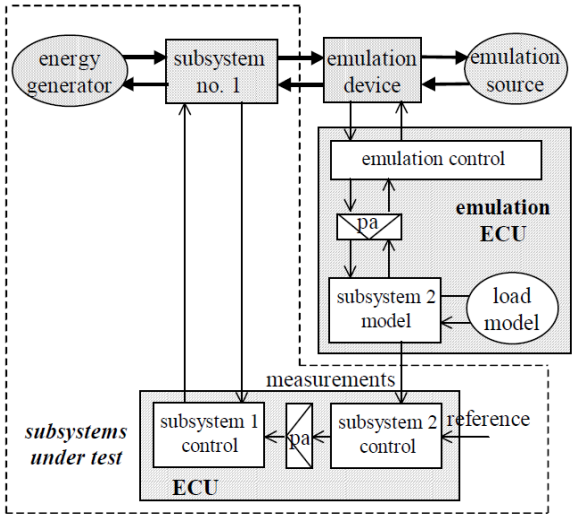

Figure 2.6 An organization of a reduced-scale P-HIL simulation [2]

As previously mentioned, it is important that the test bench is able to cover the whole reduced-scale test range. Figure 2.7 shows the comparison of limitations of both systems. The power adaptations must respect the power ratio and the limitation of the full-scale variables in order not to generate non-physical effects when the full-scale is not in limitation. In order to assure that, proposed procedure [1] shown in Figure 2.8 can be used to calculate the reduction ratios. These include the speed ratio, k_Ω, the power ratio, k_P, and the torque ratio, k_T. Subscript HP refers to high-power subsystem or the modelled part while subscript LP refers to lower power subsystems or the tested subsystems. A safety margin of 5% is also included in these calculations.

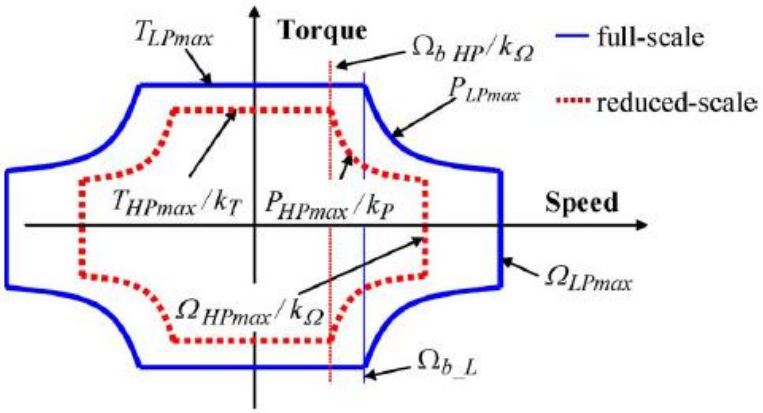

Figure 2.7 Limitations of the full-scale and reduced-scale drives [3]

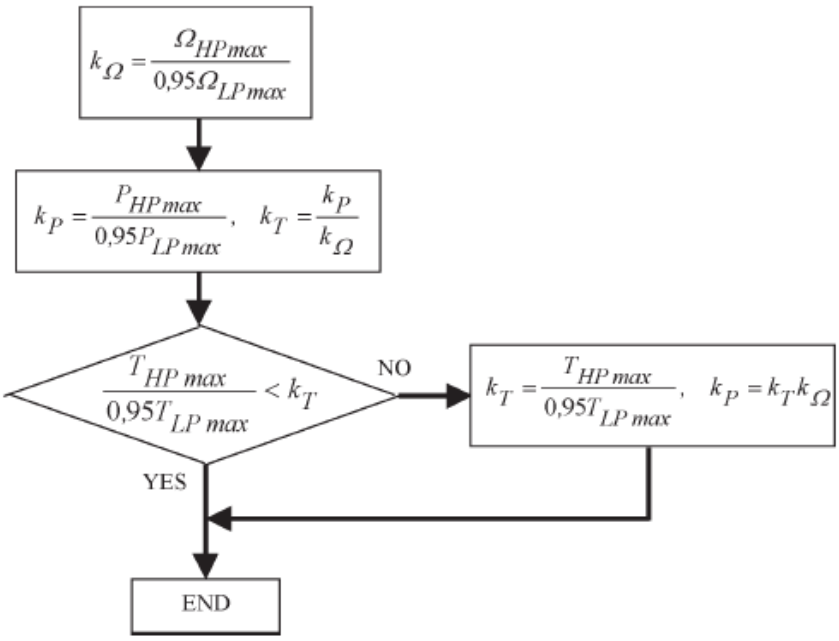

Figure 2.8 Flowchart of the adaption coefficient calculation [3]

2.2 Introduction to ISEC HIL test bench

The test bench utilized in this thesis is inherited from previous works done in ISEC-IPC. Figure 2.9 shows the initial setup of such test bench with indications of the components.

The test bench is equipped with:

- $LiFePO_4$ Sinopoly batteries: SP-LFP40AHA,
- Lithium battery charger: GWL-Power-POW72V35A,
- Battery Management System: BMS123 Main controller,
- SEVCON Synchronous Motor Controller: Gen4-72-80VDC,
- Permanent Magnet Synchronous Motor (PMSM): Heinzmann GmbH PMS120,
- Variable Frequency Drive (VFD): SEW-EURODRIVE MDX60a022050J-4-00,
- Servo Permanent Magnet Synchronous Motor (servo motor): SEW-EURODRIVE Model: CMP80M/KY/RH1M/SM1, and
- dSPACE MicroAutoBox II 1401/1511-1512 [11].

In ISEC-IPC, there is another HIL test bench which utilized CompactRIO device. It was part of Multiple Energy Storage systems Management Optimization for Electric Vehicles project (MESMO-EV). However, with this test bench, the dSPACE MicroAutoBox II is to be implemented since it simplifies the operation. With CompactRIO, the program has to be transformed from MATLAB Simulink simulation to NI-LabVIEW program in order to compile to such device. However, with dSPACE MicroAutoBox, the program can be implemented directly from MATLAB Simulink. This test bench also has higher power capacity.

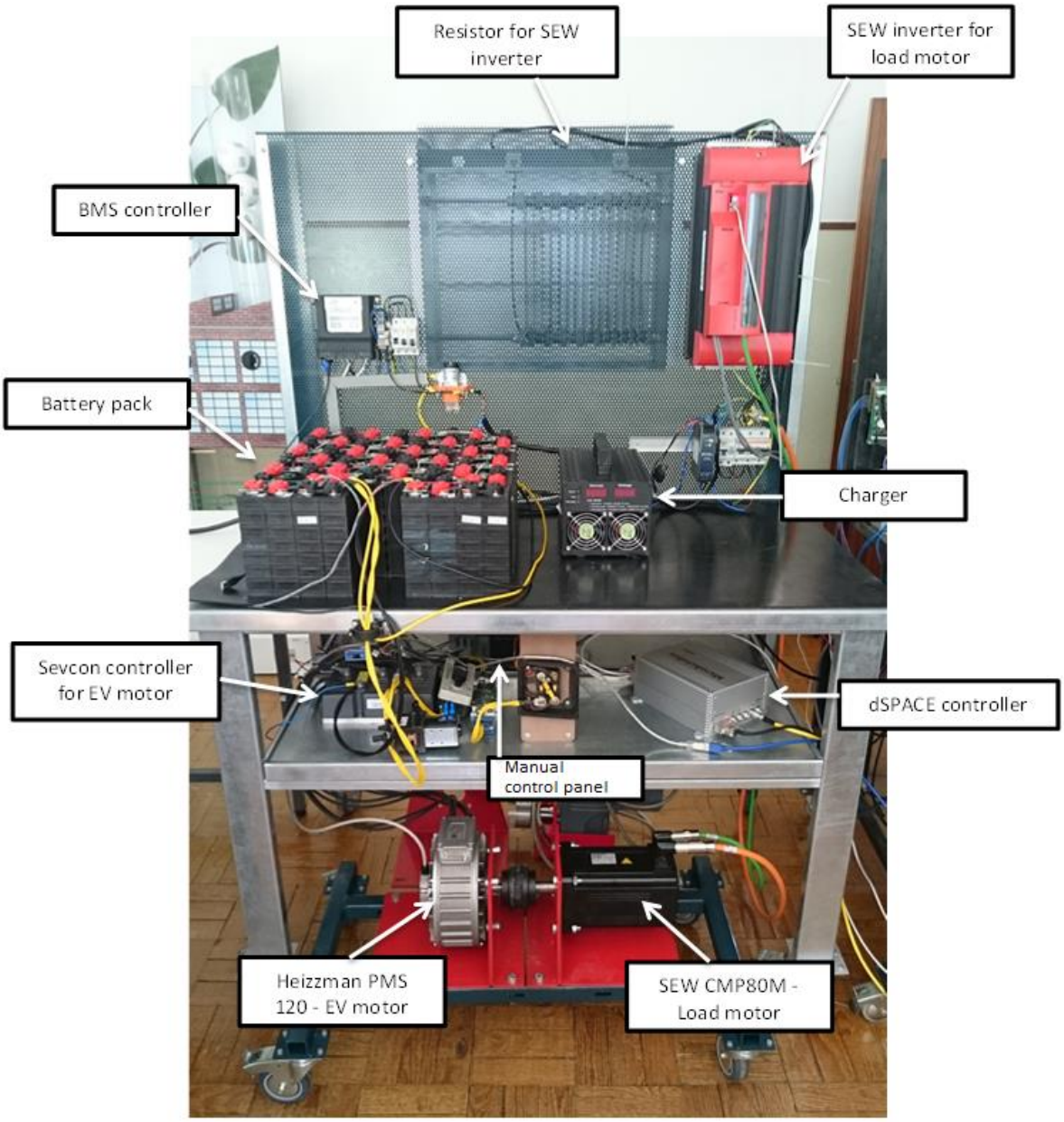

Figure 2.9 Initial HIL Test bench in ISEC with components indications

The main idea of the setup is to use the PMSM as a traction machine. This machine is controlled by SEVCON Gen4 controller. The power to this machine is provided by the $LiFePO_4$ battery. On the other hand, the load drive is composed of the servo motor and the SEW inverter. This is supplied by the grid. Furthermore, there is a central controller to communicate between the test bench and the PC. This is the dSPACE MicroAutoBox. It is in charge of supplying references from the PC to both drives and receiving the measurements from the drives to transmit to the PC. In addition, there are charging facilities which are the charger and the BMS. Several circuit breakers are employed to turn on different components of the system and to be the protection of the system along with fuses.

From the previous thesis done on the test bench [11], it was possible to:

- Manually operate the traction machine by using a push button as a foot switch

and using a knob (potentiometer) to give throttle analog signal,

- Configure the SEVCON traction machine controller through DVT software (configuration and monitoring software provided by SEVCON manufacturer),

- Monitor some variables of the traction machine through DVT software,

- Operate the load machine through “manual mode” tool in MOVITOOLS MotionStudio software (configuration and monitoring software provided by SEW manufacturer),

- Monitor and set Process Data (PD) of the load machine through MOVITOOLS MotionStudio software,

- Connect dSPACE MicroAutoBox with Simulink (analog interface) and with ControlDesk software, and

- Perform an ECE-15 driving profile simulation in MATLAB Simulink.

Nonetheless, some improvements were still required in order to operate the test bench as a HIL simulation test bench. Mainly, there were issues regarding the charging facilities which did not allow controllable charging via BMS. Moreover, the drives were not able to operate together synchronously. They were only able to operate separately and through the manufacturer software which are different for each drive. The dSPACE MicroAutobox were not completely implemented to the test bench. Under such condition, it was not possible to perform a HIL simulation. Therefore, this study will focus on refining such setup to achieve the full operation of the test bench.

2.3 Energetic Macroscopic Representation (EMR)

In developing a simulation of a system, there are several associated steps [5]. First, the system must be modelled. There may be different types of model depending on the objective of the study. In this process, assumptions are made. Only main phenomena of interest are taken into account. Then, there are several representations which can be employed to organize the model. Finally, the last step is the simulation implementation which can be done in different software. Figure 2.10 summarizes the process of developing system simulation.

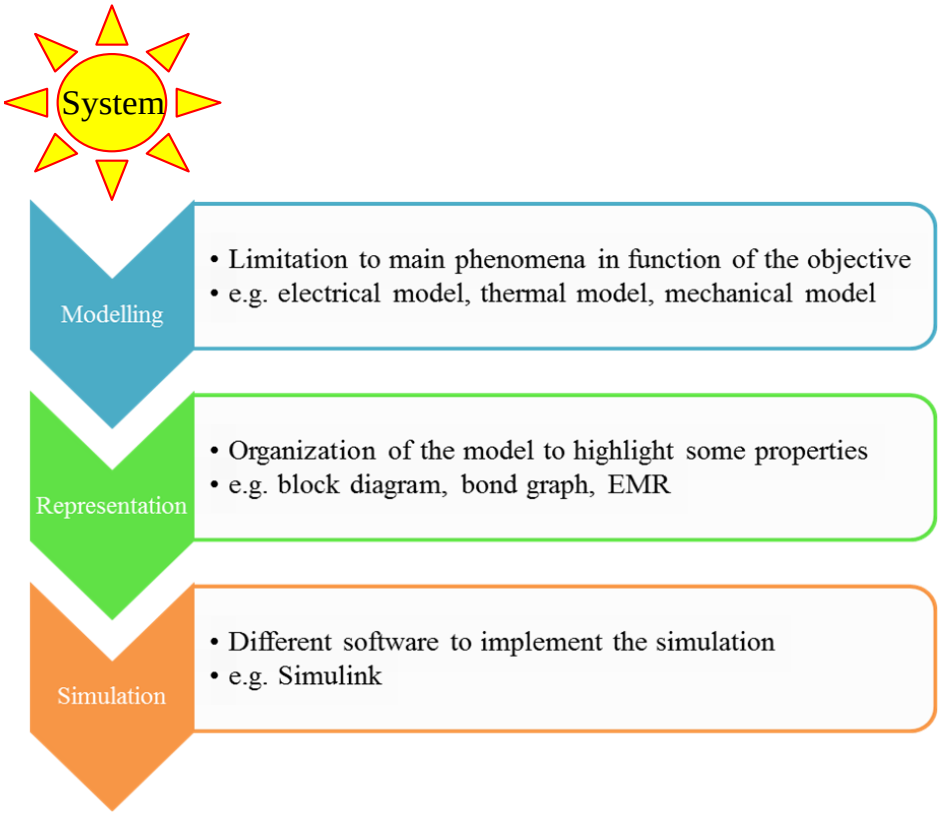

Figure 2.10 Process of developing a system simulation (adapted from [12])

In this study, different dynamic and static models will be used to model the system. In addition, Energetic Macroscopic Representation (EMR) will be utilized as a tool for the system representation. It is one of graphical descriptions which allow the user to represent the system. It has been successfully applied to may applications such as railway traction systems, wind energy systems, hybrid and electrical vehicles, and fuel cell systems. This graphic formalism shows the energetic properties of subsystems and their interactions[1]. To emphasize this, there are two principles which are the core of EMR:

1) Principle of causality: in dynamic systems, the output of a system is delayed comparing to the input of such system. This corresponds to physical reality in which the effects are delayed from the causes. In mathematical sense, the output can only be an integration of the input. It is not possible to have a derivative relationship since derivation would require knowledge of future evolution while integration only requires knowledge of previous evolution.

2) Principle of interaction: every action on a subsystem will induce a reaction. The product of them is the instantaneous power exchanged by the two elements.

There are 4 main elements in EMR which represent different energetic properties [5][1]:

1) Energy source element: it is represented by a light green, outlined in dark green oval as shown in Figure 2.11 It represents environment of the study which can generate and/or receive energy.

2) Energy accumulation element: it is represented by an orange, outlined in red barred rectangular as shown in Figure 2.11. It represents subsystem which has internal energy accumulation. Therefore, the outputs and inputs of this element must respect the integral causality i.e. an output must be an integration of an input.

3) Energy conversion element: it is represented by an orange, outlined in red square or circle as shown in Figure 2.11. If the conversion is a monophysical conversion, the element will be a square, whereas if it is a multiphysical conversion, it will be a circle. This element represents a subsystem which converts energy without internal energy accumulation. Therefore, the outputs and inputs are exchangeable depending on its adjacent elements.

4) Coupling element: it is represented by orange, outlined in red overlapped squares for monophysical coupling or overlapped circles for multiphysical coupling as shown in Figure 2.11. It distributes the energy without internal energy accumulation.

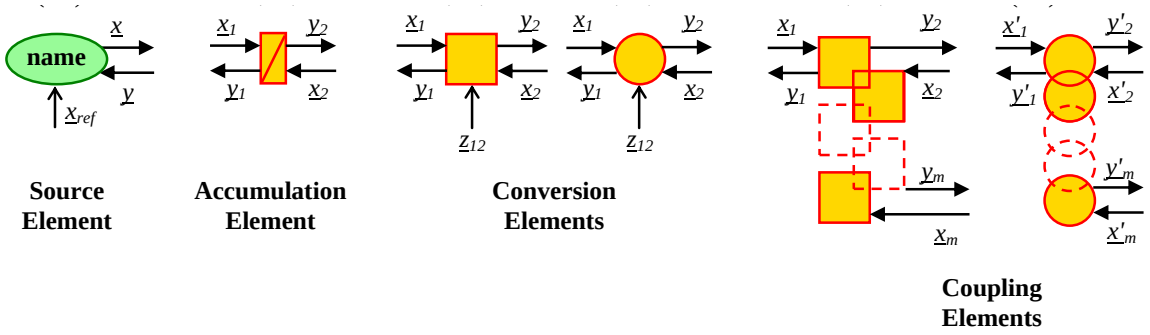

Figure 2.11 EMR elements [12]

After EMR of every components or subsystems in the system is defined, the next step is to assemble them together to build EMR of the whole system. In this step, two elements can only be connected together if their outputs and inputs match. Although inputs and outputs of conversion elements can be exchanged, they are fixed in the case of accumulation elements. Therefore, some conflicts of association may arise. These can be solved by two rules of association. As a result, a virtual subsystem with properties from the association will emerge from the real subsystems. Therefore, the system becomes represented by functional description instead of structural description.

The two rules of association are:

1) The rule of merging: this rule allows merging two accumulation elements with the same state variable.

2) The rule of permutation: this rule allows permuting two elements and obtaining a virtual element which imposes the same global outputs.

Example of the rule of emerging and the rule of permutation are shown in Figure 2.12 (a) and (b), respectively. A new global element with a global dynamic will emerge from these associations. It should be noted that this global dynamic is a dynamic of the merged element, not the combination of initial dynamics.

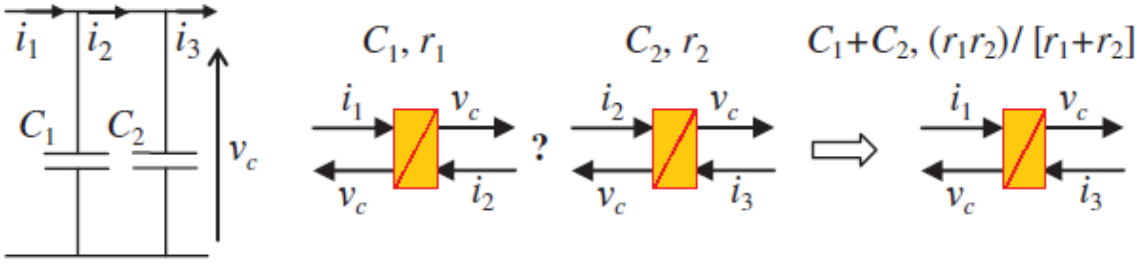

(a)

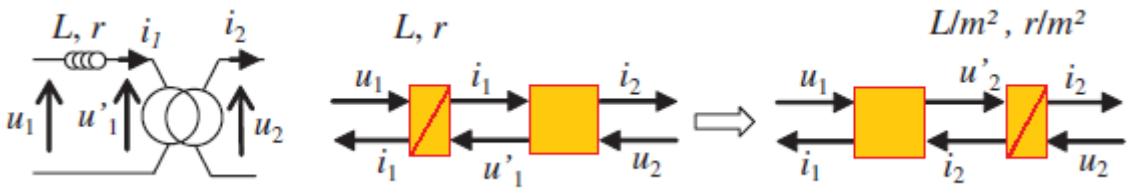

(b)

Figure 2.12 Example of (a) the rule of emerging and (b) the rule of permutation [5]

After the system is assembled, a tuning path can be defined from tunable variables to the variable which is the object of the control system. After that, a control can be obtained by inversion of elements along the tuning path. Three types of inversion elements are utilized in order to perform such task. They are represented by light blue, outlined in dark blue parallelograms as shown in Figure 2.13. These are:

1) Inversion of a conversion element: a conversion element can be directly inverted since it does not accumulate energy. If such an element has two inputs, one is chosen as a tuning input and the other becomes a disturbance input.

2) Inversion of an accumulation element: an accumulation element cannot be directly inverted due to the principle of causality. Inversion of integration would result in derivation which is not physically possible as previously described. Therefore, a closed-loop control is required.

3) Inversion of a coupling element: a coupling element can be inverted, generally, by criteria, depending on the type of coupling. In an upstream coupling, a weighting criterion is required and in a downstream coupling, a distribution criterion is required.

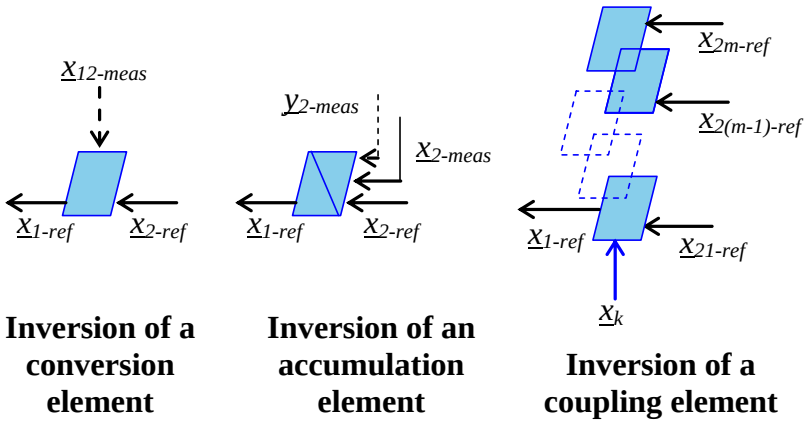

Figure 2.13 EMR inversion elements [12]

A Maximal Control Structure (MCS) is obtained as a result of these inversions. After the EMR of the system and its control are deduced, optimization and implementation processes such as simplification and estimation of variables are to be done in the next steps. In summary, the process of developing a control using EMR technique can be summarized as:

1) Defining the EMR of the system,

2) Identifying the tuning path according to the control objective and system specifications,

3) Inversion of the EMR elements along the tuning path with hypothesis that all variables are measurable,

4) Simplifications if necessary,

5) Achieving the estimations of non-measurable variables,

6) Tuning of the controllers, and

7) Implementation of the control

2.4 The electric minibus of Coimbra

As awareness of environmental impact increases extensively, CO_2 emission has come into interest of many associates. Transportation sector is one of the main sectors which cause higher Green House Gas (GHG) emission [13]. This is due to the trend of increasing quantity of personal vehicles. This trend also causes other problems such as the traffic problem. Studies show that electric buses are a potential alternative [14]. Improvement in public transportation can reduce needs of personal vehicles. This would result in reduction of energy consumption, emissions, and public health and parking space issues. Electric buses can reduce the emissions even further since they are locally emissions free. Comparing to conventional engine-driven buses, electric buses are quieter and have no energy losses during idle operation [6]. Moreover, they are easier to implement than personal electric vehicles since the driving cycles are predictable. This eases the design of the energy storage system and the charging facilities [15]. Moreover, it provides mean of transportation to people who do not drive or do not possess personal vehicle.

In Coimbra, currently, there is one line of electric minibuses which was introduced in 2003. It provides a low air and noise pollution alternative for tourists and Coimbra's inhabitants. In particular, it has provided a way of transportation for elders who would, otherwise, suffer from social exclusion. The route has characteristics of a city with hills and narrow streets in historical center. Nonetheless, the current batteries have shorter lifetime than forecasted. Due to the technological advancement in the energy storage system, particularly the battery technology, new type of battery is being considered [16][17].

The electric minibuses of Coimbra are TECNOBUS Gulliver U520 with capacity of 20 passengers and a driver. This corresponds to a fully loaded weight of 6035 kg. They employ a series DC motor of 24.8 kW and maximal torque of 235 Nm at 950 rpm. The

maximal velocity is 33 km/h and the autonomy is 6.5 hours. Other specifications which are useful for the modelling are summarized in Table 2.1.

Table 2.1 Specifications of the electric minibus of Coimbra (adapted from [16][17])

Variable	Symbol	Value	Units
Vehicle mass (without batteries)	M	2785	kg
Rolling resistance coefficient	μ_{rr}	0.01	-
Gravitational acceleration	g	9.81	m/s^2
Air density @ 20ºC	ρ	1.223	$kg.m^{-3}$
Aerodynamic drag coefficient	C_D	0.7	-
Vehicle frontal area	A_f	5.693	m^2
Wheels radius	R_{wh}	0.365	m
Gearbox transmission ratio	k_g	4.37	-
Gearbox transmission efficiency	η_g	90	%

In addition, as previously mentioned, there have been studies to employ a new type of battery in these minibuses. The current sets of batteries are lead-acid batteries while the proposed replacements are Li-ion batteries. The characteristic of these battery packs are summarized in Table 2.2.

Table 2.2 Characteristics of battery packs [16][17]

Variable	Symbol	Lead-acid Values	Li-ion Values	Units
Capacity		585	700	Ah
Battery Power (@0.5 C)	P_{bat}	[- 2.1, 10.5]	[- 25.8, 25.8]	kW
Nominal battery voltage	V_{bat_nom}	36	3.2	V
Battery State of Charge Limits	SoC_{bat}	[0.2, 1]	[0.2, 1]	-
Min. Battery open-circuit voltage	$u_{bat}^{oc\_\min}$	36.65	2.8	V
Battery no-load voltage drop	δ_{bat}	2.55	1.2	V
Battery internal resistance	R_{bat}	11.7	0.2	mΩ
Battery mass	M_{bat}	750	21	kg
Number of battery modules in series	N_s	2	23	-
Number of battery modules in parallel	N_p	1	1	-

The real driving route of the electric minibus of Coimbra is as shown in blue line in Figure 2.14. It is 2.4 km-long and it has a frequency of 10 minutes. However, there are no specific stops. The passengers can ask to enter or leave the minibus at the point that they want. The model of the minibus was tested using real driving profile collected from GPS with an average of 10 passengers. Figure 2.15 shows the velocity and slope profile of such route.

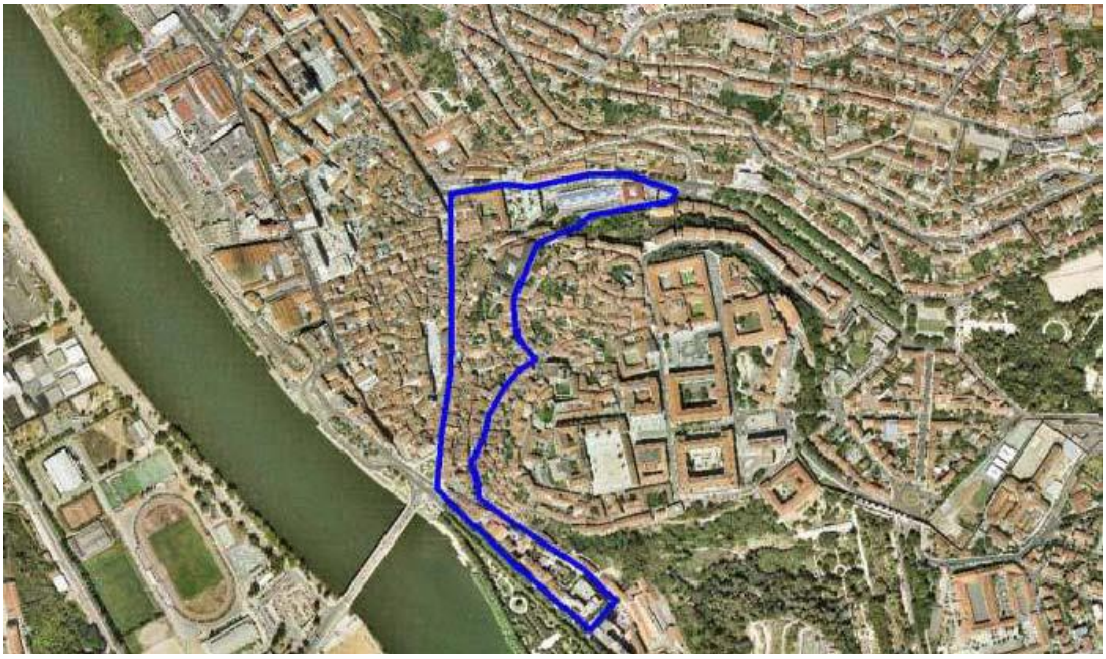

Figure 2.14 Route of the electric minibus of Coimbra [16]

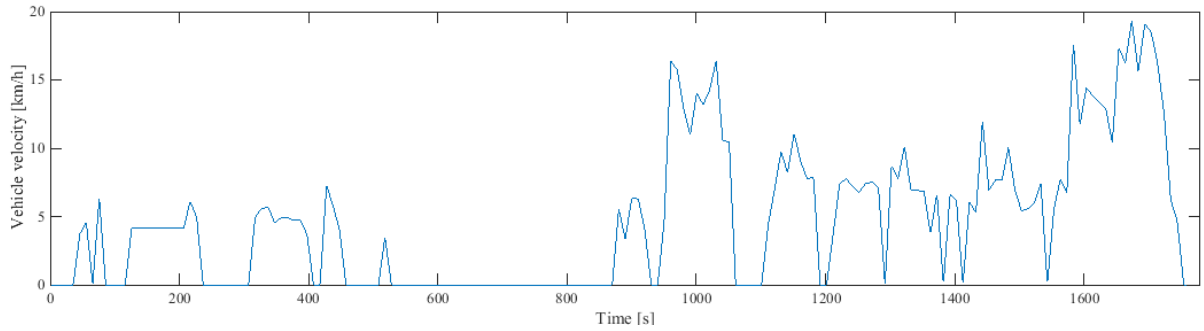

(a)

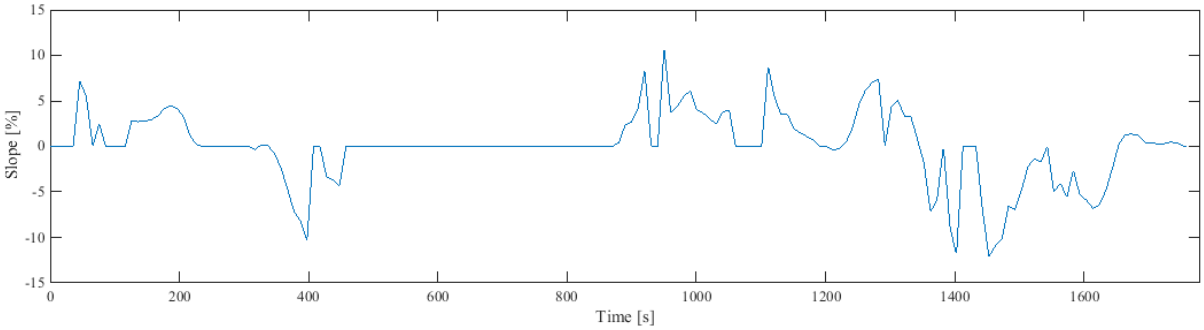

(b)

Figure 2.15 (a) Velocity and (b) slope profiles of the electric minibus of Coimbra deduced from real GPS data (adapted from [16])

Results show advantages of Li-ion battery pack. Li-ion batteries have superior characteristics of high energy density, no memory-effect, high peaks of current capability, less weight, and long life cycle comparing to lead-acid battery. Moreover, the results show lower current demand, lower voltage drop, and lower State-of-Charge (SoC) drop at the end

of the driving cycle. Comparing these SoC, it was concluded that Li-ion battery pack can last two times longer than lead-acid battery pack before needing to be charged. This could significantly save the cost of operating and charging [16][17].

Chapter 3 Improvement of Charging Procedure

From the previously developed test bench, all the connections were established and the devices were able to function individually. Regarding the charging process, the charger and the battery pack were connected in parallel through a contactor which can be closed by a circuit breaker. On the other hand, the Battery Management System (BMS) was connected to the battery pack, the charger, and the computer. It was able to take correct voltage measurement from the battery pack. However, there was a problem with accuracy of current measurement as the measurement when the battery was neither charging, nor discharging was around 26A instead of being 0A as it supposed to be. Another problem was regarding the BMS operation. Without considering the BMS, the battery pack can be charged at full power. However, the BMS did not send a proper signal to reduce or cut off charging current when certain levels were reached. In addition, in some condition (with BMS connected), the charger power was cut after it was turned on only for a short while. For such condition, it was not possible to charge the battery under a safe and proper condition. Therefore, the main objectives to improve the test bench setup for the charging process included:

1) To solve the problem of inaccurate current measurement, and

2) To develop a safe charging procedure.

In order to achieve such objectives, the procedure is as following:

1) Familiarize with the previous setup to be able to operate the test bench with previous configuration,

2) Verify all the connections and configurations with the manuals, and perform experiments to obtain addition information if necessary,

3) Analyze the result and propose solutions for each problem,

4) Implement and verify the solutions by performing an experiment. If the problem still remains or there are other issues, redo steps 2) - 3) until the final solution is reached, and

5) Summarize and create a safety charging procedure.

The first step was to familiarize with the test bench. This was a global task i.e. with the whole setup, not just the charging facilities (the BMS and the charger). After knowing how the connections were, the next step was to verify with the manuals. This was also a

global task to verify all the connections of the test bench. The purpose is to recheck all the connections and to understand the purpose of each connection as it is important to understand to be able to propose solutions.

3.1 Current measurement issue

This issue was initially suspected to be from the sensor itself. From the inspection of the charging facilities, the first potential cause discovered was associated with the current sensor. The current sensor connection provided by the manual is shown in Figure 3.1. Comparing such figure with the initial connections, a difference in the connection was found. Pin #2 of the sensor is not connected according to the manual but it was initially connected to ground at pin #1 of the BMS. Another possible solution was to tune the sensor by using two tuning potentiometers to tune the gain and offset of the output.

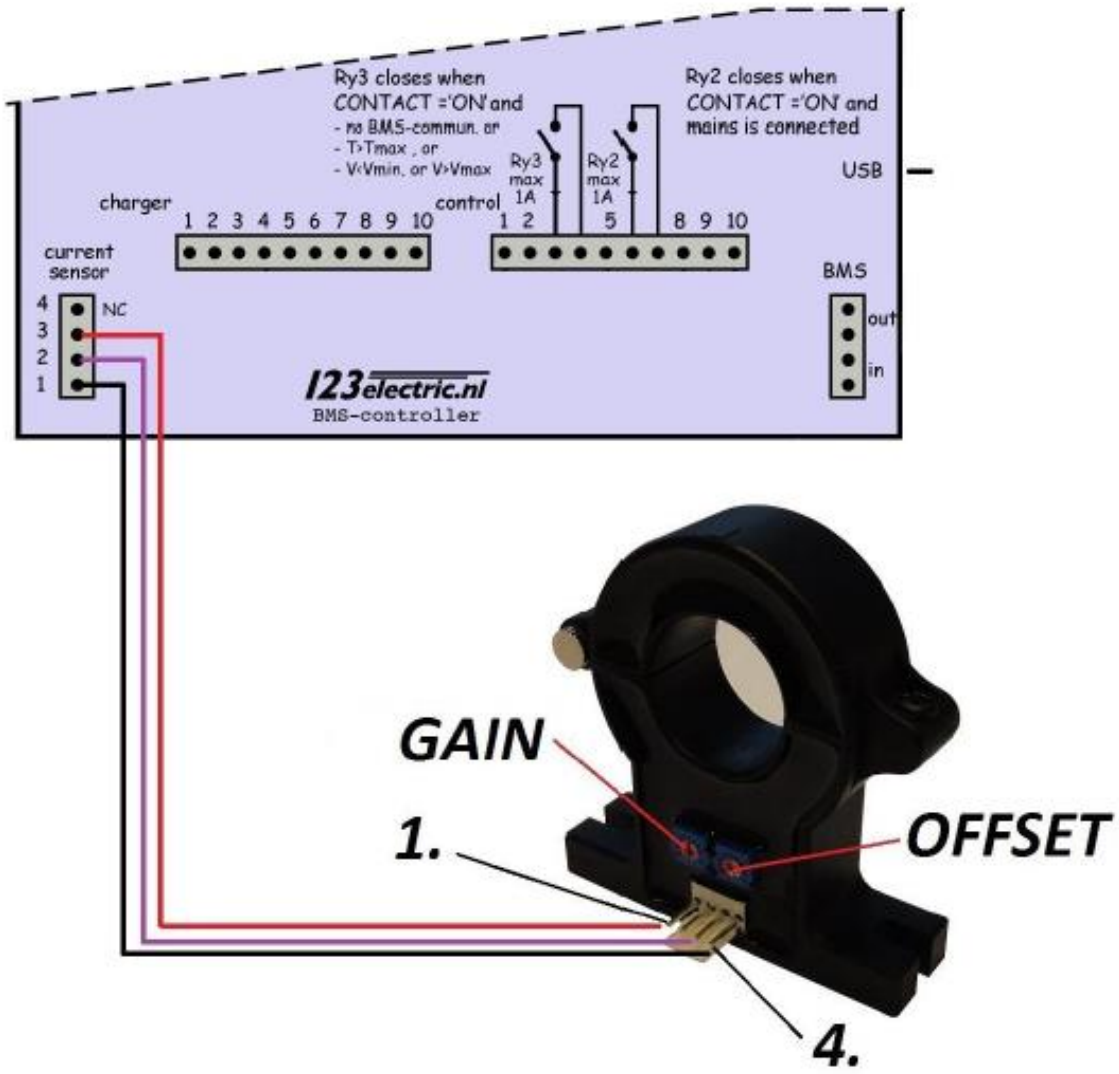

Figure 3.1 Current sensor connections from the manual [18]

Furthermore, another contrary to the manuals was the connection of the auxiliary battery (12V battery) to the system. The connection of the positive and the negative terminals

were interchanged, with regard to the connection in the manual. This might affect the supply of the BMS. In addition, since the sensor is supplied by the BMS, this might also affect the current sensor output.

From three potential causes of such issue, three possible modifications were proposed. The order of the tests was from the one which affect the setup the least to the one which affect the setup the most, to prevent danger to the setup. Therefore, the order was:

1) Remove connection of pin #2, as it would not affect any other parts and it can be undo by connecting it back,

2) Adjust the current sensor gain, as it could be adjusted back but it might affect the calibration of the sensor, and

3) Swap the battery terminal connection, as it would affect the whole supply system and should be reconfirmed with the supervisor before performing such action to prevent danger to the components.

For each test, the system was connected to BMS software to see the current measurement after each modification and verify the effect of the modification to the output. The initial inspection was to verify if the current measurement is 0A when the battery pack is neither charging nor discharging. Then, if the first requirement is fulfilled, the next verification is to compare the current measurement under operation with the measurement from external current clamp sensor.

As a result from the experiments, the observation from each modification was:

1) Connection of pin #2 did not affect the output measurement. Nonetheless, it was left not connected (with a tape on it as a protection from short circuit) to be in accordance with the manual,

2) Adjusting the potentiometers, the current measurement can be dropped down to around 2-3A when neither charging nor discharging but it could not be 0A, and

3) After verifying with the supervisor, the battery terminals were swapped. Once the system was connected, the current measurement dropped below 0A. Therefore, offset potentiometer on the current sensor was adjusted and 0A measurement was achieved when the battery was neither charging nor discharging. In addition, the motor was operated to verify the current measurement in the BMS software dashboard with the external sensor. Although the current was not constant and it was hard to verify, the range of current read from both devices were the same. Therefore, the objective of solving the measurement problem and obtaining an accurate current measurement was fulfilled.

Remark: Although the current measurement is relatively correct, for the best accuracy and resolution, the current sensor should be recalibrated with a proper calibration method since its potentiometers were adjusted during the tests.

3.2 Safe charging procedure

After the current measurement was corrected, BMS performance was inspected. The main issue regarding the BMS was that the charger is not the same model as in the manual of the BMS and there was not much information regarding the schematic inside the BMS and the signal of each pin. Figure 3.2 show two possible wirings provided by the manufacturer. In Figure 3.2 (a), Elcon battery charger with analog enable signal is employed while in Figure 3.2 (b), a BMS controllable charger is employed but only On/Off state is controllable. Initially, the connections were similar to Figure 3.2 (b) with High/Low cable also connected to ground. However, the charger employed in this test bench has both On/Off and High/Low pins. Due to this limited information given by the manufacturers, some experiments were conducted in order to test the operation of the BMS and the charger.

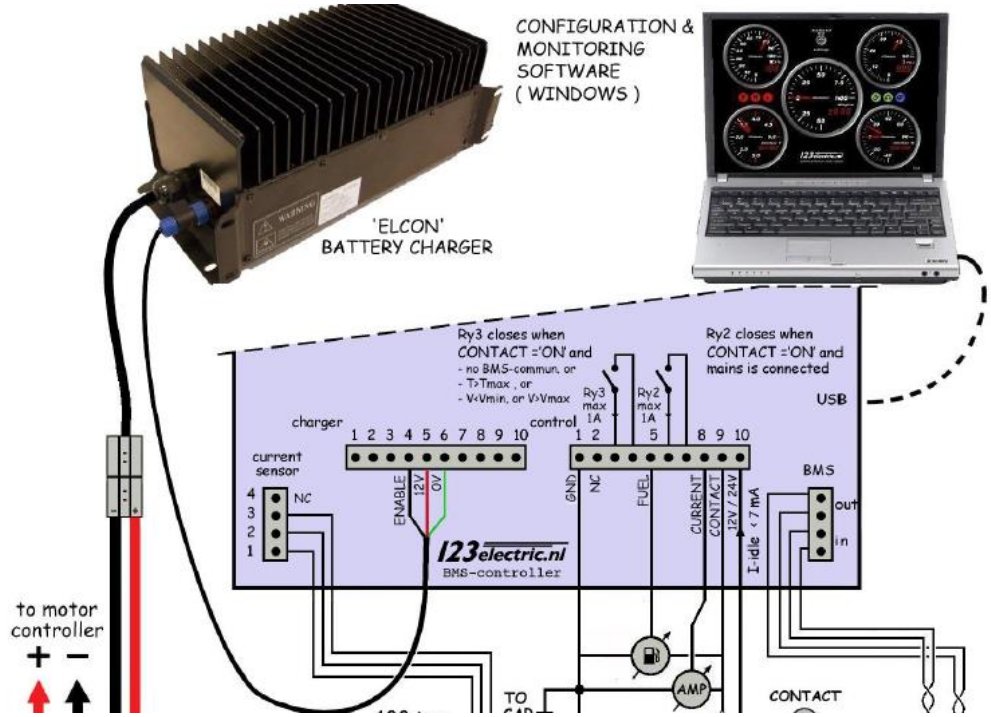

(a)

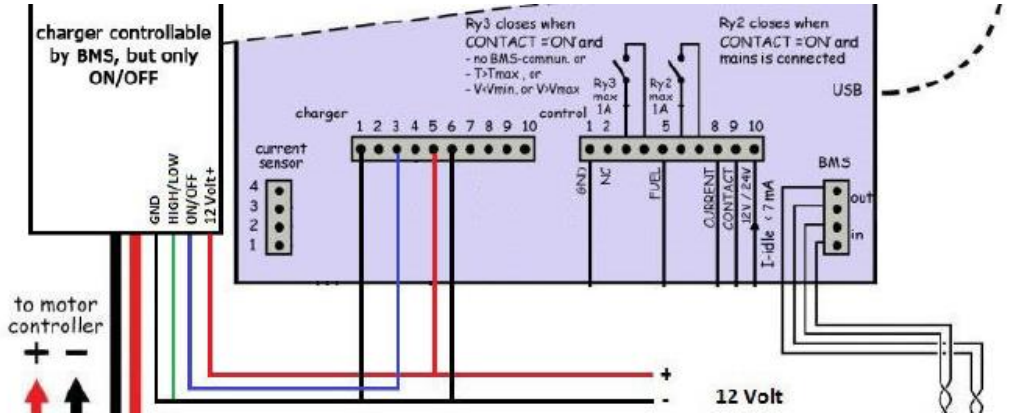

(b)

Figure 3.2 BMS wiring diagrams with (a) Elcon battery charger [18] and (b) charger controllable by BMS [19]

According to the charger manual, the manufacturer provides four conditions of charging as shown in Table 3.1. The purpose of this improvement is to allow the battery pack to be charged properly and safely until it is fully charged. For such requirement, the batteries should be charged at full power until bypass voltage level is reached. Then, it should continue charging at reduced power until the pack is fully charged. This would be possible if On/Off and High/Low pins get proper signal from the BMS. Furthermore, all cells in the pack should be in the similar level to avoid overvoltage in certain cells. This is part of the function of BMS boards. They dissipate energy from the cells which have higher voltage. Moreover, there should be safety measures to cut the power when a cell goes above cutoff voltage level.

Table 3.1 Charger operation under different connections [20]

No.	Charger operation	Contacts	Status
1	Charging at maximum power	VC12V	Not connected
		On/Off	Not connected
		High/Low	Not connected
		GND	Not connected
2	Charging at maximum power	VC12V	+12V
		On/Off	GND
		High/Low	GND
		GND	GND
3	Stop charging	VC12V	+12V
		On/Off	Not connected
		High/Low	any
		GND	GND
4	Charging at reduced power (10%)	VC12V	+12V
		On/Off	GND
		High/Low	Not connected
		GND	GND

Preliminary test was conducted with the connections as they were initially connected. On/Off was connected to pin #3 of BMS “charger” connector, pin#4 was not connected, Vc12V was connected to pin#5, and GND and High/Low were connected to pin #6. After charging for a while, the charging process stopped even though the batteries voltages had not reached set level. The SoC level on the dashboard of the BMS software showed 100%. However, this should not stop the charging process as it is not stated in the manual and the SoC was not accurate as the battery pack has to be fully charged at least one cycle in order to use this function properly. Using a multimeter, voltages measurement at each pin of the “charger” connector was taken. Vc12V at pin #5 was 5 V and GND at pin#6 was 0 V whereas pin#3 was 12V and pin#4 was 0V. Combining the issue of not utilizing the High/Low signal and unexpected output from pin #3, the BMS manual was observed and several possible modifications were proposed to achieve proper BMS functions, including:

- Utilizing output of BMS “charger” connector pin#4, and

- Utilizing the Ry3 relay inside the BMS between BMS “control” connector pin #3 and pin #4 which closes when the voltage reaches maximum voltage, the voltage is below the minimum voltage, the temperature is over the maximum temperature, or when there is no BMS connection, according to the manufacturer.

As previously mentioned, some experiments were carried out to test these components before final implementation. These included:

- Testing of output of BMS charger pins, and

- Testing of Ry3 contact.

The tests were conducted by charging the battery at reduced power, to be able to see the output clearly and to prevent danger to the battery pack. This was done by removing High/Low cable from BMS “charger” connector pin #6 so it was not connected and On/Off cable was grounded by moving it from pin#3 to pin#4 as observed from when the charger stopped working in preliminary test. It must be noted that “charger” connector pin #4 appears on the BMS manual (cf. Figure 3.2 (a)) as “Enable” for the Elcon charger, so the objective was to test if this pin’s voltage commutate when reaching overvoltage and so to use it to control the charger.

Bypass voltage and maximum voltage levels on the BMS software were set to the level close to the actual voltage level in order not to wait too long to see the result. This is also to avoid risk of passing the limit voltage in case of malfunction. A multimeter was used to measure output voltage of “charger” connector pin #4 as well as pin #3, to verify the signals from the BMS. Furthermore, 12V was supplied to BMS “control” connector pin #4 and the voltage measurement was taken at pin#3 to verify if the contact was closed or not.

Regarding balancing of cell voltage by the BMS, it was observed that the LEDs on BMS boards on top of the battery cells were blinking faster when the cells were reaching set voltage. The transistors on the boards were also getting warmer to dissipate energy in the form of heat to balance the cells. This clearly shows the function of balance charging by the BMS.

Regarding pins outputs,

- In normal charging condition, the measured voltage of pin#3 was 0V and pin#4 was around 5.6V.

- When all cells reached bypass voltage, pin#3 was 0V and pin#4 was 3V.

- When the bypass voltage was increased and all cells reached new bypass voltage, pin#3 was 0V and pin#4 was 5.6V.

- When cells reached set maximum voltage, ‘H’ indication on the dashboard was on, SoC indication was 100%, pin#3 was 0V, pin#4 was 2.56V, and Ry3 was also closed.

- After that, the charger circuit breaker was closed and the cells voltages dropped below the set maximum voltage. SoC was shown as 100% but ‘H’ was off. At this point, pin#3 was 0V, pin#4 was 2.56V, and Ry3 was open.

- Finally, the charger circuit breaker was turned on again. SoC was still shown as 100%, pin#3 was 0V, pin#4 was 2.56V, and Ry3 was open. After 1-2 minutes, 'H' indication was on.

Some pattern can be observed from BMS "charger" pin #4 but several points should be noted. First, the output is analog signal while the required input to the charger is either not connected or ground. Therefore, additional circuit such as hysteresis comparator would be required. Secondly, the voltage level was not always constant in the same condition. For instance, the voltage was measured to be 0V in the preliminary test but it was never 0V in this test and the voltage when all cells reached the increased bypass voltage was not the same as when the cells initially reached the bypass voltage. Therefore, if this is to be implemented, more controlled experiment should be conducted to verify it before utilization. In addition, the voltage of pin #3 was always 0V in this test which mean that it will never turn off the charger because On/Off pin required not connected condition to turn off the charging process, according to Table 3.1. Therefore, to keep the circuit simple, the first proposed solution is as shown in Figure 3.3. A switch was utilized to manually open the connection of High/Low pin to ground. Furthermore, a relay "-KA1" was utilized. Its coil was connected to BMS "control" connector pin #3 and its normally closed contact was connected between On/Off pin and ground. Once the Ry3 closes, the contact of "-KA1" will open and stop the operation of the charger.

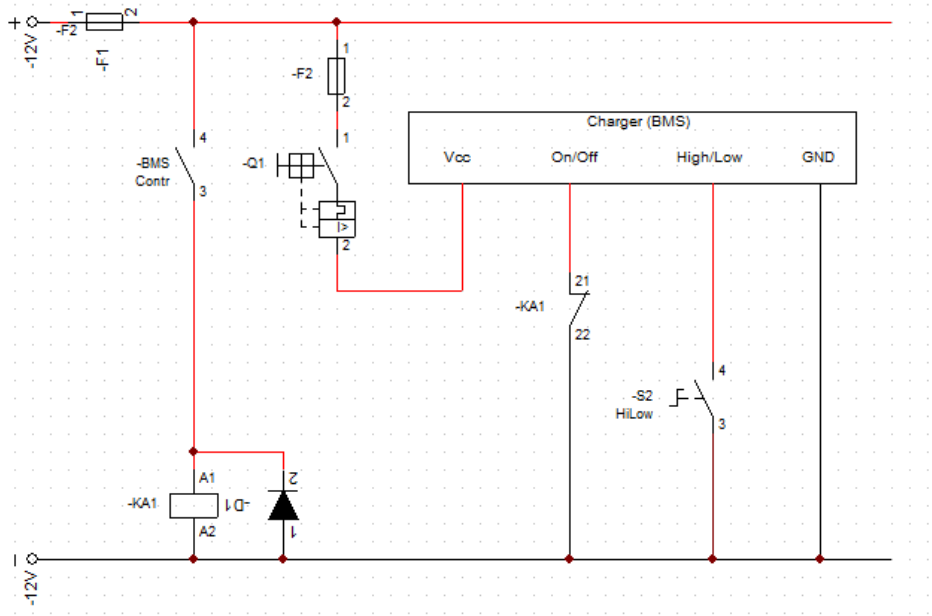

Figure 3.3 The first proposed solution for charging system

The solution was implemented to the test bench and the charging test was performed. The results show that High/Low switch was able to successfully control the charging power between full power and reduced power. The power was also cut i.e. the current went to 0 A when maximal voltage was reached. However, once the voltage dropped, the power was on again. This corresponds to the schematic. However, this is not a desirable operation since turning on and off frequently is not good for the system. Therefore, a latching circuit as shown in Figure 3.4 was proposed. The purpose of this circuit is to permanently cut the

power once a cell reached maximal voltage or any other fault condition occurs, until the reset button is pressed. This utilized another contact of the relay "–KA1" which was already in the circuit. Therefore, the only extra component required was the reset button "-S1".

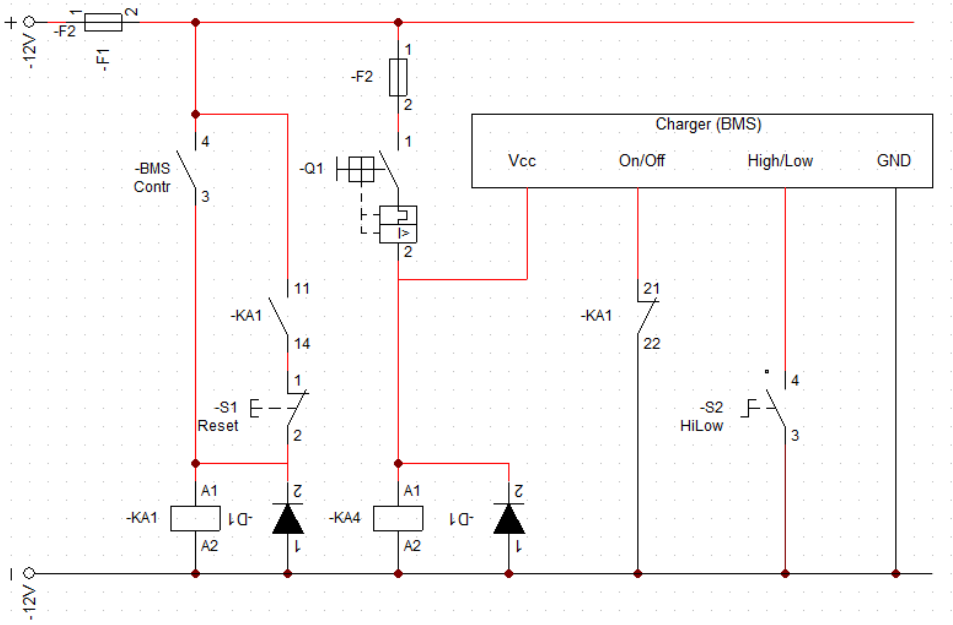

Figure 3.4 Charging system with latching relay circuit

After the latching circuit was implemented, the system was tested again. The result was satisfying. The High/Low switch was still working as it was not changed by this modification. The power output from the charger was cut once the set maximum voltage was reached by any cell. Furthermore, the power can be turned back on when the reset button is pressed.

In addition, a red indication light was added to the circuit to indicate when Ry3 is closed. Although the indications in BMS software dashboard will light up, the user might not notice it. Therefore, this light was employed to indicate such situation. This is more beneficial when deep discharge occurs since when it is overvoltage, the charging process will be cut by the relay circuit but there is no prevention for deep discharge. Nonetheless, deep discharge would occur when the test bench is under operation. Therefore, there will be a user in the area. For this reason, the indication light would tell the user to shut down the process and charge the battery pack.

At this point, it was possible to operate the charger in all desirable operations. The next step was to ensure that undesirable operation would not occur during the charging process. The main objective was to avoid full power charging in operation no.1 from Table 3.1. Although this is beneficial for charging without BMS signals and for emergency charging, it is dangerous if there are some faults which cause the contacts to be disconnected and the battery charges unintendedly. From initial inspection, such condition should not occur since the ground is permanently connected. Therefore, it is not possible that all four cables are not connected, unless there is a problem with cables connections which is unlikely. However, it is important to notice that other conditions were not specified by the

manufacturer. 12V supply depends on the circuit breaker and the fuse. Therefore, it can be disconnected. In order to test the effect of this connection, an experiment was carried out to test the condition of normal connection with 12V not connected. This was conducted by opening the circuit breaker while charging at full power and reduced power.

The results from both experiments were the same. Once the circuit breaker was open, the charger stopped working for about 2-3 seconds then it started again at full power. In addition, since there was no power to the BMS, the BMS did not detect that the batteries went overvoltage. This could be even more dangerous since this would mean that the battery will keep being charged at full power (even when the switch is selected to low power) and there is no cut off.

In order to avoid such undesirable situation, the connection between the charger and the battery should be cut if there is no power supply to BMS "charger" pin #5 which is connected to Vc12V pin of the charger. This is done by moving connection of charger output circuit breaker from directly from 12V power supply (after the fuse) to get 12V supply after BMS circuit breaker. Therefore, if the fuses or BMS circuit breaker is cut i.e. there is no supply to the BMS, the contactor will not be closed even though the charger circuit breakers are closed. Consequently, the charger will not be connected to the battery.

After the first trial, the problem found was that the BMS circuit breaker tripped after the charger was turned on. Therefore, such device was replaced by another one which has higher rating to be able to withstand the inrush current. After that, the circuit was tested again and the test result was satisfying. Several current measurements were taken by a current cramp sensor to be used as a reference for further work. The main consumption came from the charger contactor which drawn around 0.4A while the auxiliary relay for latching circuit drawn around 0.04A. The BMS draws around 60 mA.

Additionally, the last element which was added to the test bench was an emergency switch for the PMSM. This would be a safety measure before operating the machine. Since the servo motor is fed by the grid through its VFD, there was already an emergency switch to cut off grid power. However, this was not the case of the PMSM which is fed by a battery pack. Observing the manual, an emergency switch was proposed to employ between SEVCON pin#4 and the contactor. This would cut the output supply from SEVCON to the coil of the contactor. The output is at battery voltage and the maximum rating is 2A [21]. Figure 3.5 shows the test bench with charging process improvement.

In addition to the initial objectives, another issue encountered during the study was that there was no wiring diagram for the whole system. Initially, the connections were based on different wiring diagrams provided by the manufacturers. However, connections between system and adaptations applied to the test bench were not explicitly stated. These cause confusion and difficulty in understanding and tracking the system. Therefore, an additional task was to create a schematic of the whole system for ease of further study and utilization of the test bench. The developed schematic is shown in Figure A-1 in Appendix A, drawn using CADeSIMU software.

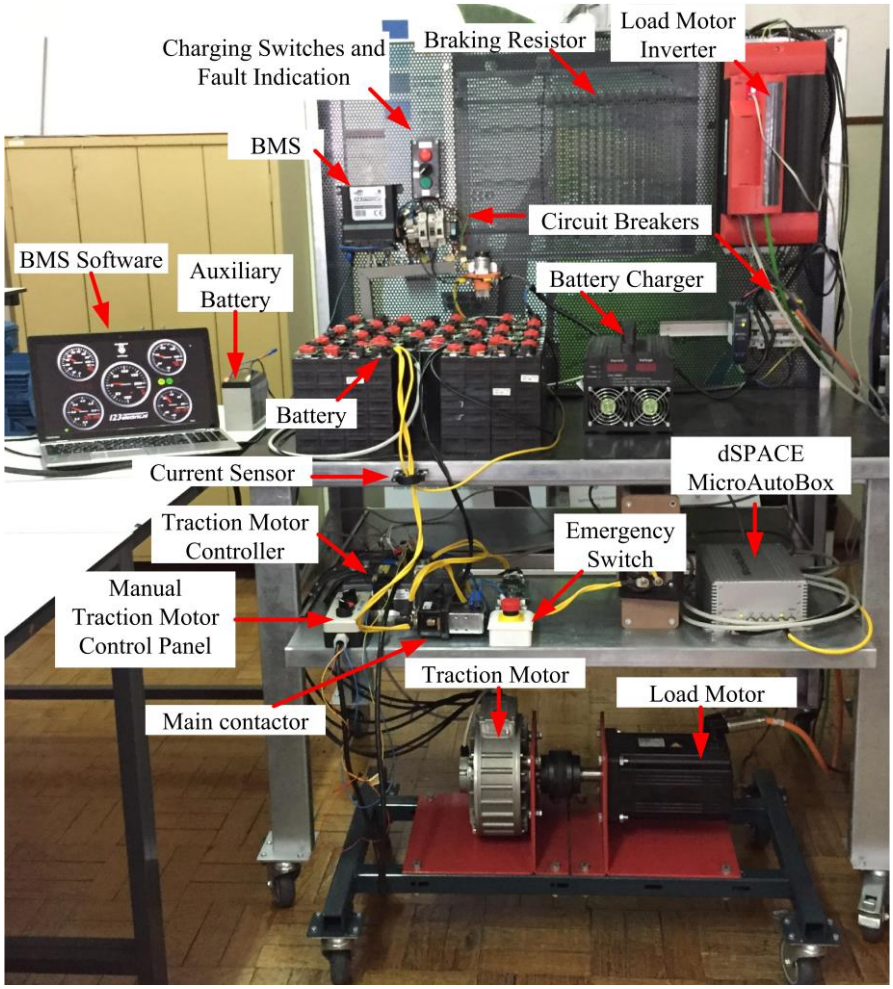

Figure 3.5 Test bench with charging process improvement

As a final step of developing a safe charging procedure, a user manual was developed as a guide for the charging procedure. This allows any user to be able to charge the battery pack of this test bench by following the steps provided by this guide. Such guideline is shown in Figure A-2. In addition, a guideline for operation of the full test bench was also developed after the test bench was completely configured (as will be further explained in following chapters). These are also shown in Appendix A.

Chapter 4 Developing of the EMR of the Electric Minibus of Coimbra

EMR of the electric minibus of Coimbra can be developed following the procedure explained in section 2.3. This is fully explained step-by-step in [22]. This chapter, on the other hand, will explain only the essential parts for the implementation to simulation. The process of developing reduced-scale P-HIL simulation for the electric minibus of Coimbra which will be explained in this chapter and next chapter are summarized in Figure 4.1. It will starts by developing the EMR and simulation of the electric minibus in Chapter 4. Then, the process of developing the EMR and simulation of P-HIL of such vehicle will be explained in Chapter 5.

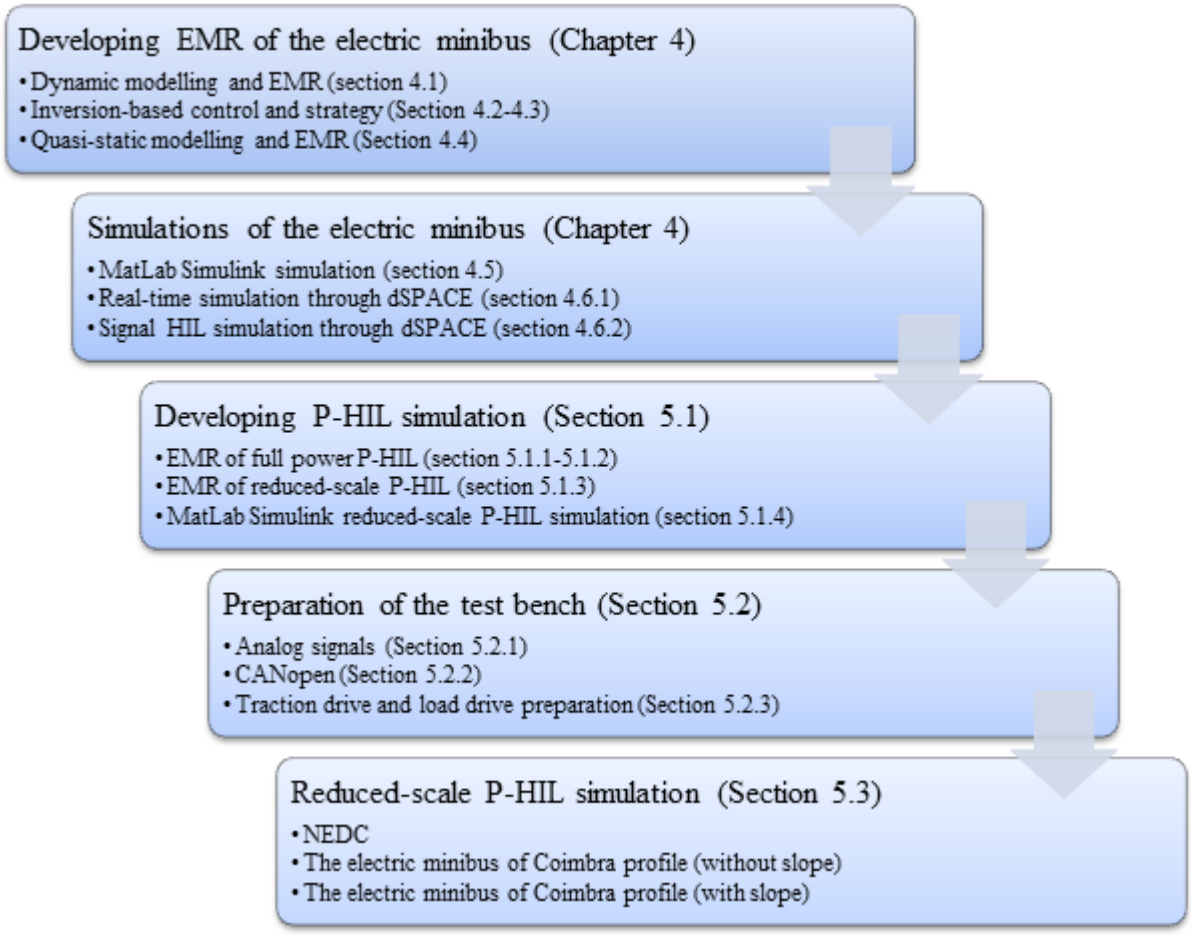

Figure 4.1 The process of developing reduced-scale P-HIL simulation in this thesis

4.1 Modelling and EMR of the electric minibus of Coimbra

As previously mentioned, the modelling of the minibus is required as the first step. Each component will be modelled separately before assembling them together. The minibus electrical propulsion system is composed of a battery pack, a DC-DC converter, a series DC motor, and a mechanical transmission with a gearbox [17]. For this study, the interest is on a linear motion with no slipping assumption. Figure 4.2 shows the topology of the minibus with an equivalent single wheel and braking system as a result from such assumption [22].

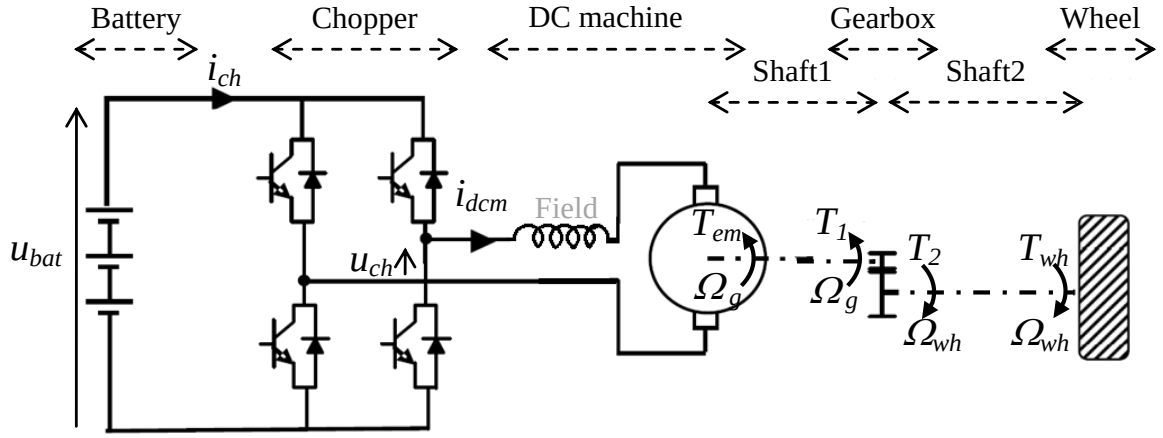

Figure 4.2 Topology of the electric minibus using an equivalent single wheel model

The first part is the battery pack which is the source of this system. As previously mentioned in section 2.4, the minibuses currently employ lead-acid batteries. However, the studies [16]-[17] recommend replacing them by Li-ion batteries. Nonetheless, the batteries are modelled as a voltage source with a voltage, $u_{bat}(t)$, depending on the State-of-Charge, and a voltage drop due to the series resistance, R_{bat}:

$$u_{bat}(t) = u_{bat}^{oc}(t) - R_{bat} i_{ch}(t) \tag{1}$$

where $u_{bat}^{oc}(t)$ is the open circuit voltage depending on SoC and $i_{ch}(t)$ is the current imposed by the chopper. This can be extended to more complicated model which also takes into account the non-linearity and thermal behavior of the battery but it is not the case of this study. This component is represented in EMR by a source element.

The DC-DC converter or chopper is modelled using an average model. A modulation ratio, $m_{ch}(t)$, is used to indicate the output voltage as a ratio of input voltage [24] as can be seen in Figure 4.3. This can be expressed as:

$$\begin{cases} i_{ch}(t) = \eta_c^n m_{ch}(t) i_{dcm}(t) \\ u_{ch}(t) = m_{ch}(t) u_{bat}(t) \end{cases} \quad \text{with } n = \begin{cases} -1 & \text{if } P(t) > 0 \\ 1 & \text{if } P(t) < 0 \end{cases} \quad \text{and } m_{ch}(t) \in [0,1] \tag{2}$$

where $i_{dcm}(t)$ is the current imposed by the machine, η_c is the efficiency of the chopper, $u_{ch}(t)$ is the voltage imposed by the chopper, and $P(t)$ is the instantaneous power. This component is represented in EMR by a monophysical conversion element.

The DC machine can be modelled as 3 parts. The first part is the electrical part. Since

the machine is a series DC machine, the currents in both windings (armature and field windings) are the same. Therefore, it can be studied using an equivalent winding which is the summation of both windings. The winding is modelled as an equivalent inductor, L_{eq}, with an equivalent series resistor, R_{eq}:

$$u_{ch}(t) - e_{dcm}(t) = L_{eq}\frac{d}{dt}i_{dcm}(t) + R_{eq}i_{dcm}(t) \tag{3}$$

where $e_{dcm}(t)$ is the back-emf of the machine. This part is represented in EMR by an accumulation element.

The second part is the electromechanical conversion which is the interaction between the rotor and the stator. This converts values between electrical and mechanical domain, with an efficiency η_{dcm}, through motor constants, k_a and k_b, and machine flux, φ. The machine flux is proportional to the machine current. However, with high value of current and torque, the machine will saturate, resulting in a constant flux. The flux is also constant in the case of a permanent field machine. Produced electromechanical torque, $T_{em}(t)$, is related to the machine current while the back-emf is related to machine speed, $\Omega_g(t)$, imposed by the gearbox:

$$\begin{cases} T_{em}(t) = k_a \varphi i_{dcm}(t) \eta_{dcm}^{m} \\ e_{dcm}(t) = k_a \varphi \Omega_g(t) \end{cases} \text{ with } m = \begin{cases} 1 \text{ if } & P(t) > 0 \\ -1 \text{ if } & P(t) < 0 \end{cases} \text{ and } \varphi = k_b i_{dcm}(t) \tag{4}$$

Since the inputs and outputs are in different domain but there are no delays between both sides, this part is represented in EMR by a multiphysical conversion element.

The last part of the machine is the mechanical part or the shaft of the machine. However, due to the conflict of association, this part is not represented by an EMR element. Its functionality is merged with other parts.

The mechanical transmission is composed of a gearbox, shafts, wheels, and a braking system. As previously mentioned, since only longitudinal motion in a straight line without slipping is considered, an equivalent single wheel model is utilized [25]. The gearbox has a fixed ratio k_g and an efficiency η_g. It reduces the speed and increases the torque of the machine by such ratio. Due to conflict of associations between the gearbox and the shafts, the relationship between outputs and inputs of the gearbox can be expressed as:

$$\begin{cases} T_g(t) = (\eta_g^{m} k_g) T_{em}(t) \\ \Omega_g(t) = k_g \Omega_{wh}(t) \end{cases} \text{ with } m = \begin{cases} 1 \text{ if } & P(t) > 0 \\ -1 \text{ if } & P(t) < 0 \end{cases} \tag{5}$$

where $T_g(t)$ is the torque imposed by the gearbox and $\Omega_{wh}(t)$ is the rotational speed of the wheel.

Since the conversion does not accumulate internal energy, this virtual component is represented in EMR by a monophysical conversion element.

The wheel changes rotational movement to translational movement with relationship of the wheel radius, R_{wh}:

$$\begin{cases} F_{tr}(t) = \dfrac{1}{R_{wh}} T_g(t) \\ \Omega_{wh}(t) = \dfrac{1}{R_{wh}} v_{ve}(t) \end{cases} \quad (6)$$

where $v_{ve}(t)$ is the vehicle velocity and $F_{tr}(t)$ is the transmission force. It is represented in EMR by a monophysical conversion element.

From Newton's second law of motion, vehicle movements depend on its mass and the total force acting on it. In traction, such force is the difference between the tractive force imposed by the wheel and the resistive force imposed by the road, $F_{res}(t)$. In addition, in deceleration, the braking force, $F_{br}(t)$, is also taken into account. However, since there are three associated forces which are more than the amount permitted by an accumulation element, the relationship has to be split into two equations. $F_{tot}(t)$ represents the total force by the vehicle (from the transmission and the braking system):

$$F_{tot}(t) = F_{tr}(t) + F_{br}(t) \quad (7)$$

This is represented in EMR by a mono-physical coupling element. In addition, the chassis can be represented by an accumulation element. However, due to the conflict of association, the mass of this element is the equivalent mass, M_{eq}, of the vehicle and shafts inertia:

$$v_{ve}(t) = \int \frac{F_{tot}(t) - F_{res}(t) - B_{eq} v_{ve}(t)}{M_{eq}} dt \text{ with } M_{eq} = M_{tot} + \frac{J_{eq}}{R_{wh}^2} \text{ and } B_{eq} = \frac{f_{eq}}{R_{wh}^2} \quad (8)$$

where M_{tot} is the total mass of the vehicle, J_{eq} is the equivalent shafts inertia from the association, f_{eq} is the equivalent rotational friction coefficient from the association, and B_{eq} is the equivalent friction coefficient of the vehicle. Full calculation of these equivalent parameters can be found in [22].

The resistive force is the summation of rolling resistance, aerodynamic drag force, and grading force as expressed by:

$$F_{res} = \mu_{rr} M_{tot} g + \frac{1}{2} \rho C_d A_f (v_{ve}(t) + v_w(t))^2 + M_{tot} g \sin \alpha(t) \quad (9)$$

where μ_{rr} is the rolling resistance coefficient, g is the gravitational acceleration, ρ is the air density, C_d is the aerodynamic drag coefficient, A_f is the vehicle frontal area, $v_w(t)$ is the wind velocity, and $\alpha(t)$ is the road angle. Since the road is considered as environment of this study, this is described by a source element.

In addition, another source element in this system is the braking system. The braking force, $F_{br}(t)$, is given by the reference, $F_{br\text{-}ref}(t)$:

$$F_{br}(t) = F_{br-ref}(t) \quad (10)$$

Combining all the elements together, Figure 4.3 shows the developed EMR of the electric minibus.

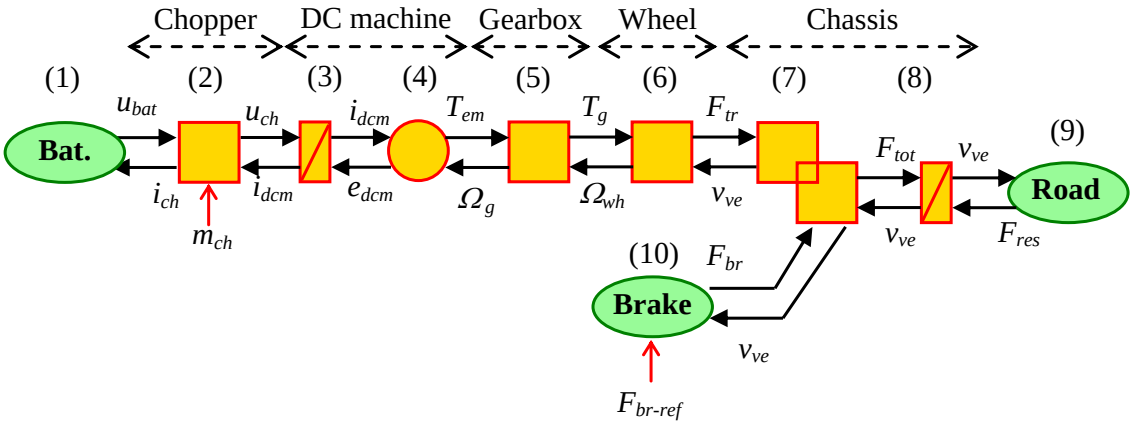

Figure 4.3 EMR of the electric minibus

4.2 The inversion-based control of the electric minibus of Coimbra

After the EMR of the electric minibus is defined, the next step is to identify the tuning path. The objective of the control is to control the velocity of the vehicle whereas the tuning variables are the modulation ratio of the chopper and the braking force reference. Therefore, taking Figure 4.3 as a reference, the tuning path can be identified as in Figure 4.4.

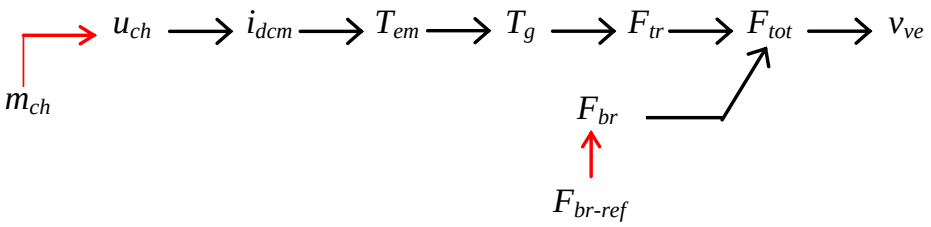

Figure 4.4 Tuning path of the traction system of the electric minibus

Using an inversion-based control, a Maximal Control Structure can be obtained by inverting all EMR elements according to the identified tuning path. This process is done from the final element in the tuning path back to the tuning variables according to the principle explained in section 2.3.

The first element to be inverted is the chassis which is an accumulation element. A closed-loop controller such as PI controller (or others) is required for this inversion. This is done by feeding the error between the references (with subscript *-ref*) and the measured values (with subscript *-meas*) as can be seen in Figure 4.5. In addition, disturbances can be feedforward to the system to improve the control. For the chassis, its control can be achieved using a closed-loop velocity controller, $C_v(t)$:

$$F_{tot-ref}(t) = C_v(t)[v_{ve-ref}(t) - v_{ve-meas}(t)] + F_{res}(t) \qquad (11)$$

Then, the chassis coupling is inverted. A distribution criterion, $K_D(t)$, is required to invert relationship (7). As a result, the control is given by:

$$\begin{cases} F_{tr-ref}(t) = K_D(t) F_{tot-ref}(t) \\ F_{br-ref}(t) = (1 - K_D(t)) F_{tot-ref}(t) \end{cases} \quad (12)$$

After that, the equivalent wheel is directly inverted. The control of the wheel can be achieved by inversion of equation (6):

$$T_{g-ref}(t) = R_{wh} F_{tr-ref}(t) \quad (13)$$

Similarly, the control of the gearbox which is a conversion element can be achieved by direct inversion of equation (5):

$$T_{em-ref}(t) = \frac{1}{k_g} T_{g-ref}(t) \quad (14)$$

The control of the EM conversion of the DC machine can be achieved by inversion of equation (4):

$$i_{dcm-ref}(t) = \frac{T_{em-ref}(t)}{k_a \varphi} \quad (15)$$

On the other hand, the winding of the DC machine is an accumulation element. Its control can be achieved using a closed-loop current controller, $C_i(t)$:

$$u_{ch-ref}(t) = C_i(t)[i_{dcm-ref}(t) - i_{dcm-meas}(t)] + e_{dcm-meas}(t) \quad (16)$$

Finally, the control of the chopper can be achieved by a direct inversion of equation (2) to obtain the modulation ratio, $m_{ch}(t)$, which is the tuning variable of this system:

$$m_{ch}(t) = \frac{u_{ch-ref}(t)}{u_{bat-meas}(t)} \quad (17)$$

4.3 Control strategy

Additionally, there is another level of control called the “strategy” level. This is a global level which provides the references and identifies the criteria necessary for inversion of coupling elements[1]. For this system, a distribution is required to split the braking force between electrical and mechanical brakes. However, due to the construction of the DC machine which is a series DC machine, regenerative braking is not possible with the current condition. Therefore, the braking force must be provided entirely by mechanical braking. On the other hand, the total force is provided entirely by the electrical machine during traction. These can be interpreted to an equation for the distribution criterion as:

$$K_D = \begin{cases} 1 & \text{if acceleration; } F_{tot-ref} > 0 \\ 0 & \text{if deceleration; } F_{tot-ref} < 0 \end{cases} \quad (18)$$

The EMR of the electric minibus with Maximal Control Structure (MCS) is shown in Figure 4.5.

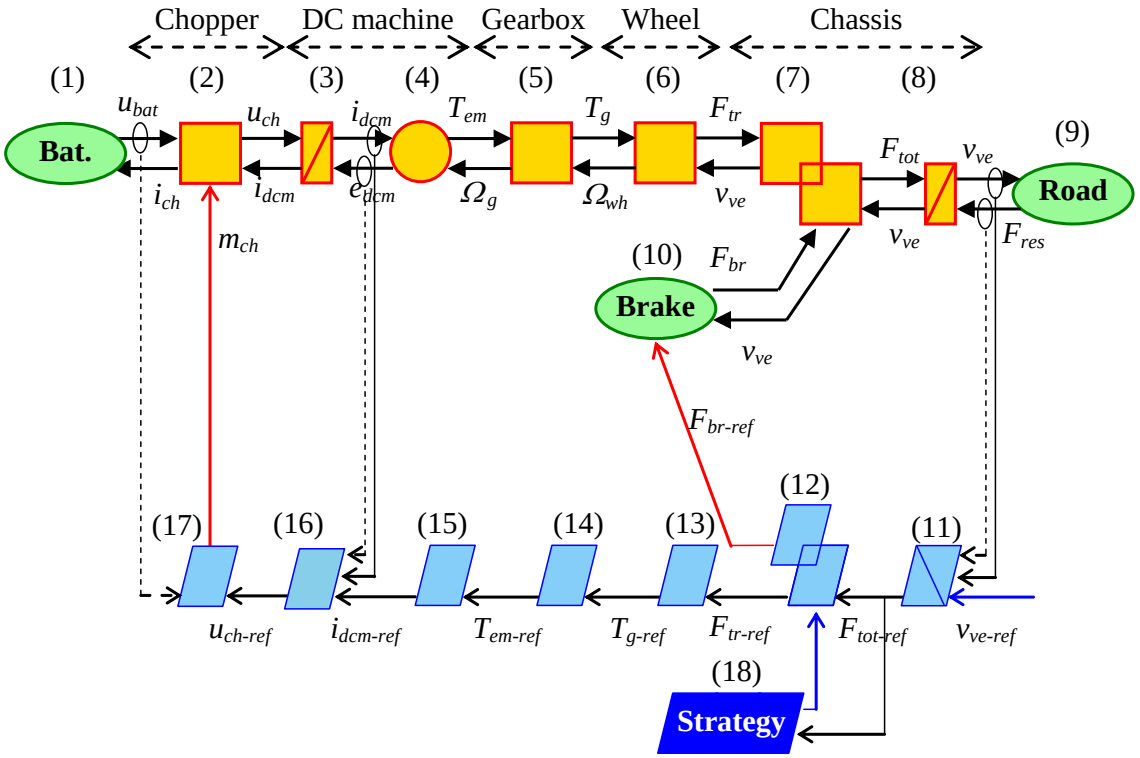

Figure 4.5. The EMR with MCS of the electric minibus

4.4 Quasi-static model of the electric minibus of Coimbra

In addition to the dynamic model, depending on the objective of the study, other models such as a static model can be used. This would simplify the simulation and reduce computational time and power without leading to significant error [22]. In this study, a static model of the machine is utilized. This includes the DC machine, the chopper, and their controls. This helps to overcome the issue regarding machine parameters. Nonetheless, since the dynamic of the vehicle is still considered, globally, the system is considered as a quasi-static model.

Neglecting the dynamic of the machine, the torque, $T_{em}(t)$, is assumed to be instantaneously equal to the reference, $T_{em\text{-}ref}(t)$. In addition, the current imposed by the chopper, $i_{ch}(t)$, can be calculated from the power equation, taking into account the efficiency of the drive, η_d:

$$\begin{cases} T_{em}(t) = T_{em-ref}(t) \\ i_{ch}(t) = \dfrac{\eta_d^m T_{em}(t)\Omega_g(t)}{u_{bat}(t)} \end{cases} \quad \text{with } m = \begin{cases} 1 \text{ if } & P(t) > 0 \\ -1 \text{ if } & P(t) < 0 \end{cases} \tag{19}$$

Replacing the dynamic model of the machine by the static one, the EMR of the system becomes as shown in the upper part of Figure 4.6, in orange and green pictograms. Consequently, the MCS can be deduced from such an EMR. This is similar to the MCS of the dynamic model except that the inversion for the dynamic model is removed. The torque

reference is directly fed to the machine model. This is shown in the bottom of Figure 4.6, in blue pictograms.

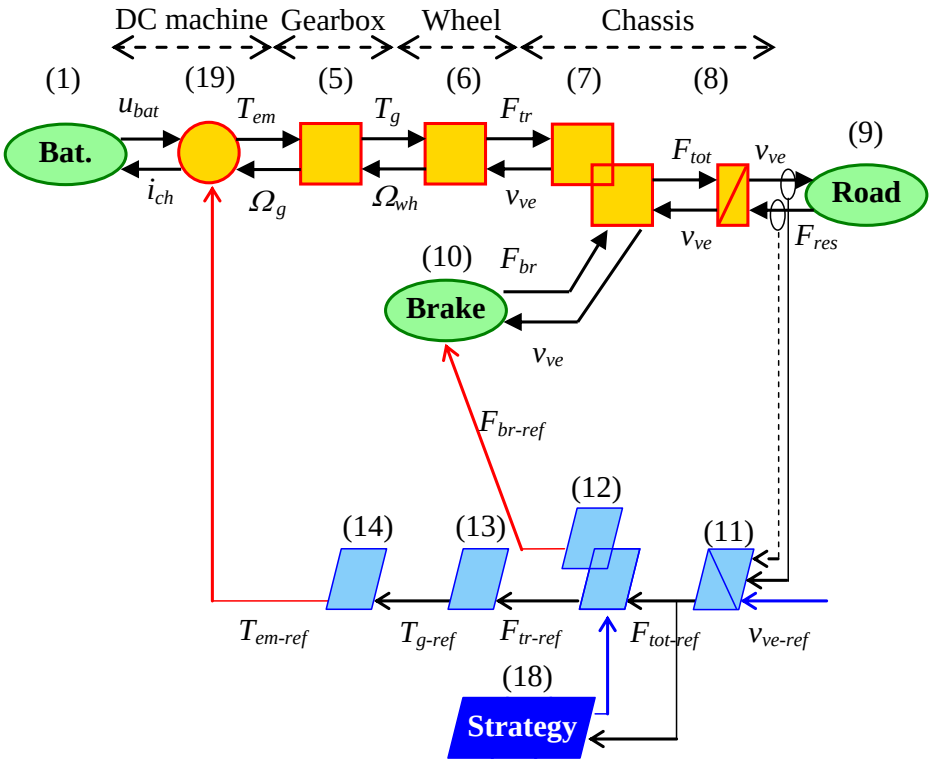

Figure 4.6 EMR and MCS of the electric minibus (quasi-static model)

4.5 MatLab simulation of the electric minibus of Coimbra

After the model and the EMR of the minibus were developed, the next step is to implement them in a simulation. Figure 4.7 shows the developed EMR of the electric minibus in MatLab Simulink software. The structure is the same as in Figure 4.6 except the limitations due to software structure. All inputs of a block are on one side and all outputs of the same block are on the other side. Furthermore, the outputs of the chassis block which is an accumulation element are labeled as Vve and Vve2 even though they are the same. This is due to the restriction of the software which does not allow more than one port or element with the same name. Each block represents an element in the EMR. Corresponding equations are implemented inside each block with parameters from Table 2.1 and Table 2.2. In addition, due to lack of information and for simplicity of the study in this stage, general values such as 80% efficiency for the traction drive were utilized. The friction coefficient was also neglected. Furthermore, the New European Driving Cycle (NEDC) was employed as a reference. No wind or road slope was taken into consideration.

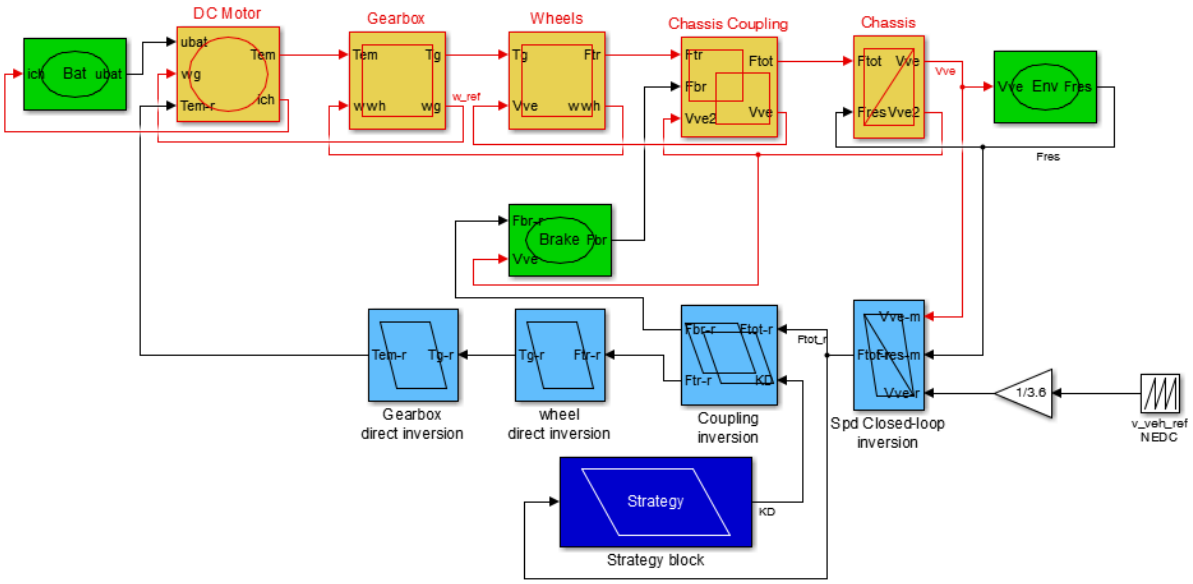

Figure 4.7 Simulink program of the EMR of the electric minibus simulation

Comparing the lead-acid batteries and the Li-ion batteries, the main differences which can be observed from the specifications are the capacity and the weight of the batteries. The total weight of lead-acid batteries is 1500 kg while it is 483 kg for the Li-ion batteries. This affects the weight of the vehicle which is an important variable in resistive force calculation. Consequently, the power required for the minibus to overcome such force and follow the velocity profile is higher in the case of lead-acid batteries as can be seen from Figure 4.8. Both batteries allow enough power and the minibus is able to follow the velocity reference very well. However, the maximal power required in the case of Li-ion batteries is reduced from around 12 kW in the case of Lead-acid batteries to around 10 kW. The machine torque and the discharging current are also greatly reduced. Moreover, the state of charge for one reduced-NEDC cycle (3km.) is reduced around 1.1% in the case of Li-ion batteries and around 1.9% in the case of Lead-acid batteries. This implies longer autonomy which would be beneficial in operating time. These results correspond to the results from previous studies [16][17]. Therefore, only Li-ion batteries will be considered in following sections.

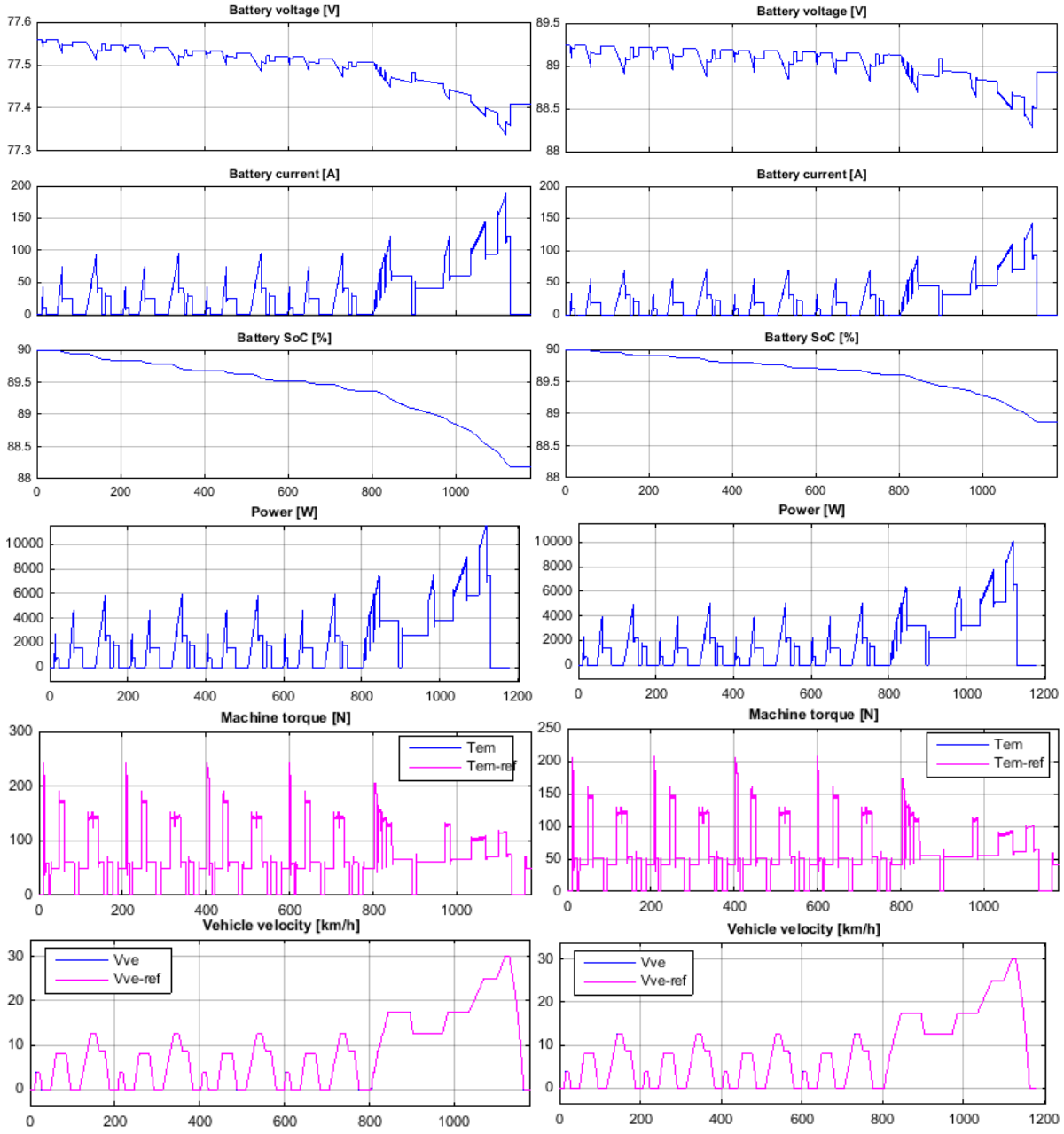

Figure 4.8 Simulation results of Lead-acid (left) and Li-ion batteries (right)

4.6 Real-time simulation and Signal HIL simulation of the electric minibus of Coimbra (Performed in Lille)

In addition to the developed EMR of the electric minibus of Coimbra, this section will extend the software simulation to real-time simulation and S-HIL simulation. This is an intermediate step or a bridge to continue to P-HIL simulation in the next chapter. This would ensure the compatibility of the developed Simulink program to be used for P-HIL simulation through a dSPACE platform.

4.6.1 Real-Time simulation

After the program was developed in MatLab Simulink software, the next step towards HIL simulation was to perform a real-time simulation of the system. This was to be carried out through a dSPACE controller board. The main objective of this step is to ensure that the developed model is able to run in real-time and that it is compatible with dSPACE which is the platform for HIL simulation. Connection between MatLab Simulink software and dSPACE MicroAutoBox hardware is through dSPACE ControlDesk software. Such software allows changing and observing variables in real-time through different virtual instrumentations. In order to do so, the model had to be transformed into discrete domain. Mainly, all the continuous integrators had to be replaced by discrete ones. There must be no algebraic loop in the program. After that, the model was built and .sdf file was linked to the dSPACE experiment.

For this system, the only main change required in the program was to add extra blocks to stop and start the simulation and the reference from velocity profile. Plotters were utilized to observe variables in a similar manner to scopes in Simulink program. However, since the simulation would take more time, only the case of interest (Li-ion batteries) was simulated. The step-time in this test was 1e-3 second. The results were similar to the ones obtained from Simulink. Therefore, they are not shown here. Nonetheless, this verifies validity of the simulation in real-time.

4.6.2 Signal HIL simulation

Although the objective of this project is the power HIL simulation, another intermediate step which could be implemented before going to power HIL simulation is the signal HIL simulation. This allows testing of control signals without risks from real power. In order to perform such simulation, the system was decoupled into the system part and the control part. The control was implemented in a dSPACE board. Then, another dSPACE board was used as an interface system. It connected the control in the main board with the system in the program. In this system, the vehicle velocity and the resistive force are the inputs to the main board. On the other hand, the machine torque reference and the braking force reference are the outputs of the main board. Figure 4.9 shows the Simulink implementation of the signal HIL simulation of the electric minibus of Coimbra. All the system parts are grouped inside the yellow block while all the controls are grouped inside the blue block. They are connected to sensor input and output blocks which are the inputs and outputs of dSPACE boards. These boards were connected together with external wires. In addition, there is a security block which allows starting and stopping the program. This block is more critical in power HIL since it would stop the system to avoid damage which could occur if some values exceed safety levels.

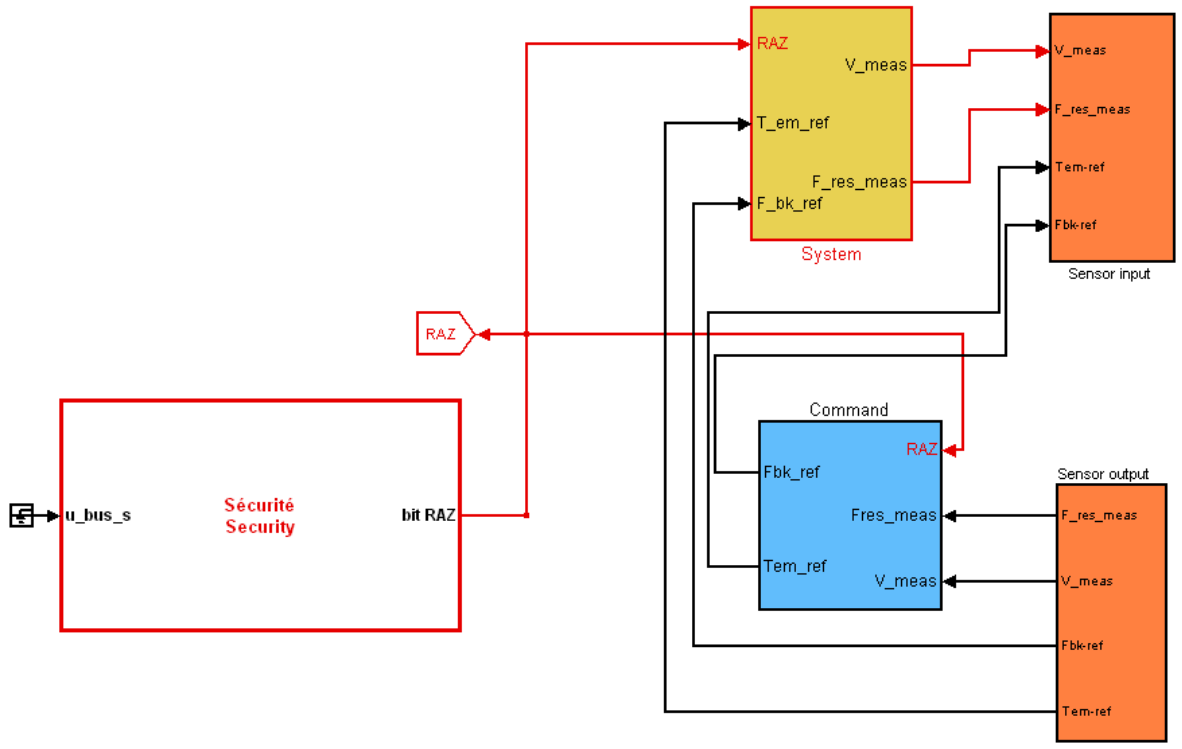

Figure 4.9 Simulink program for signal HIL simulation of electric minibus of Coimbra

After the Simulink program was built, it was implemented in dSPACE ControlDesk software, as previously stated. Figure 4.10 shows the ControlDesk screen of such developed program. The simulation can be controlled by buttons on the top left of the screen. In addition, there are a velocity gauge and several plotters to show results from the simulation. In this figure, the results from the simulation with NEDC reference are shown. The velocity reference and the measured velocity in km/h are shown in the upper left plotter. The middle left plotter shows the battery current, the lower left plotter shows the battery voltage, and the lower right plotter shows the battery SoC in %. Furthermore, the forces in N are shown in the upper right plotter. These include the transmission force, the braking force, and the resistive force. The electromechanical torque in Nm and the rotational speed in rad/s are shown in the middle right plotter. The results are observed to be similar to the results obtained from software simulation. However, some ripples and delays can be observed. In addition, it should be noted that this is the result from a refined version of the simulation. A low-pass filter was added to the voltage measurement output from the emulated board. This is feasible since real devices actually have dynamics with certain bandwidths.

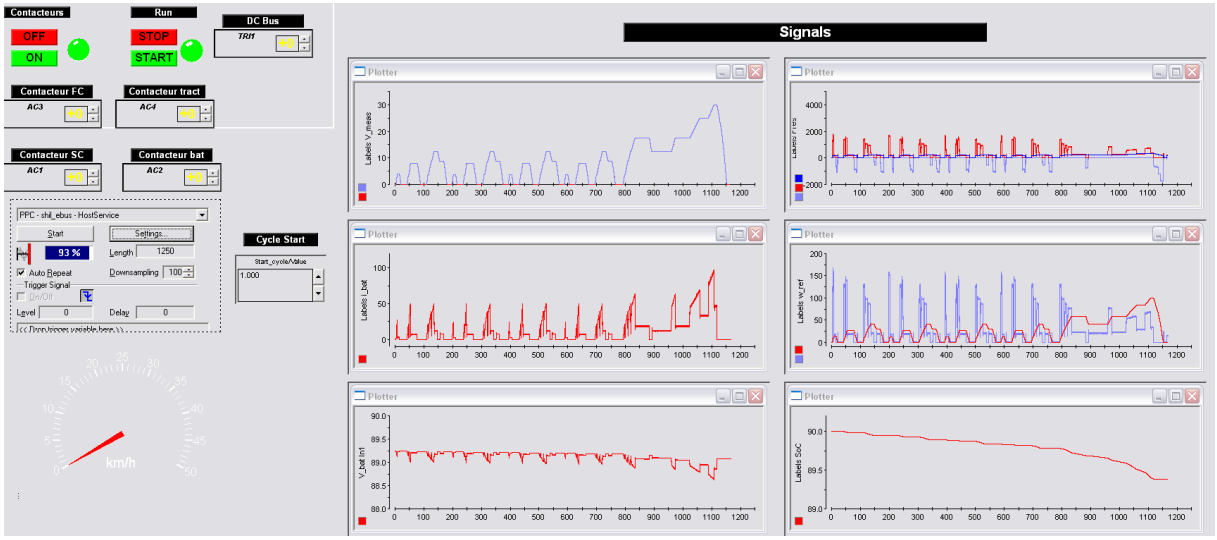

Figure 4.10 ControlDesk screen with results of S-HIL simulation of the electric minibus

Chapter 5 Power HIL Simulation Implementation through dSPACE

After the electric minibus was modelled and implemented into Simulink simulation using EMR method in the previous chapter, this chapter extends such concept into P-HIL simulation. This would allow studying with real physical conditions. The organization of such simulation is explained in the first part. The P-HIL was initially organized in full-scale. Nonetheless, the implementation in this study is in reduced-scale. A reduced-scale simulation is a valuable intermediate step to study a system with high capacity. It allows testing without risks of full power [9]. The setup in ISEC-IPC as explained in section 2.2 will be tested instead of the actual batteries and electric drive of the minibus. Several configurations were required in order to prepare the test bench for such simulation. These processes will be explained in this chapter. Finally, the simulation results will be provided with discussions.

5.1 EMR of P-HIL of the electric minibus of Coimbra

5.1.1 Organization of the HIL simulation

In order to test the system with new batteries and the electric drive, the system is split into two parts. The first part is the “Subsystem to test”. This is composed of the battery and the traction drive which are the real components in this system. The other part is the “Subsystem to emulate”. This is the part which is in software simulation. This part must impose proper interaction with the “Subsystem to test”. From the EMR previously developed, the variables between both parts are the torque T_{em} and the rotation speed Ω_g. Figure 5.1 shows the decomposition of the system into two parts.

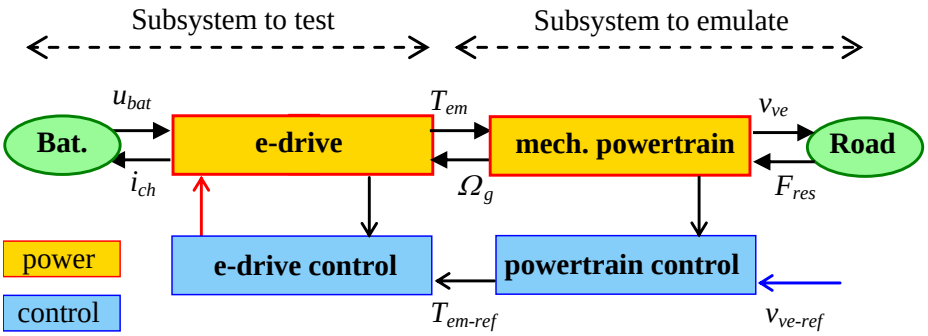

Figure 5.1 Electric minibus subsystem decomposition

In order to link the "Subsystem to test" which is hardware and the "Subsystem to emulate" which is software, an interface system is required to impose the right interactions between both parts. This interface must:

1) Accept torque as input,

2) Deliver rotational speed as output, and

3) Receive the rotational speed of the model as reference.

To fulfil these requirements, another electric drive with a speed control loop will be utilized as the interface. Figure 5.2 shows such HIL organization. Torque measurement will be taken from the real system. Then, counteract rotation speed of the machine will be calculated through the model. This speed will be given to the "Subsystem to emulate" as a reference so that the system can provide the interaction as if it is a real mechanical powertrain.

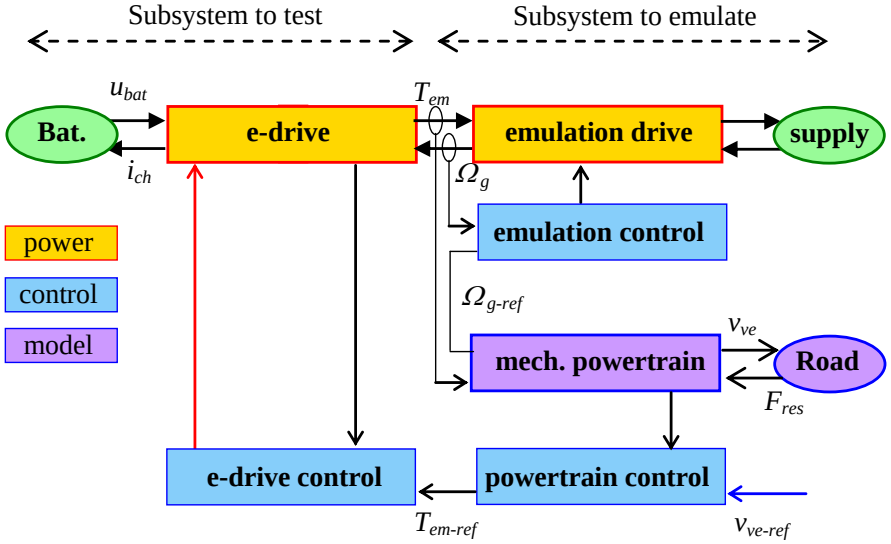

Figure 5.2 HIL organization

5.1.2 Full power HIL simulation

For the full power HIL simulation, the real batteries and DC machine and its

controller would be used. The emulation subsystem is the load drive. This is another machine with its inverter. The inverter is assumed to have a good control over the DC link voltage. Therefore, the DC bus has a constant voltage, V_{dc}:

$$V_{dc} = const. \tag{20}$$

Neglecting the dynamic of the machine in a similar manner to the traction drive, the torque, $T_L(t)$, is assumed to be instantaneously equal to the reference, $T_{L\text{-}ref}(t)$. The current imposed by the inverter, $i_L(t)$, can be calculated from the power equation with the efficiency of such drive, η_L:

$$\begin{cases} T_L(t) = T_{L-ref}(t) \\ i_L(t) = \dfrac{\eta_L^m T_L(t)\Omega_g(t)}{V_{dc}} \end{cases} \quad \text{with } m = \begin{cases} 1 & \text{if } P(t) > 0 \\ -1 & \text{if } P(t) < 0 \end{cases} \tag{21}$$

The traction drive shaft and the load drive shaft are coupled through a coupling which has one-to-one relationship. Combining the mechanical part of both machines, the relation between the torques of both drives can be expressed as a function of total machines inertia, J_{tot}, and total machines friction coefficient, f_{tot}:

$$T_{em}(t) - T_L(t) = J_{tot}\frac{d}{dt}\Omega_g(t) + f_{tot}\Omega_g(t) \quad \text{with } J_{tot} = J_{em} + J_L \text{ and } f_{tot} = f_{em} + f_L \tag{22}$$

where J_{em} is the traction machine inertia, J_L is the load machine inertia, f_{em} is the traction machine friction coefficient and f_L is the load machine friction coefficient.

From such a relationship, this machine can be controlled by a closed-loop speed controller, $C_j(t)$:

$$T_{L-ref}(t) = C_j(t)[\Omega_{g-ref}(t) - \Omega_{g-meas}(t)] + T_{em-meas}(t) \tag{23}$$

The EMR of the full power HIL simulation can be developed using the same principles as when developing the EMR for the electric minibus. The DC bus is represented by a source element since it marks the end of the study. The load drive is represented by a conversion element as it does not accumulate energy. Finally, the coupling is represented by an accumulation element. The EMR of the full power HIL simulation of the electric minibus of Coimbra is shown in Figure 5.3.

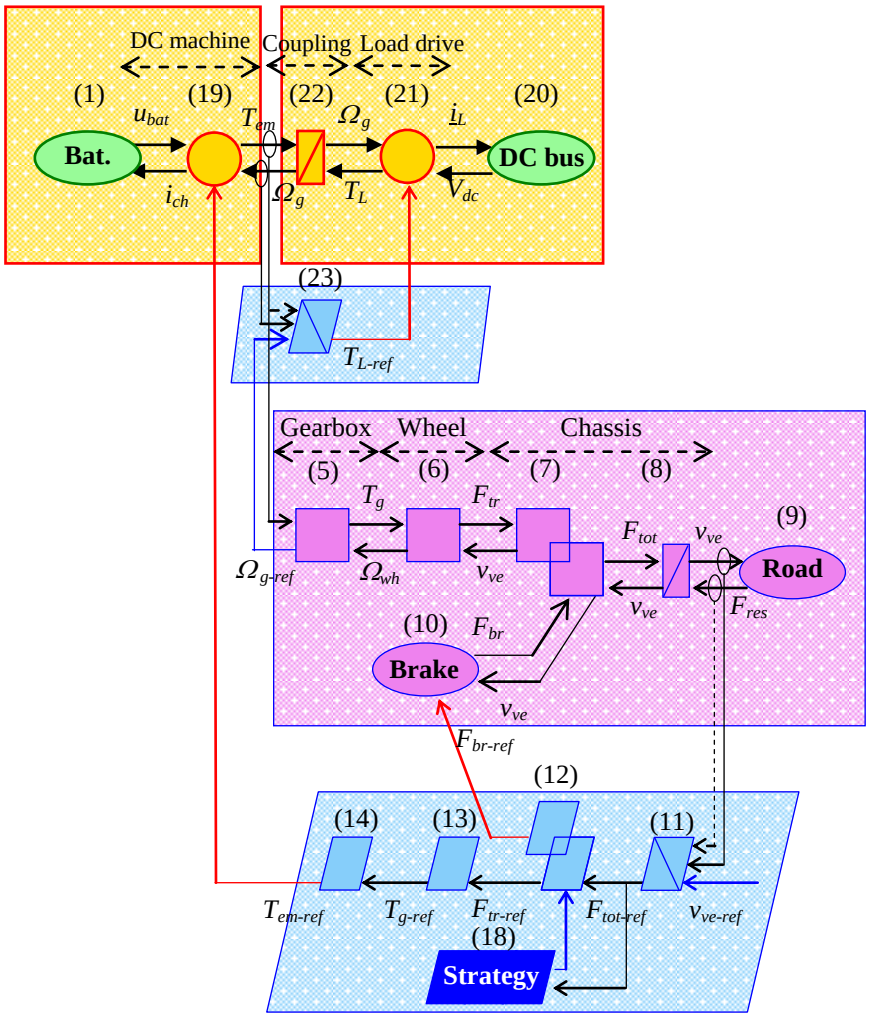

Figure 5.3 EMR of full-power HIL of the electric minibus of Coimbra

In addition, the load machine or the emulation machine must have greater capacity in order to cover the whole range. The power must be greater than 24.8 kW, the maximal torque must be greater than 14.9 Nm, and the speed greater than 4500 rpm. Moreover, in order for the speed control loop to impose the required speed, the control loop should be faster than the dynamics of the tested subsystems.

5.1.3 Reduced-scale HIL simulation organization

Before performing a full-power HIL simulation, a reduced-power simulation is a valuable intermediary step [2]-[4]. It allows testing without risks and issues of full power as well as to emulate systems that do not exist yet or where full power testing (e.g. in MW) is not feasible. From the available setup, a reduced-power HIL testing is considered. The HIL organization is modified by keeping the full-power model of the emulated subsystem. This implementation will allow:

1) Maintaining behavior of the system, including the non-linear behavior of the mechanical powertrain [3], and

2) Using the same model for both full-power and reduced-power HIL simulations.

The organization of the reduced-power HIL simulation is shown in Figure 5.4.

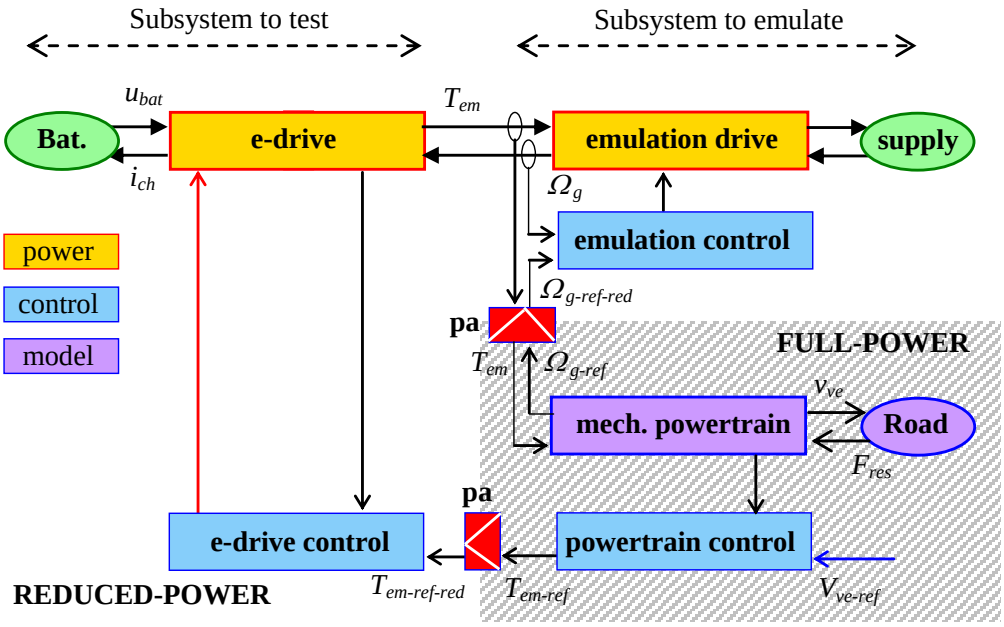

Figure 5.4 Reduced-power HIL organization

For such aim, power adaptation (pa) elements are added between the full-power part and the reduced-power part, using speed ratio k_Ω and torque ratio k_T:

$$\begin{cases} \Omega_{g-full} = k_\Omega \Omega_{g-red} \\ T_{em-full} = k_T T_{em-red} \end{cases} \tag{24}$$

$$T_{em-ref-full} = k_T T_{em-ref-red} \tag{25}$$

Subscription *–full* refers to full-power subsystems while subscription *–red* refers to reduced-power subsystems. These ratios are defined by the ratio of the maximal values of the full-power and the reduced-power subsystems. Table 5.1 shows the specifications of the full power subsystem and the test bench. The reduction ratios can be calculated using the flow chart shown in Figure 2.8 in section 2.1. A 5% safety margin is included in this calculation. The speed ratio was calculated to be k_Ω =0.24 and the power ratio was initially calculated to be k_p=3.73. This gave the torque ratio k_T =15.53. However, this did not fulfil the condition of $T_{Hmax}/0.95T_{Lmax} < k_T$. Therefore, the torque ratio was re-calculated to be k_T = 16.6 and the power ratio was calculated to be K_p=16.6*0.24=3.98.

Table 5.1 Full-power (Minibus) and reduced-power subsystem specifications

	Full-power simulation [16]	**Test bench [26]**	**Reduction ratio**
Power	24.8 kW	7 kW	3.98
Torque	235 Nm	14.9 Nm	16.6
Speed	1044 rpm	4500 rpm	0.24

The organization of such testing facility is complex and the EMR formalism is a valuable tool to propose a strict organization and interconnection of the different parts. The EMR of the reduced-scale power HIL simulation of the electric minibus of Coimbra is shown in Figure 5.5.

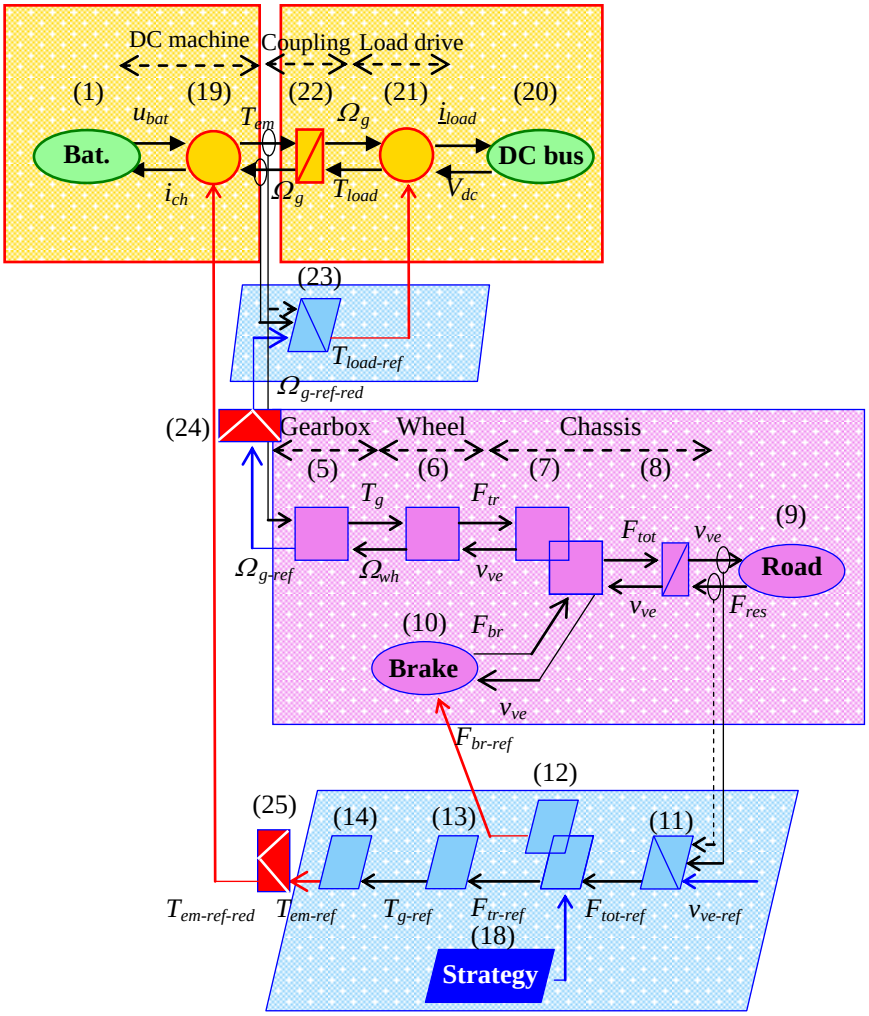

Figure 5.5 EMR of reduced-power HIL simulation of the electric minibus of Coimbra

5.1.4 Reduced-scale HIL software simulation

Before the actual HIL simulation, the system was tested through software implementation. The EMR of reduced-scale HIL simulation of the electric minibus of Coimbra in Figure 5.5 is implemented in Simulink program as shown in Figure 5.6.

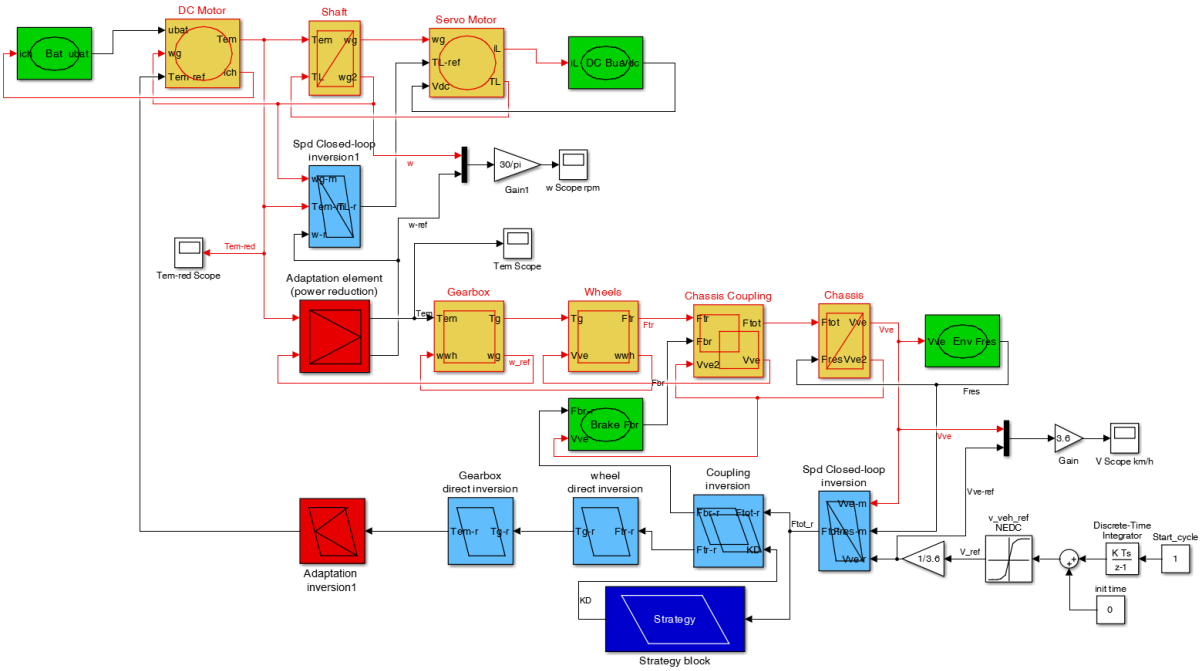

Figure 5.6 Simulink program of reduced-scale HIL simulation of the electric minibus

The results of the vehicle velocity, the machine rotational speed, the full torque, and the reduced torque are shown in Figure 5.7 (a) - (d), respectively. The vehicle velocity and machine speed references have the same shape but different value due to the wheel radius and the gearbox reduction ratio. The NEDC reference was reduced by a factor of ¼ to have the maximal velocity which corresponds to the minibus. As a result, the maximal velocity is 30 km/h and maximal reduced-power machine rotational speed is 4000 rpm. This speed is within the speed range of the machine. Moreover, the simulation is able to follow both references very well. On the other hand, the full-power maximal torque is around 140 Nm while the reduced-power maximal torque is around 8 Nm. Both maximal values are within the limit of the machines. These verify the organization of this HIL simulation.

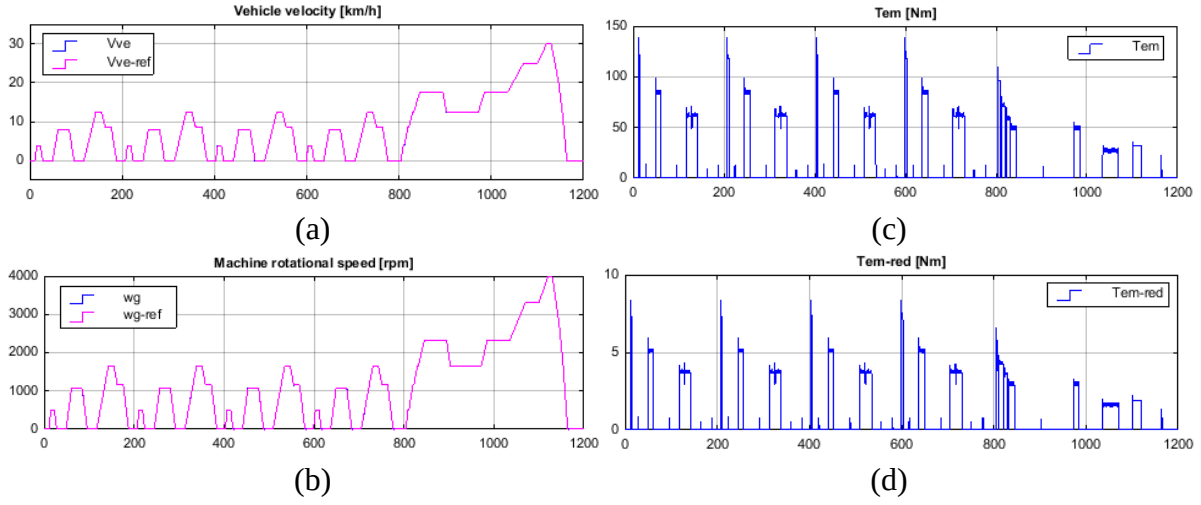

Figure 5.7 (a) Velocity, (b) speed, (c) full torque, and (d) reduced torque results of the reduced-scale P-HIL software simulation of the electric minibus using NEDC reference

5.2 Test bench preparation for P-HIL implementation

In order to perform a power HIL simulation, the dSPACE MicroAutoBox must be able to send commands to the controllers and receive measurements from the machines. Analog signals are used to deliver the commands and CANopen protocol is used to deliver the measurements. Before implementing the simulation of the minibus, the configurations were verified through several tests in order to ensure that the setup was ready to perform the final P-HIL simulation. In the first stage, analog signals and CANopen protocol were tested. Then, they were implemented to control each actual drive separately.

5.2.1 Analog signals tests

In order to use analog signals as references for the machines, first, programs were developed to test the analog signals from dSPACE. This includes:

1) Analog output test

In this test, analog signal was given through the output of the MicroAutoBox. Then, the output voltage was measured using a multimeter. The reference given in the ControlDesk screen was compared with the value read through the multimeter to verify the program.

2) Analog output and input test

In this test, after ensuring that the output signal given in the program corresponds to actual output, analog input was tested. The objective was to utilize the input and to be able to monitor the output values through ControlDesk screen in real-time. The analog input and output wires were connected together. Then, the values of reference voltage on the screen and the value read from analog input were compared.

In order to develop the programs, it is essential to do signal scaling. From the datasheets, the analog input and output voltage ranges are as shown in Table 5.2. As can be seen from the table, the dSPACE I/O (Input/Output) voltage ranges and the Simulink DAC (Digital-to-Analog converter) and ADC (Analog-to-Digital Converter) I/O ranges are not the same. Therefore, gains are required before the DAC block and after the ADC block in order to obtain proper voltage level.

Table 5.2 Analog inputs and outputs voltage ranges

	dSPACE I/O Voltage range [27]	**Simulink DAC and ADC I/O range [28]**	**Gain**
DS1511 Analog outputs	0…4.5 V	0…1 V	1/4.5
DS1511 Analog inputs	0…5V	0…1 V	5

Figure 5.8 shows the developed Simulink program. The program mainly consists of the input part and the output part. The upper part is the output part. DAC_Output constant block is used to specify the output level. This can be changed through an instrument in

ControlDesk. A gain is added as previously stated. Then, a DAC block is used to convert digital signal to analog signal. This block comes from rti library which depends on the dSPACE unit. It must be configured to specify the module and channel in which the signal will be outputted from. On the other hand, the input part is in the bottom of the program. This consists of an ADC block which is also from rti library, a gain, and a scope. The scope is used to monitor the variables of interest. These variables can be shown in various instruments in ControlDesk.

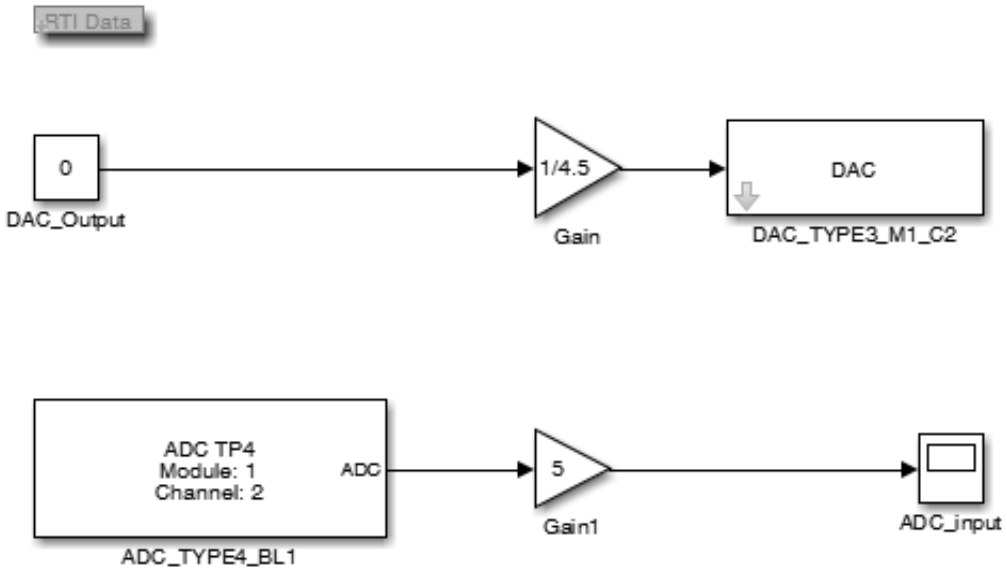

Figure 5.8 Simulink program for the analog I/O test

After the program was developed in Simulink, it was built and a .sdf file was obtained. After that, the file was used for dSPACE ControlDesk experiment. The layout of ControlDesk experiment is shown in Figure 5.10. The ADC_output is linked to the slider and the numerical input. It is also shown in the plotter along with the DAC_input which is taken from the scope. The latter is also shown in the indicator.

As a result, the measurements obtained are:

1) Analog output test

Using the slider in ControlDesk to vary the voltage reference, similar measurements can be observed through a multimeter. Figure 5.9 shows an example of the measurement when the reference in ControlDesk is set to 2V. Slightly lower output comparing to reference value can be observed. However, this different is relatively small. The used multimeter is not calibrated so it might also have some measurement errors. This verifies that the program is able to give required output voltage level.

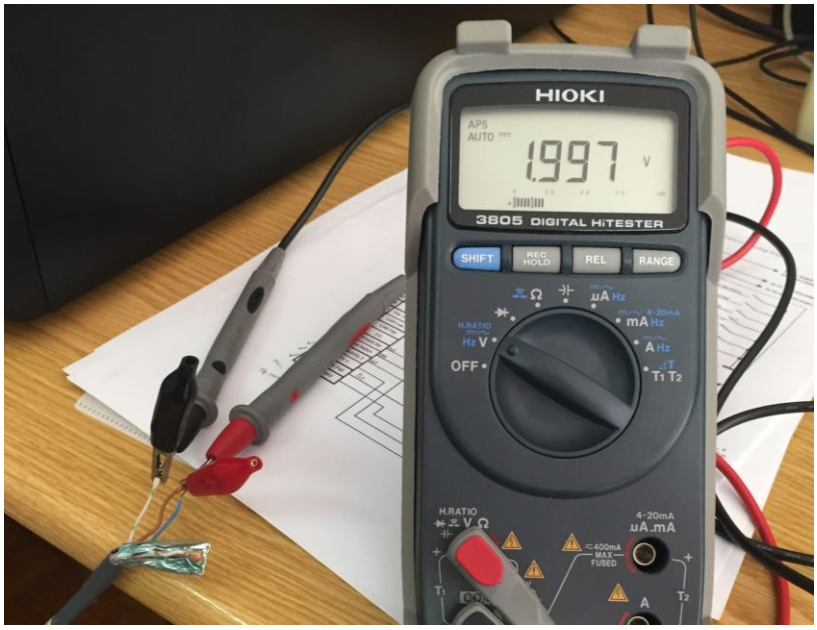

Figure 5.9 The multimeter measurement with 2V reference in the analog output test

2) Analog input and output test

After the output was verified, the output and input wires were connected together. Consequently, the analog input was able to show a value similar to the value of the analog output. Figure 5.10 shows the screen of ControlDesk for analog output and input test. Several points can be noted from this figure. The plotter on the right shows the analog output signal from Simulink in green and the analog input signal read in Simulink in red with respect to the time in second (in x-axis). It can be seen that both lines overlap. This shows that the Simulink program and dSPACE implementation can be used to give good analog output signal. However, once reached 4.5 V, the input read was 4.5 V even though the signal from Simulink was increased further. This is because, as previously stated, that the maximum output of the dSPACE analog output is 4.5 V. Therefore, although output signal sent was above 4.5 V, the output was limited to 4.5 V. In addition, observing the values from the indicator on the left, some deviation can be observed as the ADC input reading is slightly lower than 4.5V. Nonetheless, this deviation is comparatively low.

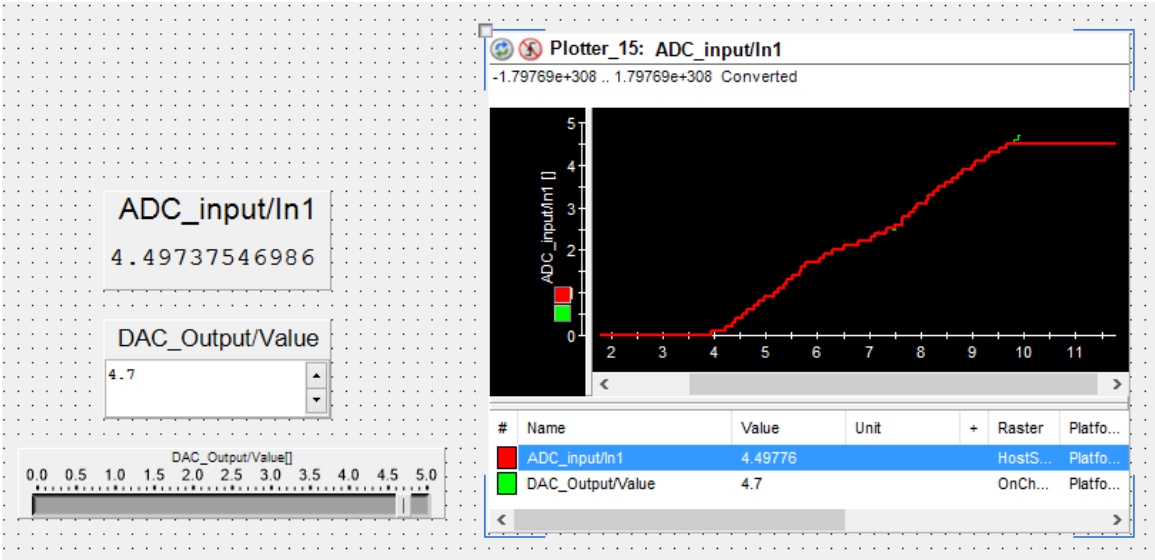

Figure 5.10 ControlDesk screen for the analog input and output test

5.2.2 CANopen test

CANopen protocol is a communication protocol which is based on CAN system. It comprises higher-layer protocols and device profile specifications [29]. It provides greater standardization and interoperability between devices [21]. The most important part of CANopen is the Object Dictionary (OD). Device setup, configuration, and diagnostics are done by reading and writing values in its object dictionary. The CANopen communication objects allow transferring of information. The protocols comprise of SDO (Service Data Object) protocol, PDO (Process Data Object) protocol, NMT (network management) protocol, Special function protocols, and Error control protocols.

The main communication objects are the SDO and the PDO. SDOs are typically used for device configuration while PDOs are used for exchanging of information in real time. In this study, all the configurations will be done through DVT software which is the software provided by the SEVCON manufacturer. Therefore, direct accessing of SDOs are not necessary and only PDOs configurations are of interest. PDOs allow transferring the data of the object dictionary. These data are specified by their index and sub-index. Table 5.3 summarizes the index, sub-index, and other characteristics of variables of interest in this study from the object dictionary of SEVCON.

These variables are accessed through TPDOs (Transmit Process Data Objects). DVT software was used to select the variables to be mapped through TPDOs. SEVCON allows five TPDOs. Each TPDO has 8 bytes or 64 bits. TPDOs and RPDOs (Receive Process Data Objects) can be set through DVT by going to “DVT Helper” which is the tool to “Manipulate settings via GUI” then select “TPDO/RPDO” tab. After that, the user can click “Setup TPDO” to configure each TPDO as shown in Figure 5.11.

Table 5.3 Characteristics of variables of interest from the object dictionary of SEVCON

Index	Sub-Index	Scaling	Units	Name	Data Type
2220h	2	1/256	V	Throttle Input Voltage	Integer16
4600h	5	1/8	A	Target Id	Integer16
4600h	6	1/8	A	Target Iq	Integer16
4600h	7	1/8	A	Id	Integer16
4600h	8	1/8	A	Iq	Integer16
4600h	9	1/8	V	Ud	Integer16
4600h	10	1/8	V	Uq	Integer16
4600h	11	100/255	%	Voltage modulation	Integer16
4602h	18	1/8	V	Capacitor Voltage	Unsigned16
4600h	12	1	A	Actual AC Motor Current	Integer16
4600h	13	1/8	V	Actual AC Motor Voltage	Integer16
4602h	11	1/8	Nm	Torque demand value	Integer16
4602h	12	1/8	Nm	Torque actual value	Integer16
4602h	17	1/8	V	Battery Voltage	Unsigned16
4602h	29	1/2^24	Henry	Measured inductance	Integer16
5100h	2	1/8	A	Battery Current	Integer16
606ch	0	-	rpm	Speed	Integer32
60ffh	0	-	rpm	Target speed	Integer32

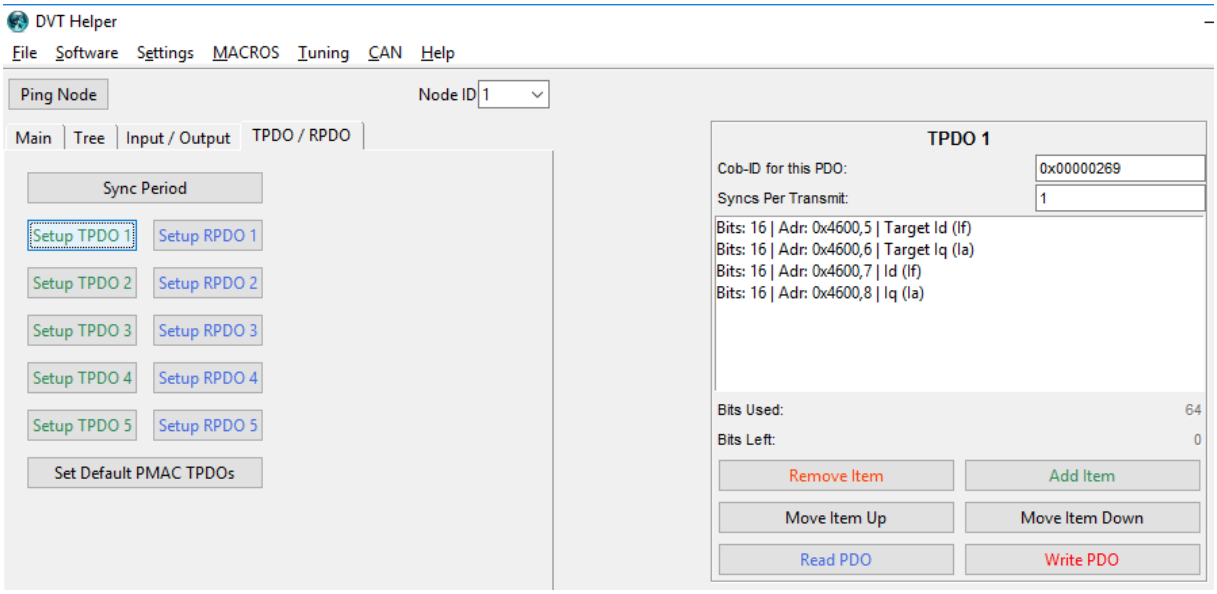

Figure 5.11 DVT interface for setting up messages in TPDOs

This must be set in pre-operational operating mode. The operation mode can be selected in “Main” tab. Then, the setup must be transferred to the controller through “Write PDO” button. In the main DVT screen, index number and “ok” messages will appear

if the variable is successfully mapped or “abort” message will appear if it is not successfully mapped. This can also be check by clicking “Read PDO” afterward. “Read PDO” will download the setup from the drive. Some variables in the object dictionary have restrictions and cannot be mapped. Therefore, the user should always check if the variable is successfully mapped or not before proceeding to another step.

Furthermore, another important part of CAN protocol is the message ID. Since CAN is a multi-messages bus, message identifier is used to identify which message is of interest for each node. In the case of CANopen, this identifier is referred to as a COB-ID (Communication Object Identifier). In order to receive the correct message, the receiver and the transmitter must have the same identifier. In this study, the measurements from SEVCON are received by the dSPACE through the CAN communication. Therefore, the COB-ID specified in DVT as can be seen on the top right field of Figure 5.11 will be used in setting up CAN receiver in dSPACE. COB-IDs of all TPDOs of SEVCON are specified in Table 5.4. As part of CANopen conditions, each TPDO must have a different COB-ID. Moreover, another parameter which has to be check is the sync period. This tells the period in which the information will be synchronized between the controller and the PC.

Table 5.4 COB-ID of SEVCON TPDOs

TPDO no.	**COB-ID**
TPDO 1	0x00000269
TPDO 2	0x00000369
TPDO 3	0x00000155
TPDO 4	0x00000172
TPDO 5	0x00000141

After variables of interest were configured in DVT, Simulink program was developed accordingly. “RTICAN controller setup” block was required in order to specify general information about the CAN node. This block can be found from dSPACE RTI CAN library. Then, “RTICAN Receive (RX) message” blocks were used to receive CAN messages. COB-ID and sync time must be specified for each block in order to receive the messages. In addition, since one message can contain different information, the user can specify these data by indicating the name of the data, the starting bit, and the length of the data, as well as the type of the data. For instance, in TPDO1, the first part of the message is the target d-axis current which starts at bit 0 and is 16 bits long. Depending on the data, gains may be needed to scale the data into actual value. This gain is given by the scaling in Table 5.3. Simulink program for CANopen test is shown in Figure 5.12.

In addition, there are sender status detection blocks. This block was adopted from CAN rti example. The purpose of this block is to check reception of the system. If no message is received for 6 consecutive execution steps or the message is not received within expected time for 6 consecutive times, the sender will be considered in trouble and the 'RX Warn' output will be set to 1.

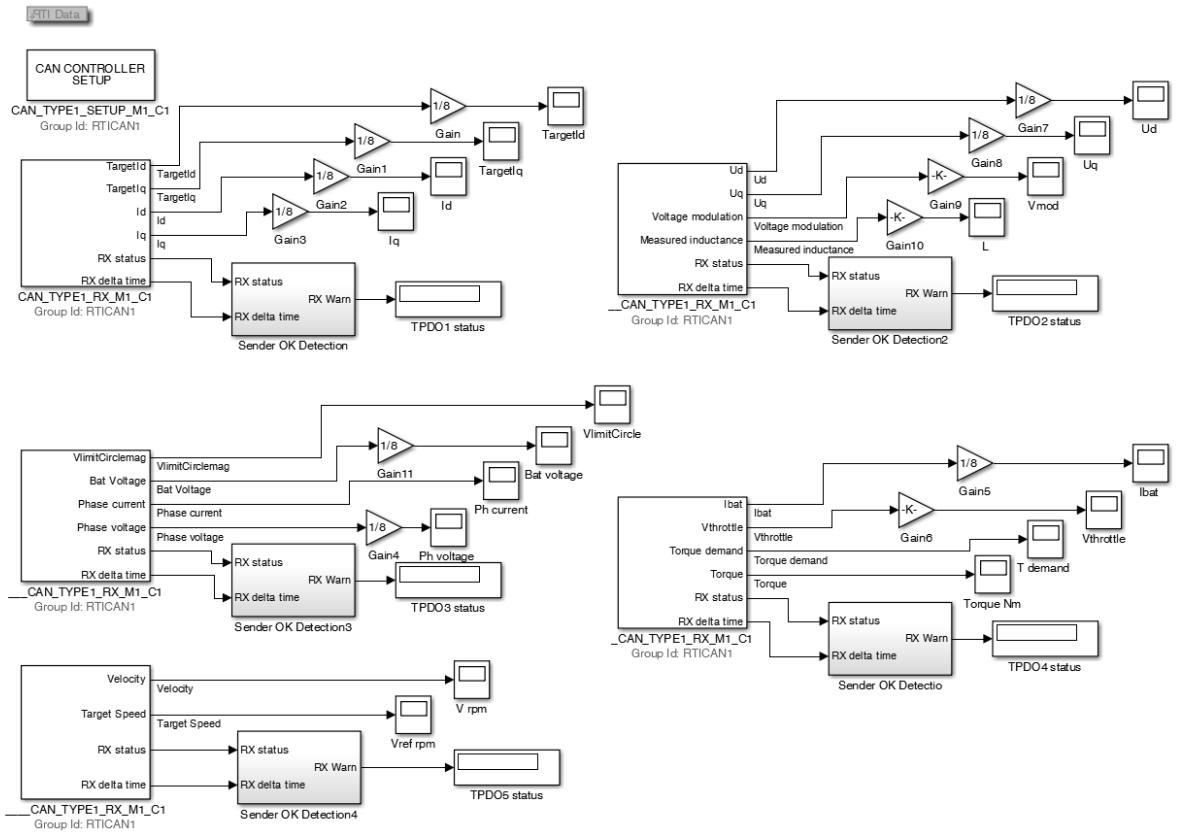

Figure 5.12 Simulink program for CANopen test

After that, the program was built and linked to a ControlDesk experiment. Several variables were put to plotters to observe and compare with data from DVT “Vehicle Interface” window as shown in Figure 5.13. Although some delays can be observed, the data are in the same range. The data is also observed with respect to the real value. For instance, no torque reference is given to the machine. Therefore, there should be no current from the battery. In addition, the voltage of the machine and battery is 80V and the capacitance voltage corresponds to that number. This verifies the ability of the program to take measurements of the machine through CAN bus.

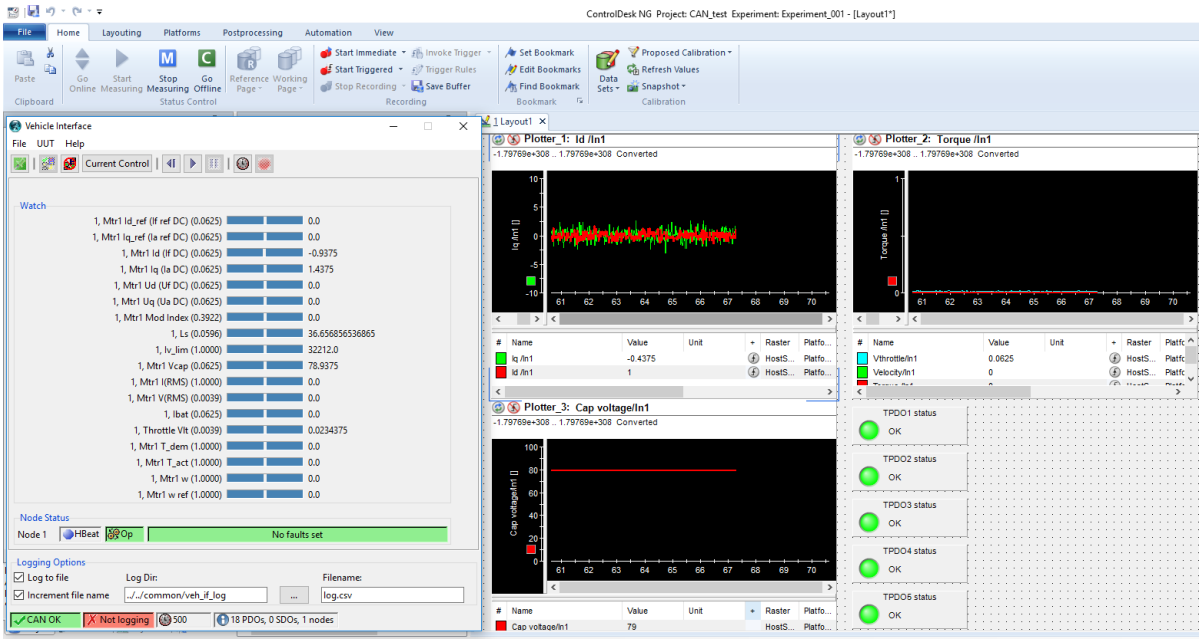

Figure 5.13 ControlDesk and DVT vehicle interface screen for CAN testing

5.2.3 Separate drive control tests

Before putting the machines to operate together, the machines were tested separately to ensure that they both operate well and provide desirable output, corresponding to the given reference. First, the drives were tested using manual analog signals as references. Then, they were tested with a driving cycle reference to see their ability to provide required torque to follow the speed reference.

According to the EMR of the HIL shown in Figure 5.5, torque control is required for the traction drive and speed control is required by the load drive. However, the speed control of the load drive is performed through Simulink implementation. The load drive will also receive torque reference. Therefore, both drives must operate in torque mode. The load drive was already operated in torque operation. Therefore, no additional configuration was needed. However, the traction drive was initially configured in speed mode. Therefore, some extra parameters had to be configured in order to operate in torque mode.

1) Analog reference test

Analog reference signals were given to the machine through a slider in ControlDesk. However, before being able to do so, some configuration had to be done to the drives. For the traction drive, from the user manual, pin 22 of the connector is the analog input1 pin. It is specified that this pin is suitable for potentiometers in the range 500 Ω to 10 kΩ, or voltage-output device of 0 to 5 V or 0 to 10 V [21]. However, the range of the analog input can be further configured in the DVT software in the “Throttle setup” in “Tree” of “DVT Helper” as shown in Figure 5.14. In this case, the end voltage is set to 4.5 V to correspond to maximum analog output of the MicroAutoBox. It should also be noted that the start voltage is set to 0.1 V to avoid effects of noises. However, due to limitation of the program, read back values are slightly lower than set values.

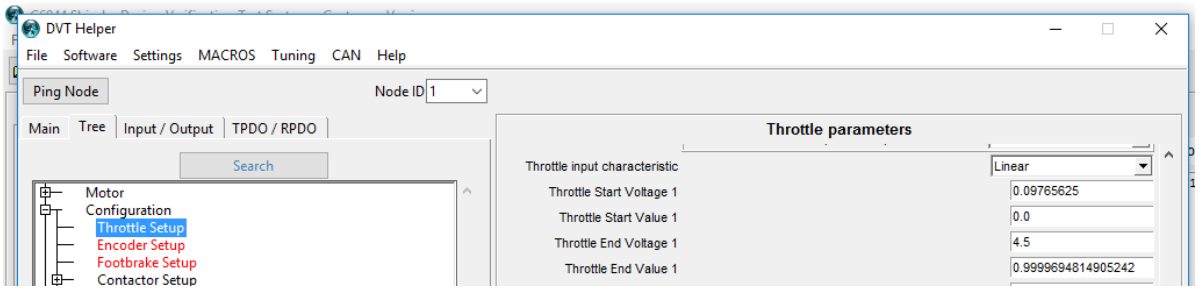

Figure 5.14 Throttle setup through DVT software

For the load drive, analog output 2 of dSPACE is connected to terminal X11:2 of SEW VFD while the ground is connected to terminal X11:4. Analog input 2 is also connected to terminal X11:2 to be able to measure the analog signal in real time for purpose of fault detection. Then, the configuration was done through MOVIDRIVE MOVITOOLS software which is the software from the SEW manufacturer. Parameters of interest can be set and monitor through “Parameter tree”. In order to have the machine run with analog input, the setpoint source was configured to UNIPOL./FIX.SETPR [30]. This allows the machine to receive setpoint from analog inputs or internal fixed setpoints. Being unipolar, the negative analog setpoints are interpreted as zero and the direction of rotation is specified by control signal. Additional specifications such as the input scaling or offset can also be set. This can be done through P11X parameters.

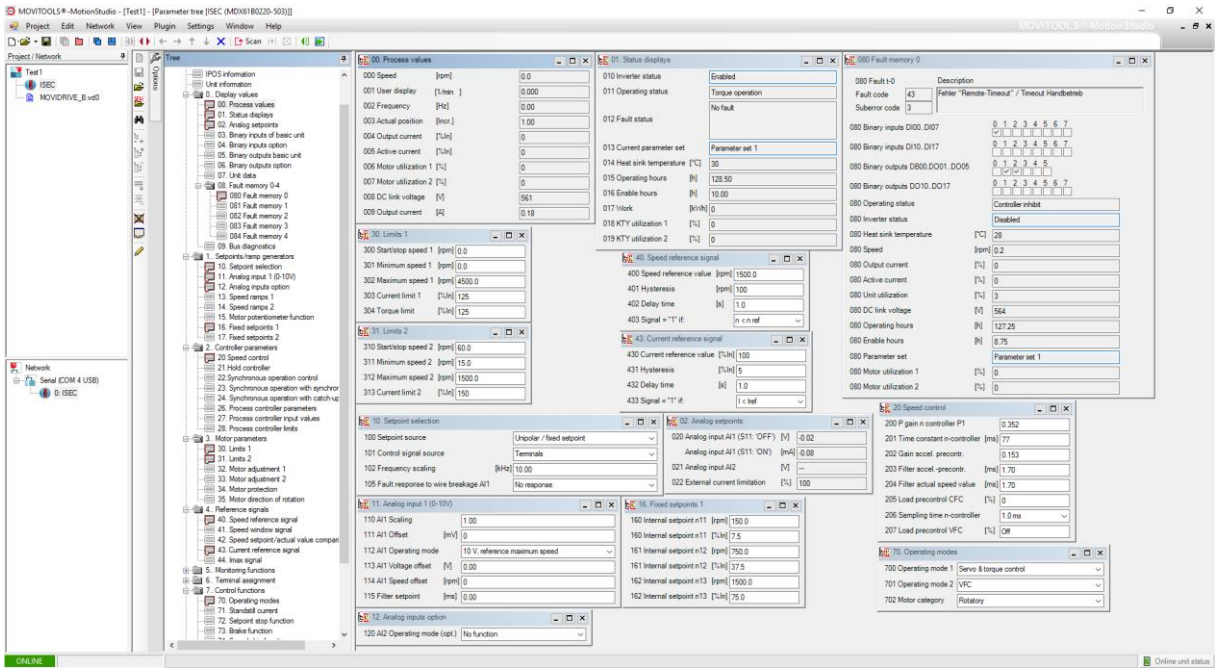

Figure 5.15 MOVITOOLS software configuration for analog input

Once the wires were connected and the configurations via manufacturer software were done, preliminary tests can be performed. These were performed separately for each drive. The program from the analog output and input test can be applied. The blocks must be set to channel 1 for the traction drive test and channel 2 for the load drive test. In these tests, the analog output of dSPACE was slowly increased from zero. This must be done with care

to avoid risk of damaging the drives from too high reference. The reference was increased until the motor starts to move and it was increased further to see if the speed increases. These can be done by visual observation, listening to the sound of the motor, and/or through indications in manufacturer software.

The results of both drives were satisfying. After applying some torque reference, the drives were able to move and the speed increased as the slider was moved to higher value. These verified the ability of the analog output signals of dSPACE to operate the drives.

After that, specific Simulink programs were developed to further verify the configuration for the purpose of the control. As previously mentioned, torque control is required for the traction drive. The desirable output would be to have the machine torque following the torque reference perfectly without delay. In order to test the torque response of the drive, a Simulink program was developed to provide different torque reference to the machine. The developed Simulink program is shown in Figure 5.16.

In this program, both analog signals and CAN protocol are implemented together. Measurements inputs are taken through CAN protocol inside “CAN monitoring” block. Then, these measurements are given to the “Security” block which serves as a protection system. These include two protections. First, the system will only provide outputs if enable signal is set as “on”. Furthermore, if there is any measurement which exceeds the safety limit, the output will be set to zero. This logic is done through the switch. Then, for the reference of this test, there are two types of reference, selectable through a switch. The first reference is a constant setpoint. This reference is given through “Tref” block which is changeable through ControlDesk. The other type of reference is a ramp reference. This reference would allow observing ability of the drive to follow increasing reference instead of a fixed setpoint. Furthermore, it would allow observing the machine torque response to different levels of torque reference. If there is a fault or no “on” signal, the enable bit will not be zero and the reference will be changed to zero to stop the drive. Gain blocks of “1/17.8” are added to scale the reference torque in Nm to a value between 0 and 1 which corresponds to the output of Simulink. The gain of 17.8 corresponds to the stall torque of the machine which was configured as the peak torque of the machine in DVT software. Moreover, 0.05 V are added to the final voltage in order to compensate for the threshold voltage which was set in DVT software. This voltage is only added when there is an enable signal.

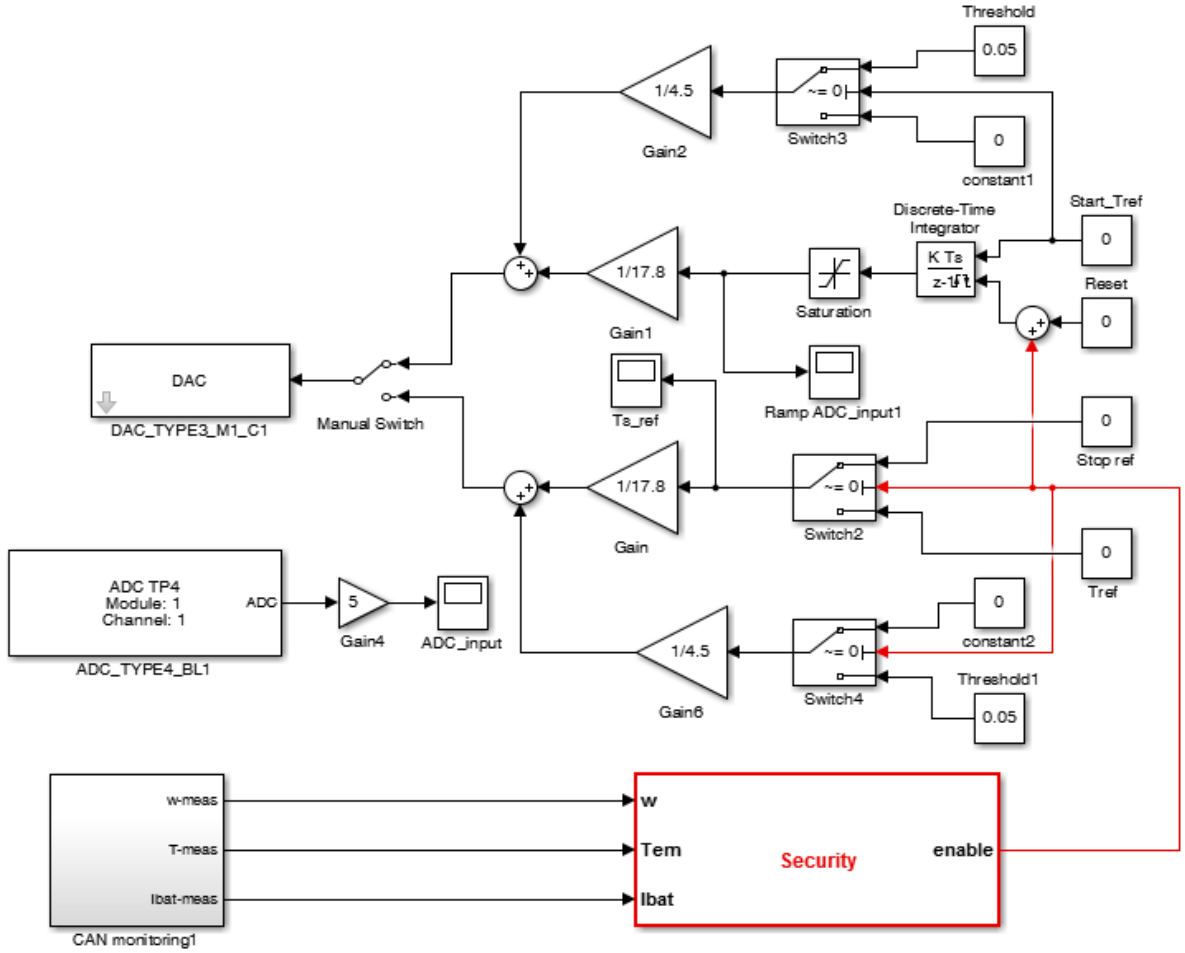

Figure 5.16 Simulink program for the traction drive, analog reference test

The results of analog reference tests with step setpoint and ramp reference are shown in Figure 5.17 and Figure 5.18, respectively. For the step setpoint test, the system was turned on at t = 1 s. Consequently, higher throttle voltage level (dark blue line) can be observed. This is due to the threshold voltage which was added. In addition, the setpoint was set to 1.5 Nm at t = 6 s. The machine torque was able to follow the torque demand with very small delay. However, a small error between the actual torque and the torque demand can be observed as the green line on the upper plotter is slightly lower than the red line. Some ripples can also be observed. Furthermore, the speed rises as a result of the machine torque.

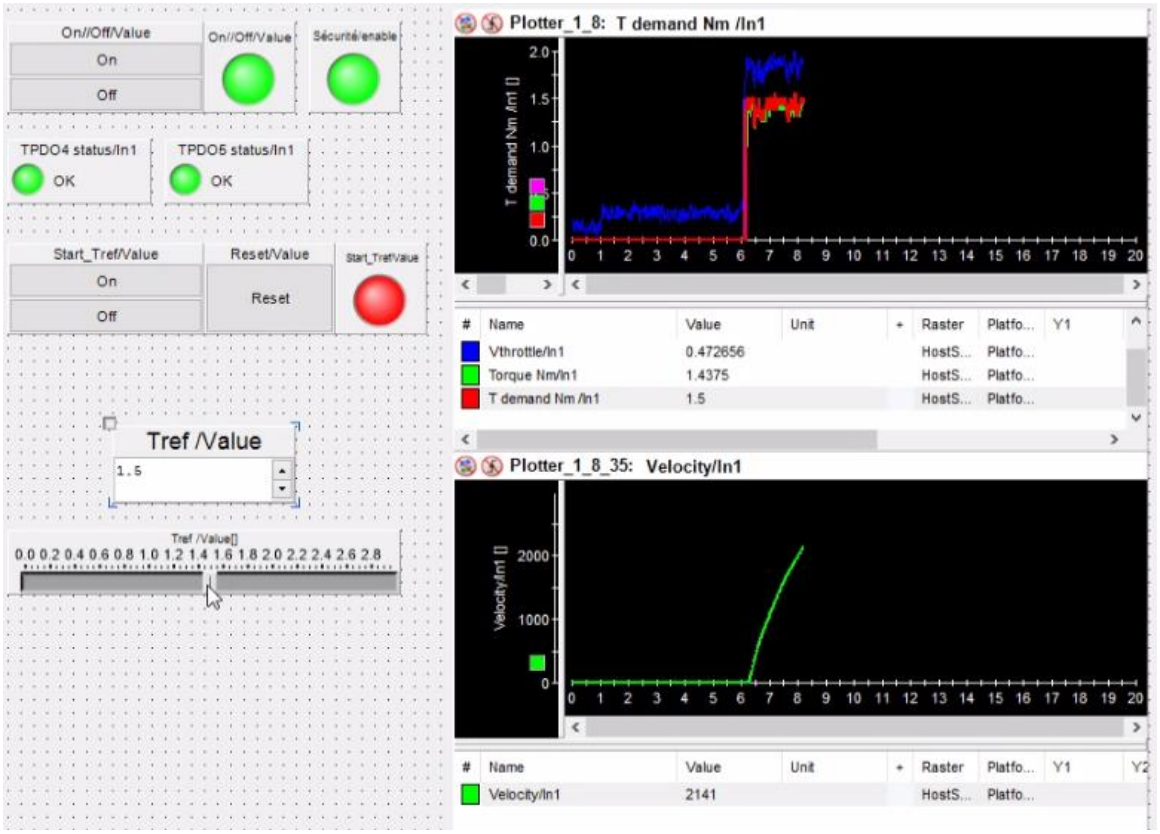

Figure 5.17 ControlDesk screen for the traction drive, analog reference test

For the test with a ramp reference, several points can be noticed. First, the torque was able to follow the torque demand quite well with some error as seen from the case of constant setpoint. However, the torque reference from the program and the torque demand of the machine are not the same. This is suspected to be due to the noise in the analog channel and the threshold voltage. As a result, there are some error between torque reference in the program and the torque demand and torque measurement in the machine. In addition, comparing the torque and the speed plots, it can be seen that some torque was required to overcome the static friction. This corresponds to around 1 Nm in order for the machine to start its rotation. Furthermore, once the machine reaches maximal speed, large torque ripple appears. Ripples in the speed can also be observed. This is because the drive had reached the maximal configured speed. SEVCON controller limits the maximal speed of the machine to such value. It should be noted that the machine must be set to have speed limit at maximal speed (in DVT). If the machine is set to have speed limit depending on the throttle opening, the torque will be limited once the speed reached a certain level. In such case, the torque might not be able to reach the demand. This would also result in ripple in the speed as can be seen when the speed reaches maximal value.

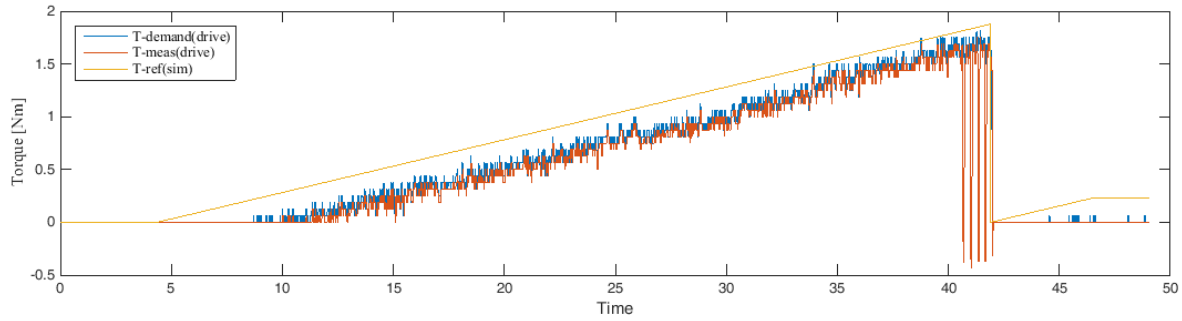

(a)

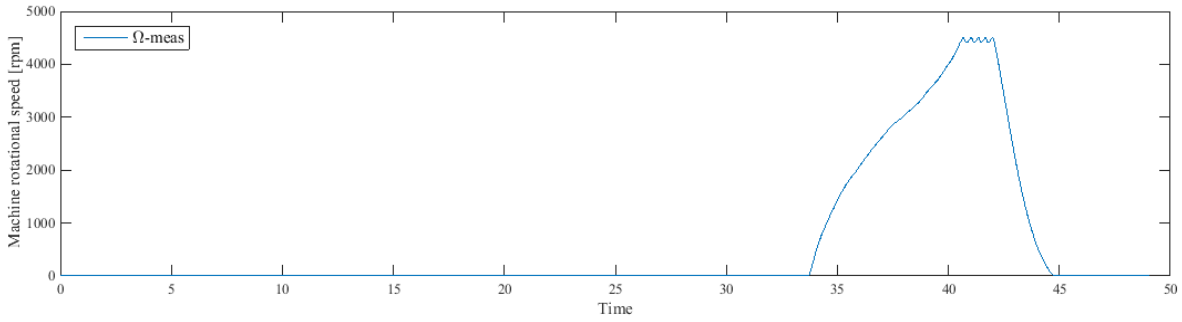

(b)

Figure 5.18 (a) Torque and (b) speed response of the traction drive, analog reference test

For the load drive, a driving cycle reference with a speed control through Simulink was applied. The ECE driving cycle was applied instead of the full NEDC which would take much longer to complete each experiment. Figure 5.19 shows the Simulink program for the load drive, ECE reference test. The speed control is implemented in the blue "Control of Emulator" block. Since only one motor is under operation in this test, the disturbance torque from PMSM, T_{em}, is set to zero. In order to assure this condition, the maximal torque of the traction machine in DVT software must be set to zero to avoid the traction drive generating braking torque to counteract the torque from the load machine. Furthermore, since the driving cycle provides reference as a velocity of the vehicle, gains have to be added in order to obtain machine rotational speed reference. For the controller, a classical PI with an anti-wind up integrator structure is utilized. One important thing that should be noted is that the speed measurement from CANopen is in rpm. Therefore, a gain is required to convert it to rad/s. These are implemented inside "reference" block. Moreover, an integrator of a constant is implemented in order to start the driving cycle reference when desired to. This can be done by changing the value of such constant by a switch in ControlDesk.

For the measurements, similar approach as previous test was applied to the load drive. However, since the measurements are taken from the traction controller, the variable which is used for protection is the speed since it is the only shared variable. It must be noted that "-1" gain is required since the load machine spins in the opposite direction. Therefore, the speed measurement from the traction drive is in negative value. Furthermore, the enable bit is also given to other block to reset the integrator when error occurs.

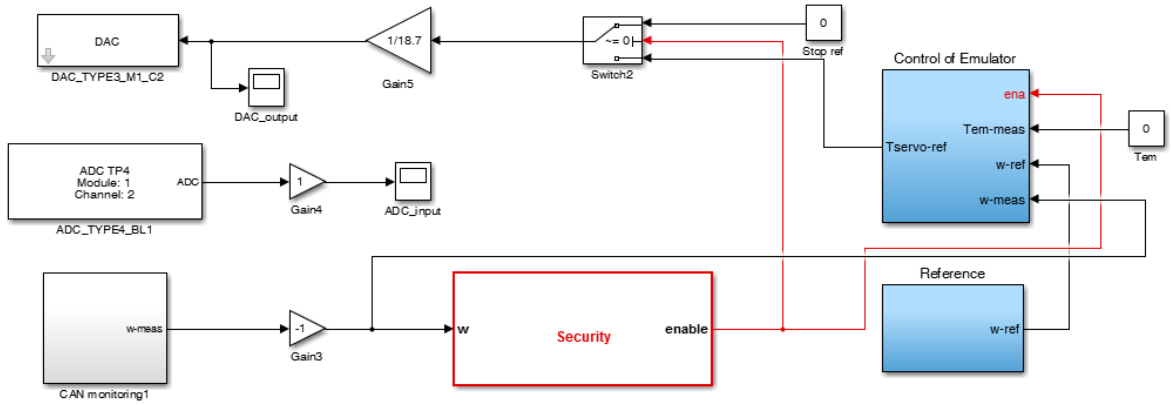

Figure 5.19 Simulink program for the load drive, ECE reference test

Figure 5.20 shows the ControlDesk screen with comparison to MOVITOOLS screen for the load drive, ECE reference test in the beginning of the driving cycle. Although the torque of the machine is not explicitly shown in MOVITOOLS, the ability to follow the torque reference of the machine can be observed through the output current. From the figure, the output current is 2% of the nominal current. Considering that the current is proportional to the torque, this would mean that the torque is 0.02*18.7 Nm =0.374 Nm which is close to 0.347 reference. It should be noted that the percentage is only shown as an integer (with no decimal point). This could be the source of the error. In addition, the measured and reference machine rotational speed, and the reference torque of the full ECE cycle are shown in Figure 5.21. It can be seen that the speed follows the reference very well. However, there are several points which can be observed, especially from the torque plot. First, there are ripples in the results. This could be overcome by better tuning the controller. Secondly, there are small spikes at the beginning of each cycle. This can be explained by the fact that the machine requires a certain torque in order to overcome the static friction. However, once the machine starts to move, this torque becomes in excess and result in a spike. The response can be improved by setting small torque to be applied as soon as speed reference is given. This torque is the torque to overcome the friction or the torque required to achieve initial movement [21]. Tuning the controller of having low speed gains should also help obtaining better response. Finally, the torque does not return to zero at the end of each cycle. This can also be explained by the reason similar to the first observation. Since the machine has some friction, lower amount of torque can be applied without rotor movement.

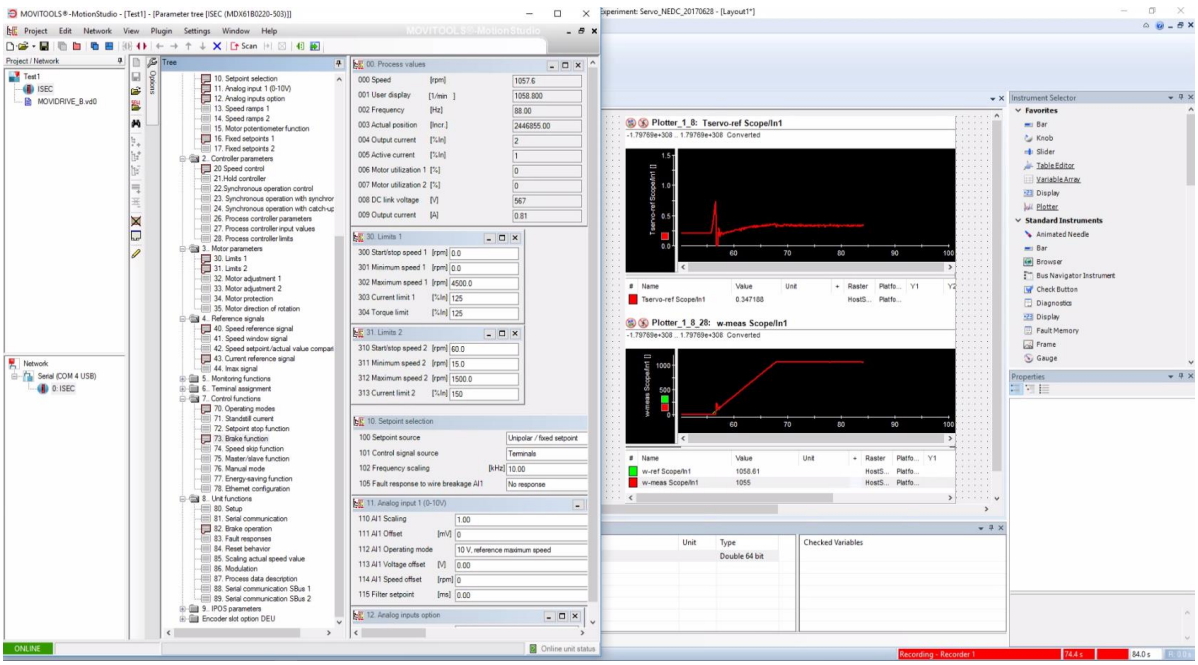

Figure 5.20 ControlDesk and MOVITOOLS screen for the load drive, ECE test

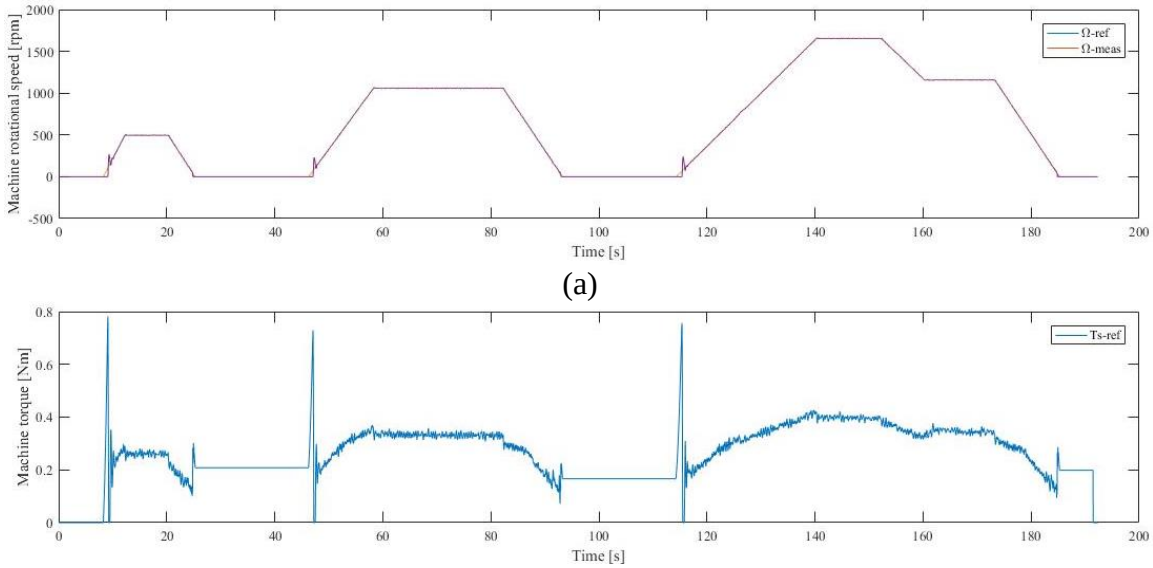

Figure 5.21 (a) Machine speed and (b) torque from the load-drive, ECE test

In addition, the friction, *f(t)*, can be calculated from machine torque behavior:

$$f(t) = f_{cons} + k_b\Omega(t) + k_a\Omega^2(t) \qquad (26)$$

where f_{cons} is the constant friction, k_b is the bearing friction coefficient, k_a is the aerodynamic friction coefficient, and $\Omega(t)$ is the machine rotational speed in rad/s. Given that the torque should be zero when the speed is zero, the measured torque during such condition is the torque which can be applied to the drive without movement or the constant term of the friction. From the figure, it is observed to be around 0.2 Nm. In addition, using two points with constant speed, the bearing friction coefficient, k_b, was calculated to be 7.95e-4 and the

aerodynamic friction coefficient, k_a, was calculated to be 4.22e-6. Thus, these could be implemented as friction terms in (8) and (22).

Furthermore, this calculated friction was implemented to the simulation to improve the drive response. This was done by adding these terms as a feedforward after the output of the speed controller. Several logics should be implemented to achieve the best results. Mainly, there are two conditions for the constant term. In the beginning of the cycle, large starting torque is required to overcome the static friction. However, once the machine starts to move, this constant term decreases to a lower value. In addition, logic was added to set the torque reference to zero when the speed reference is zero. The results from such implementations are shown in Figure 5.22. It can be seen from Figure 5.22 (a) that the response of machine rotational speed in the beginning of the cycle has improved from Figure 5.21 (a). The speed follows the reference from low speed and without significant overshoots as in previous test. In term of torque, there are still large peaks in the beginning of the cycles since they are required to overcome the static friction and start the movement. However, slightly lower values can be observed.

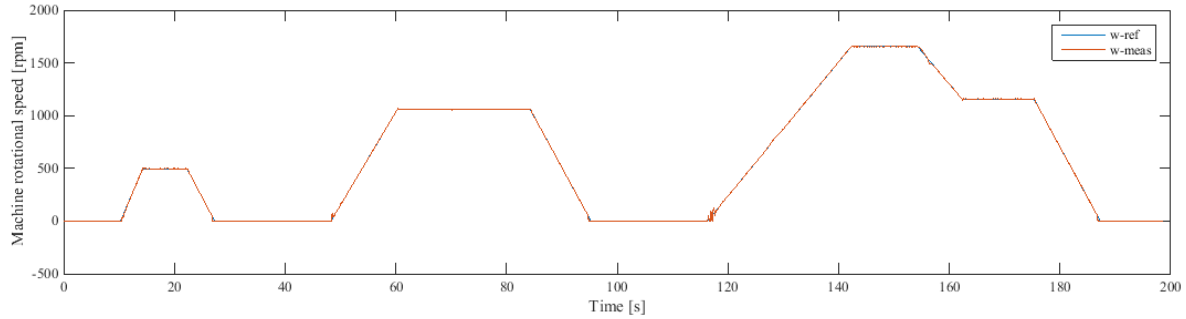

(a)

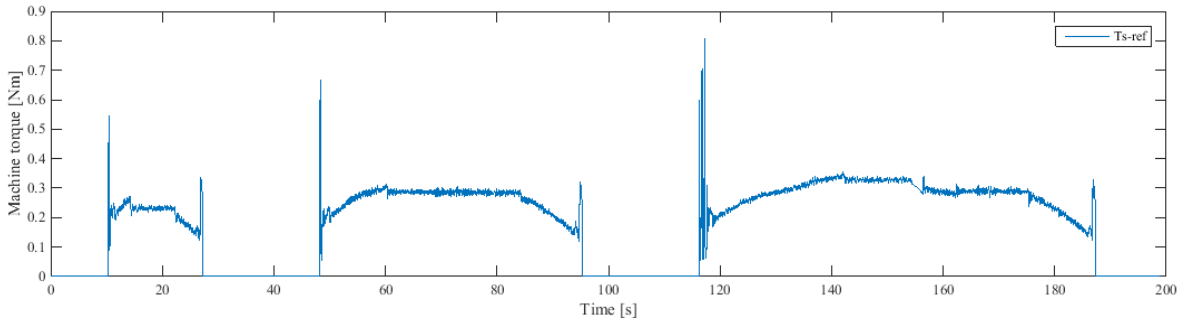

(b)

Figure 5.22 (a) Machine speed and (b) torque from the improved load-drive, ECE test

5.3 Reduced-scale P-HIL simulation of the electric minibus of Coimbra

5.3.1 Reduced-scale P-HIL setup

After all parts of the HIL simulation were prepared, they were assembled together to perform the reduced-scale P-HIL simulation. Figure 5.23 shows the Simulink program for such simulation. The program from Figure 5.6 was adapted to give the references to the drives and take the measurements from the real system instead of within Simulink. The blocks inside the "Control" block are shown in Figure 5.24. This is the same structure as Figure 5.6 except that the models of real subsystems were removed. Furthermore, some compensation is added to the torque reference in order to overcome the friction. This compensation is adapted from the calculation in section 5.2.3 as by (26). In addition, there are switches to set the torque references as zero when the velocity reference is zero. The ControlDesk screen for this simulation is shown in Figure 5.25. The simulation will be perform, first, with the NEDC and, then, with the real driving profile of the electric minibus of Coimbra. It should be noted that several tunings were required in order to achieve the best results. These include tuning of the speed and velocity PI controllers and the compensation block. The PI controllers were initially tuned using the pole placement method. The response time and damping factor were varied. In addition, the value of the moment of inertia for gains calculation was modified from the value from datasheets. The aim of this modification is to find the actual moment of inertia of the setup which might not be exactly the same as datasheets.

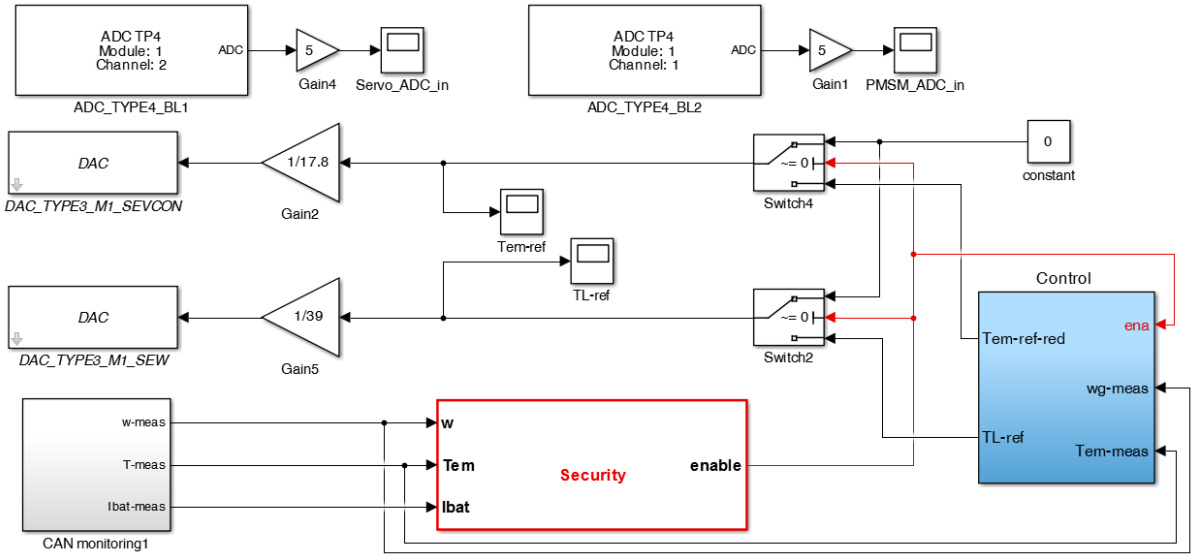

Figure 5.23 Simulink program for the reduced-scale P-HIL simulation

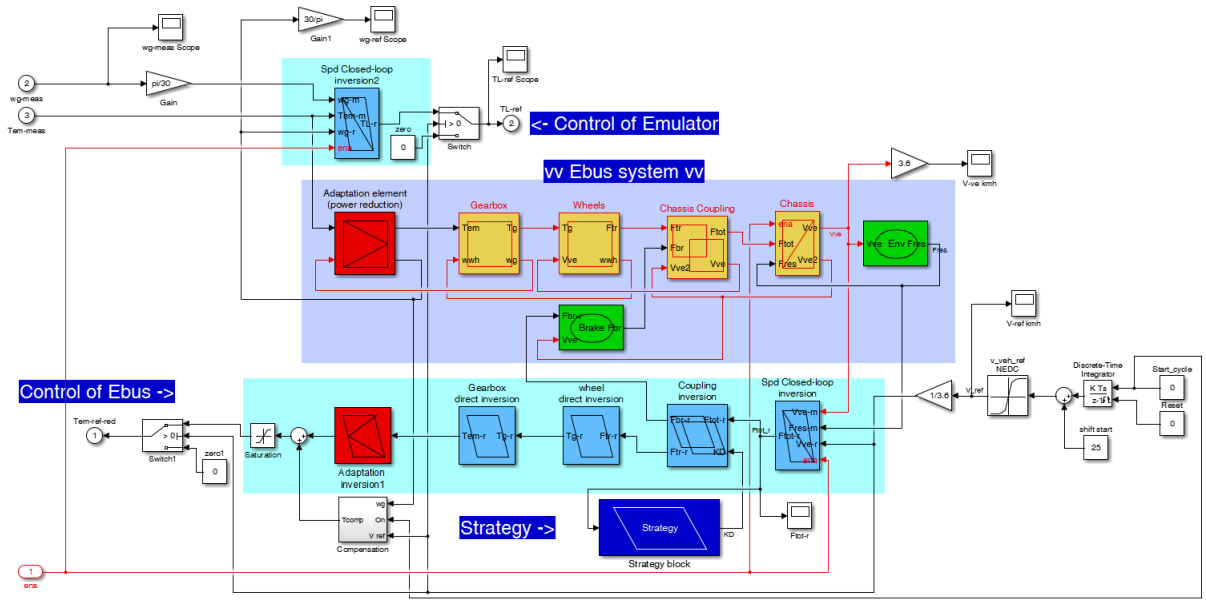

Figure 5.24 Inside “Control” block of Simulink program for P-HIL simulation

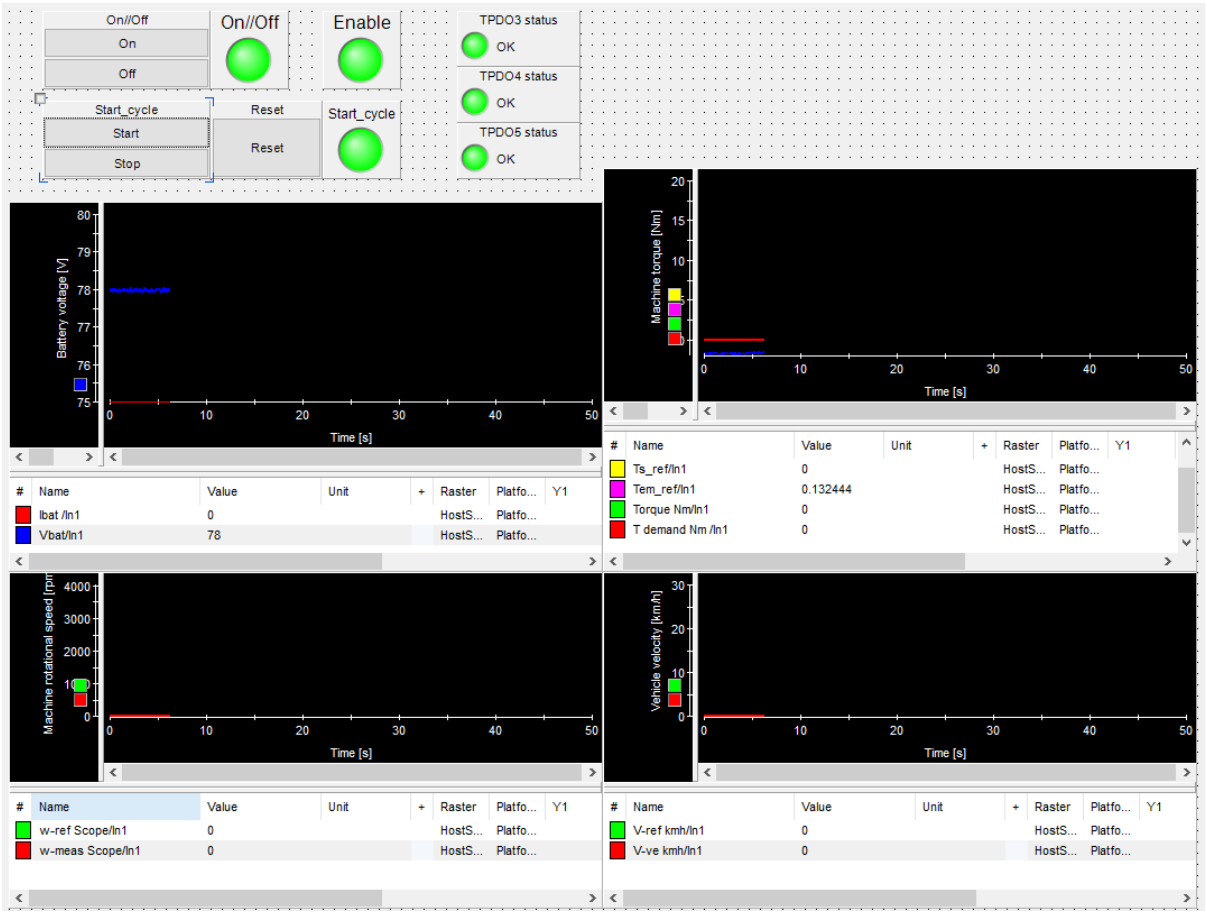

Figure 5.25 ControlDesk screen for HIL simulation

5.3.2 NEDC reference, reduced-scale P-HIL results

In the first part, the simulation was performed using NEDC driving cycle as a reference velocity profile. The results of such simulation are shown in Figure 5.26. As can be seen from Figure 5.26 (a), the velocity of the emulated minibus ($V_{ve\text{-}meas}$) follows the reference very well. The machine rotational speed also follows the reference very well except some small overshoot and ripples as can be seen from Figure 5.26 (b). Observing the torque results in Figure 5.26 (c), the small overshoot in the machine speed can be explained by the peak torque when the speed torque changes its value from one to another such as when starting from zero or when the torque reduces from accelerating torque to constant speed torque. Furthermore, the battery voltage and current are shown in Figure 5.26 (d).

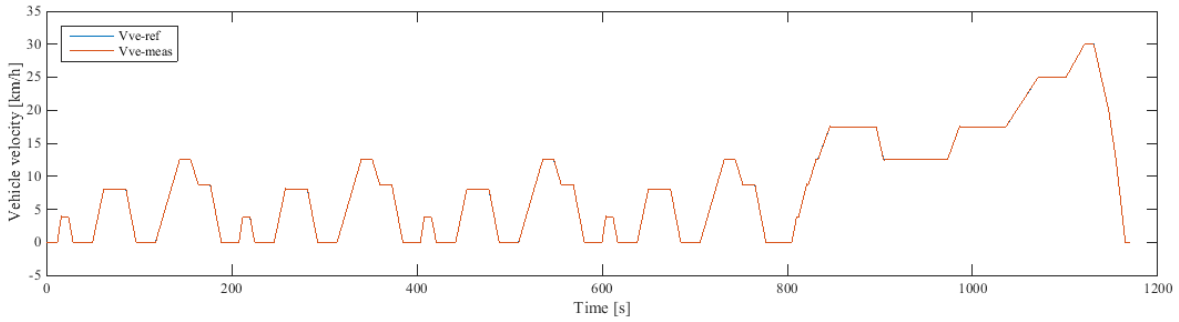

(a)

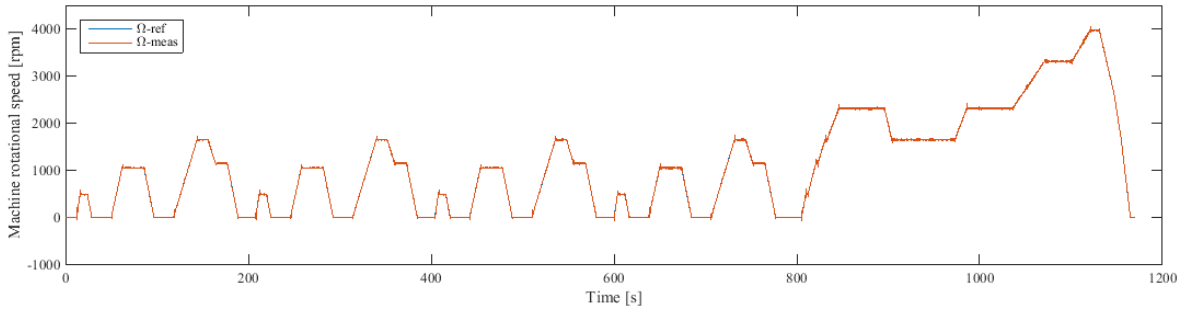

(b)

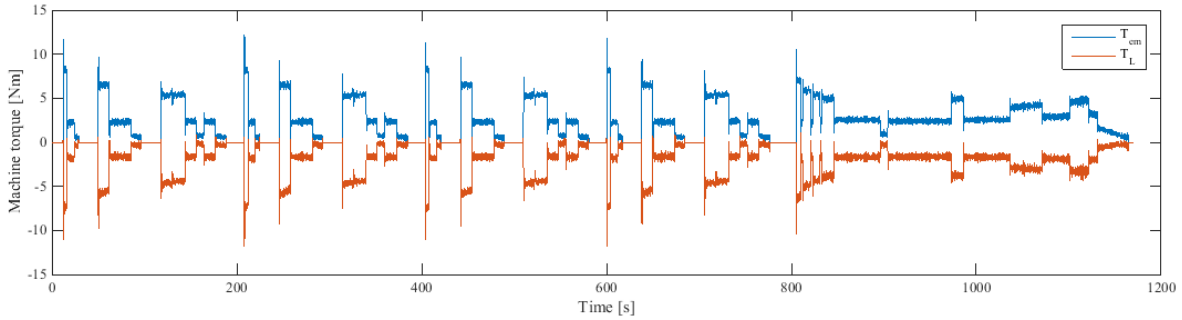

(c)

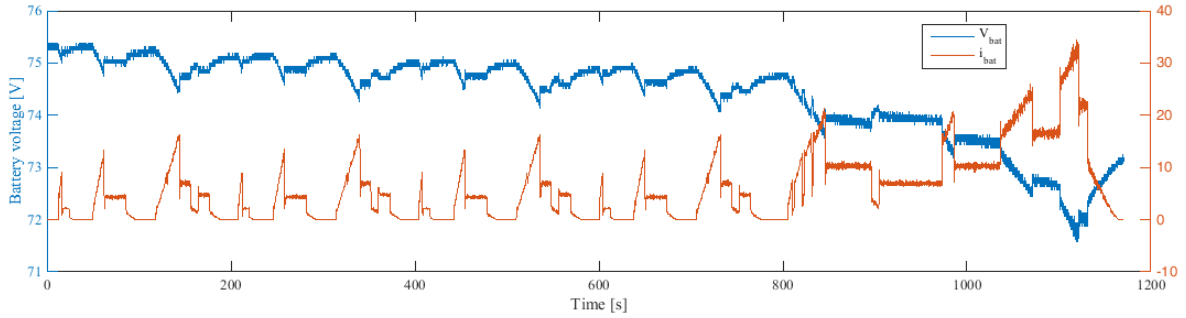

(d)

Figure 5.26 (a) Vehicle velocity, (b) machine rotational speed, (c) machine torques, and (d) battery voltage and current results from the NEDC HIL emulation

5.3.3 Minibus driving profile reference, reduced-scale P-HIL results (without slope)

After the NEDC simulation, real driving profile was implemented as a reference for the HIL simulation. In this section, only the velocity profile is applied. The slope is not considered yet. Before going to HIL simulation, the organization was first verified in software simulation. The results of the software simulation are shown in Figure 5.27. Both the vehicle velocity and the machine rotational speed follow the reference very well as in the case of NEDC reference. Furthermore, the torques are in permitted levels. Therefore, the simulation was carried on to the HIL simulation.

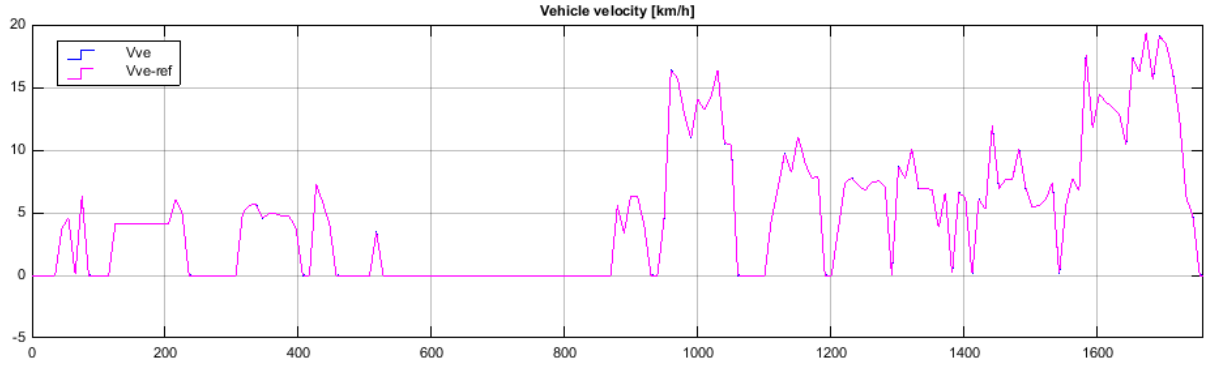

(a)

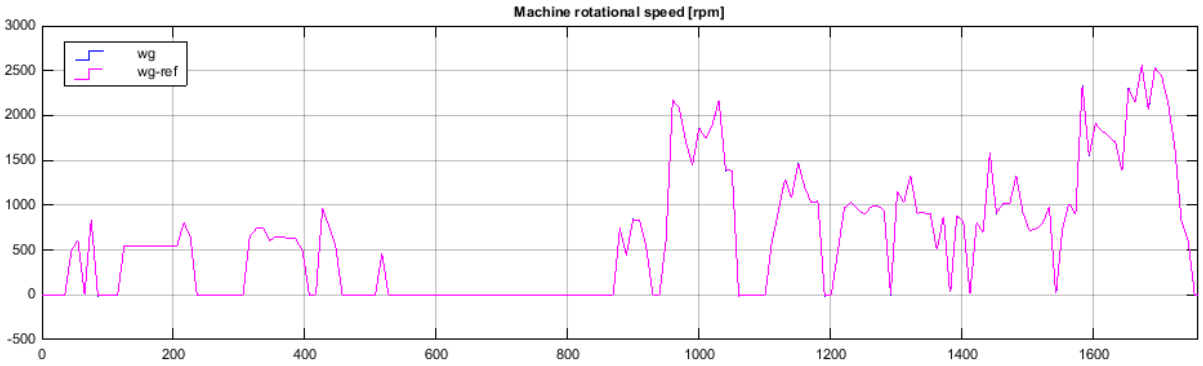

(b)

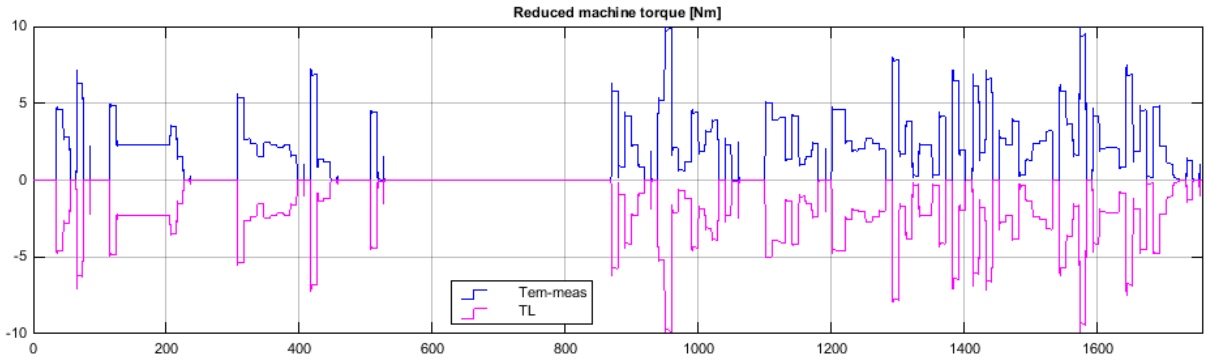

(c)

Figure 5.27 (a) Velocity, (b) machine speed, and (c) torques, results from the minibus driving profile software simulation (without slope)

The results from HIL simulation using the electric minibus of Coimbra driving profile without slope are shown in Figure 5.28. The vehicle velocity is shown in Figure 5.28 (a) while the machine speed is shown in Figure 5.28 (b). Both variables follow the reference very well. Only some small ripples can be observed in some cycle of the machine speed as in the case of NEDC reference. Moreover, the machines' torque are shown in Figure 5.28 (c). The torque of the traction drive is labelled as T_{em} and the load torque which emulates the torque from the road is labelled as T_L. It should be noted that although the load torque is shown as negative values in this plot, this negative sign is taken into account in the real implementation as a counter clockwise direction of rotation. The reference is given in positive value. Furthermore, battery voltage and current are shown in Figure 5.28 (d). Battery voltage drops from around 73.8 V to around 70.5 V with the lowest peak around 69.8 V. The highest battery current peak is around 38 A. These are in the permissible range.

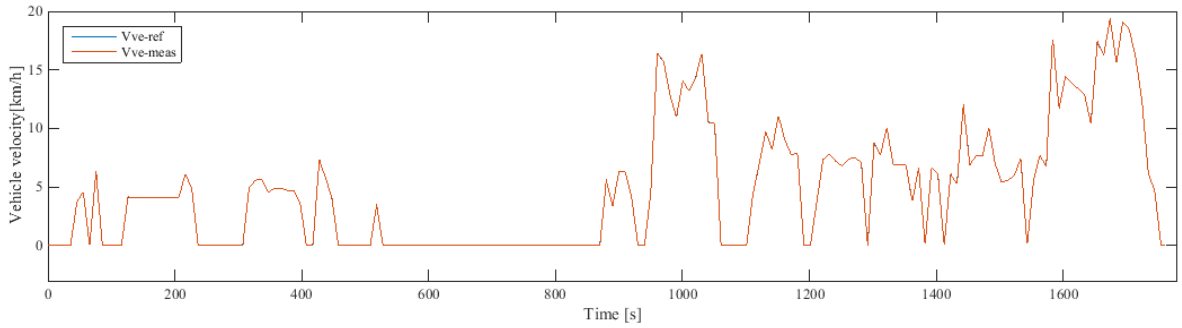

(a)

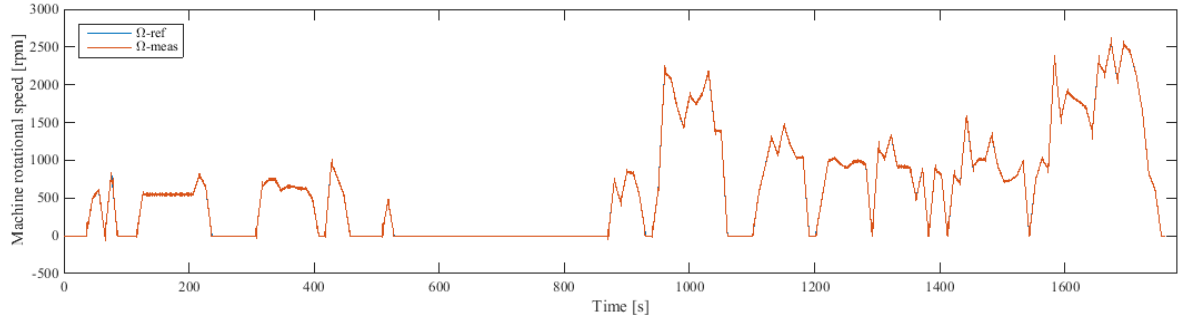

(b)

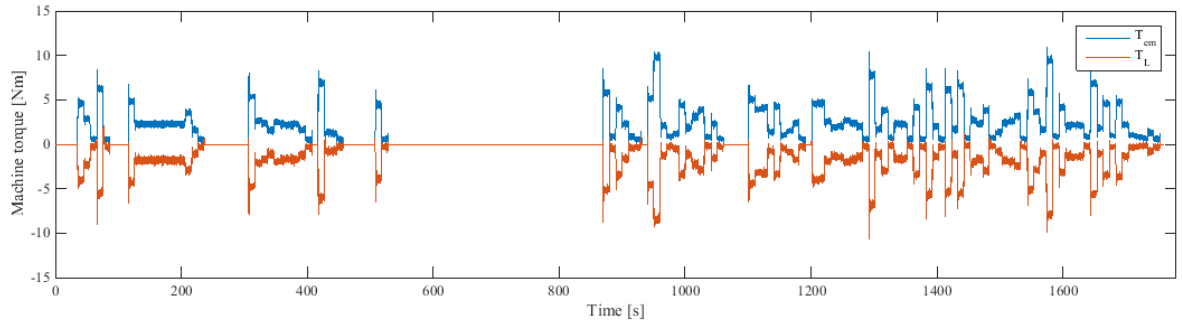

(c)

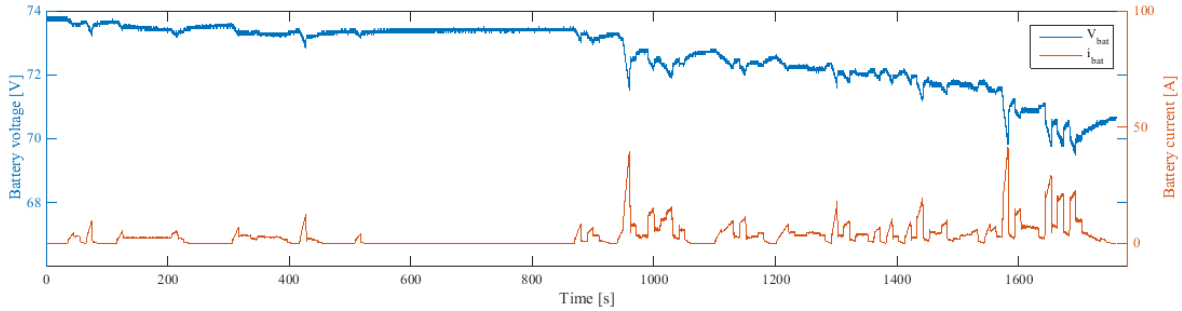

(d)

Figure 5.28 (a) Velocity, (b) machine speed, (c) torques, and (d) battery voltage and current results from the minibus driving profile HIL simulation (without slope)

Comparing the HIL and the software simulation, the vehicle velocities are observed to have the same characteristic. However, for the machine speed, the software simulation has slightly better response. The speed is able to follow the reference without any overshoot or ripples which is not the case of the HIL simulation. For the torque in figures (c), several differences can be noticed. First, the overshoots in HIL simulation are higher than in software simulation. This result in the overshoot in the speed as previously mentioned. In addition, no torque is required for deceleration in the software simulation. However, due to the friction, the compensation block was added in the HIL simulation. This results in additional torque in real HIL simulation. Without this compensation, the machine speed would not be able to follow the reference during the deceleration. The speed would drop to zero just after the traction torque is removed. These differences show the importance of HIL simulation as a mean to study the system in more realistic way.

5.3.4 Minibus driving profile reference, reduced-scale P-HIL results

After a successful reduced-scale P-HIL simulation with the real electric minibus driving cycle without slope was achieved, a slope was added to such profile. First, this was done through a software simulation. The main concern was the torque required by the machine since the weight of the minibus is quite high and the driving route is quite hilly. This could significantly increase the torque demand by the machine. The full-power machine torque from such simulation is shown in Figure 5.29. As suspected, the slope increases the torque demand significantly. There are several peaks which exceed the maximal continuous

torque of the machines. The highest peak is around t=950s and it has a value of around 500 Nm. This corresponds to 2.1 times the maximal continuous torque.

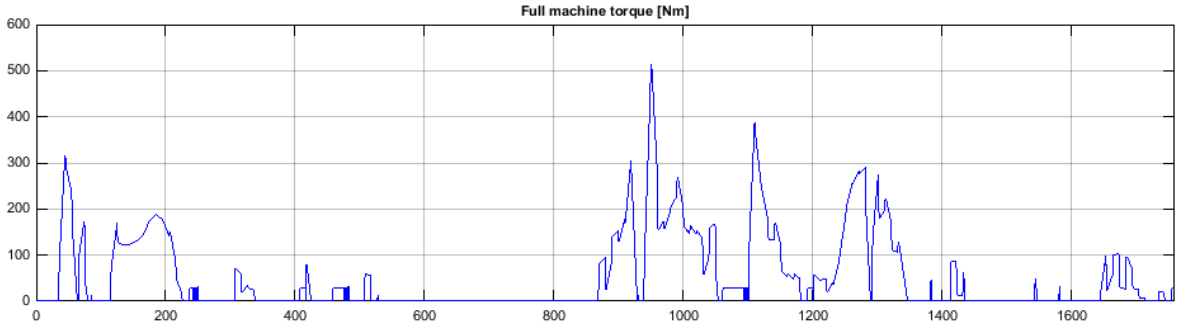

Figure 5.29 Full machine torque from the minibus driving profile software HIL simulation

In order to study the test bench behavior with limited torque, a saturation block with maximal limit of 30 Nm was added to the traction machine torque reference. On the other hand, the limit of the load machine was set at 35 Nm. The results from this software simulation are shown in Figure 5.30. It can be observed from Figure 5.30 (c) that the torque reached its limit around t=950s. This results in a flat-top shape. Consequently, this results in the vehicle velocity which did not follow the profile perfectly. A small difference can be observed at that time as shown in Figure 5.31. Nonetheless, the machine rotational speed follows the reference very well. The battery voltage and current are also in the permitted levels. It should be noted that in this section, the velocity controller was retuned to have slower response than in the previous section. This helps smooth the required torque and reduce the maximal value. It can be seen from Figure 5.30 (a) that the reference and the actual velocity are not exactly overlapped. There is a small delay between both values. Nonetheless, this is realistic since the velocity is a result of mechanical system and it would generally have slower response time.

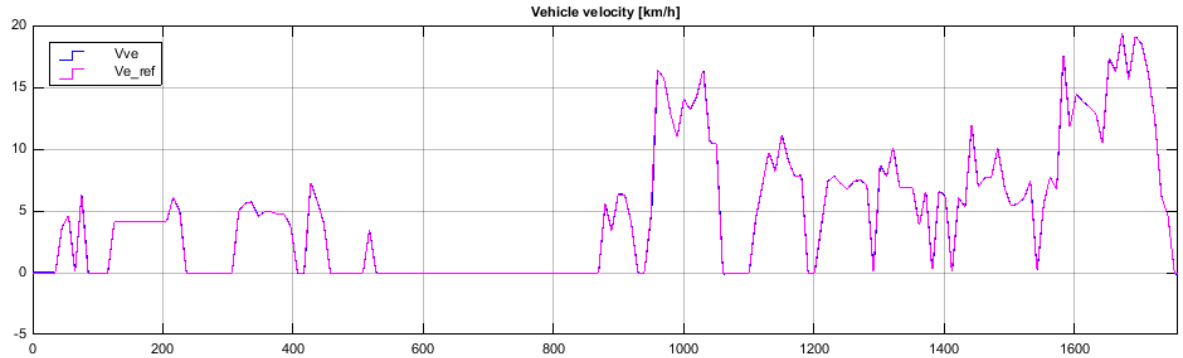

(a)

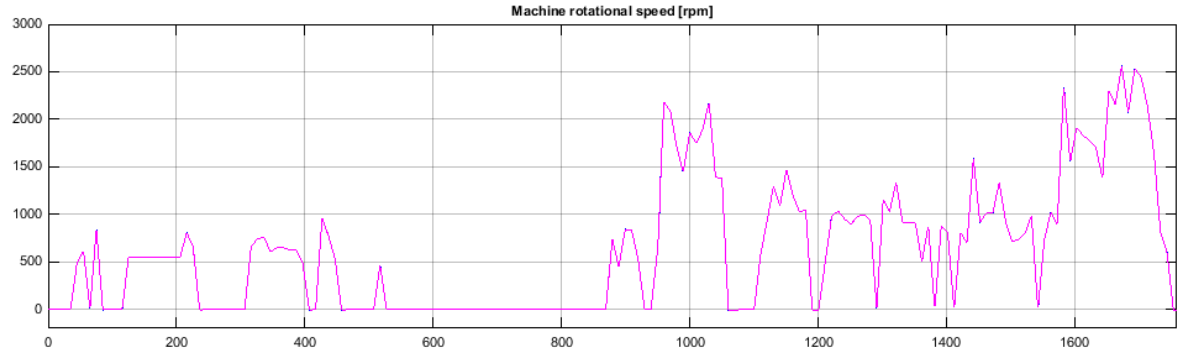

(b)

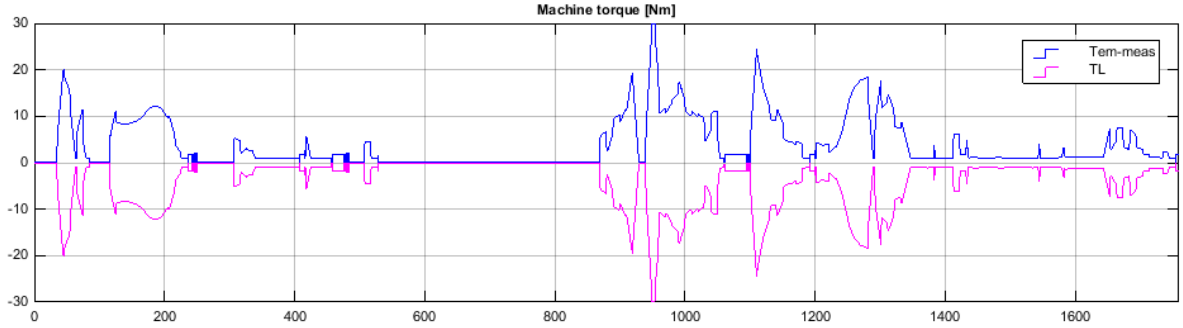

(c)

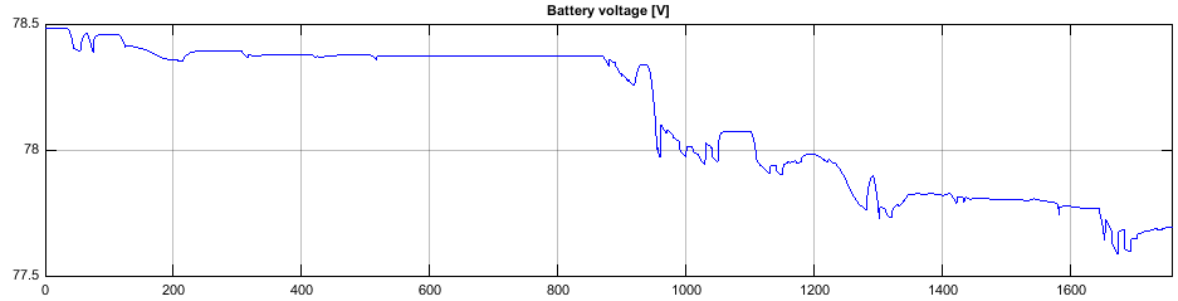

(d)

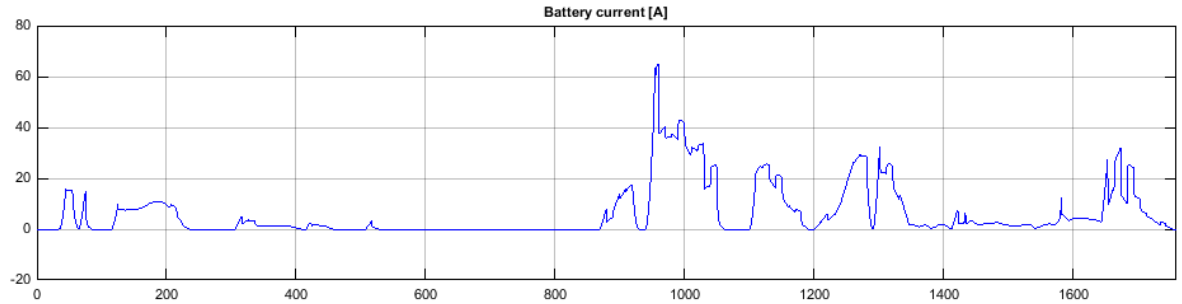

(e)

Figure 5.30 (a) Velocity, (b) machine speed, (c) torques, (d) battery voltage, and (e) battery current results from the minibus driving profile software simulation

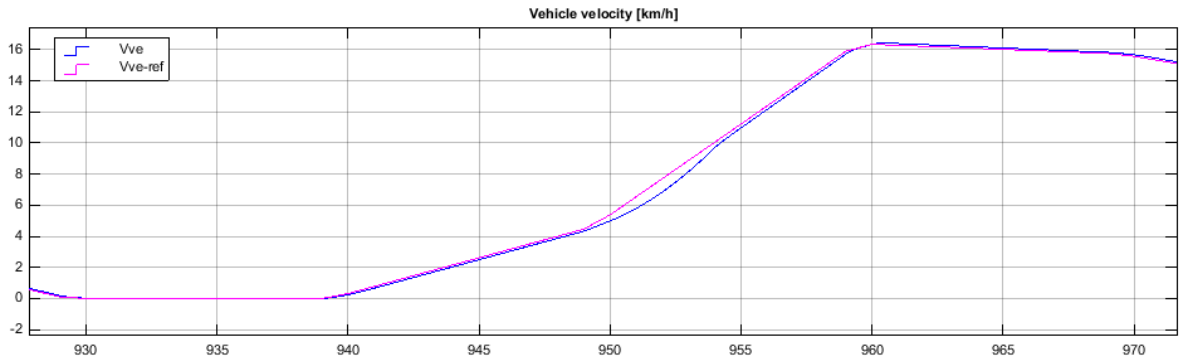

Figure 5.31 Velocity at t=920-980s from the minibus driving profile software simulation

As observed from the software simulation, the required torque exceed the continuous maximal torque limit. In order to allow the traction drive to follow such reference, several configurations had to be done. First, the datasheets of the battery, the controller, and the machines were checked. The maximal values of these components are summarized in Table 5.5. Then, the maximal allowable torque of the machine in DVT software has to be increased. It was increased to 30 Nm for this experiment. In addition, the limit of the saturation block in Simulink has to be increased. The limits in the security block should be set accordingly. Finally, the limit of the saturation block of the load drive torque reference also had be increased. These process must be done carefully as exceeding the limits could damage the devices.

Table 5.5 Maximal values of components in HIL setup

Device	**Variable**	**Value**
Battery	Discharging current	3C or 240A (for 2 in series)
SEVCON Gen4	Continuous current (60 min)	140 A
	Peak current (2 min)	350 A
	Boost current (10 sec)	420 A
Traction machine (PMS120)	Nominal torque	14.9 Nm
	Current	98.5 A
	Stall torque	17.8 Nm
	Stall current	118.2 A
	Max. stall torque	45 Nm
	Max. stall current	300 A
	Power	7 kW
SEW inverter	Rated output power	31.9 kVA
	Nominal current (at 400 Vac)	46 A
	Max current	150% of nominal current
SEW motor CMP80M	Nominal torque	18.7
	Current	20.10 A
	Peak torque	62.6 Nm
	Max. current	103 A

The results from such HIL simulation are shown in Figure 5.32. As anticipated from the software simulation, the velocity follows the reference very well except for around t=950 s. This can be more clearly observed from the ControlDesk screen which is shown in

Figure 5.33. Although the torque demand is limited at 30 Nm, the actual torque (green line) did not reach 30 Nm which is set value. This could be due to the power limit. The shape of the machine rotational speeds in Figure 5.32 (b) corresponds to the measured vehicle velocity in Figure 5.32 (a). It follows the profile very well. Nonetheless, some relatively small overshoot and ripples can be observed as in all previous HIL simulations. In addition, the battery voltage and current are shown in Figure 5.32 (d) and (e). Large drop in the voltage and large peak in the current can be seen at the time when peak torque occurs. The voltage dropped around 2.7 V and the current was around 100 A. Nonetheless, these are still in permittable ranges. The maximal discharge current of the battery is 3C or 240A and the voltage did not drop below the lower voltage limit.

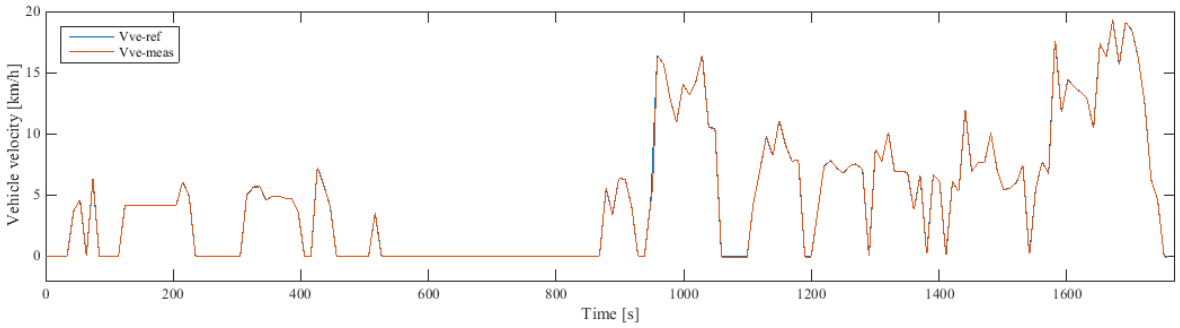

(a)

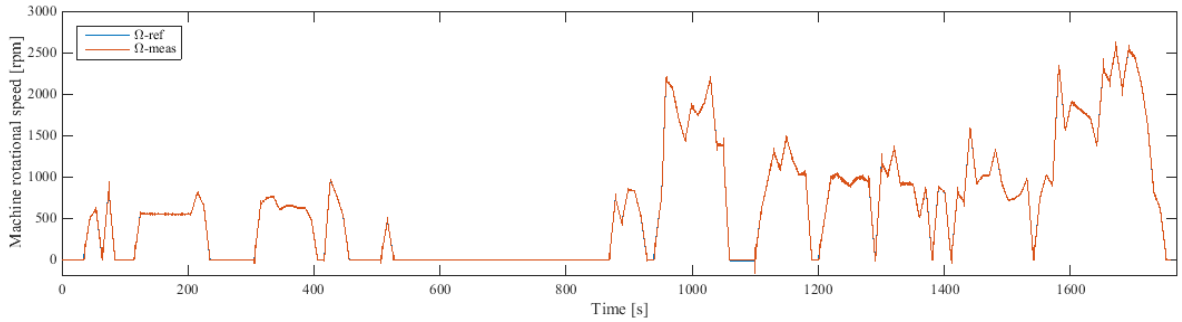

(b)

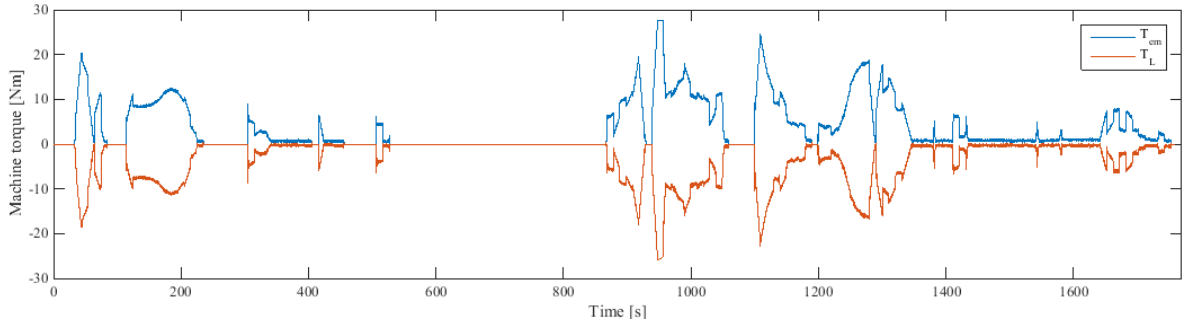

(c)

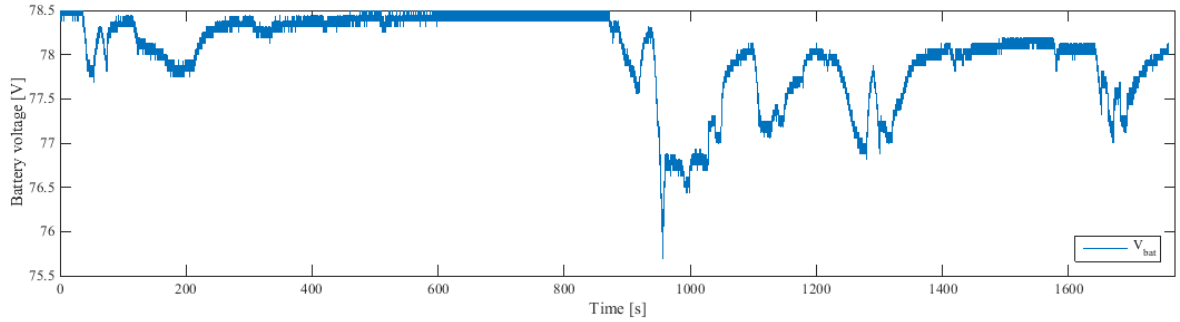

(d)

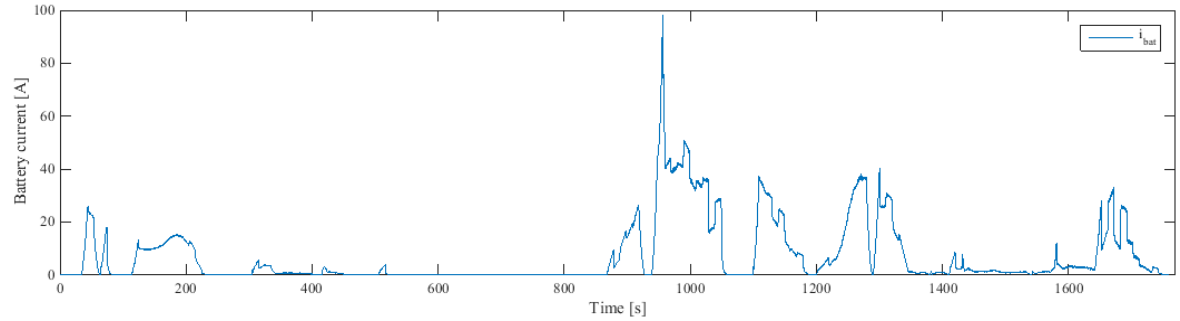

(e)

Figure 5.32 (a) Velocity, (b) machine speed, (c) torques, (d) battery voltage, and (e) battery current results from the minibus driving profile HIL simulation

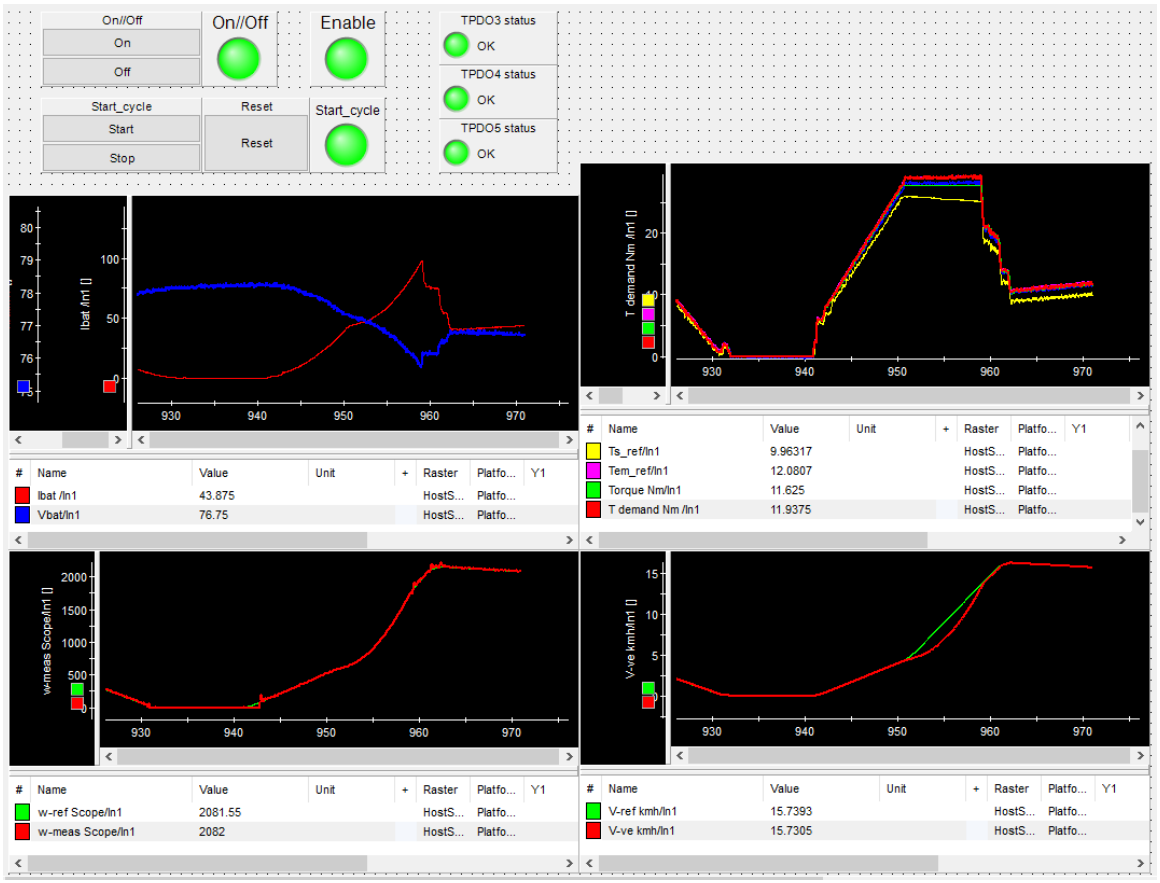

Figure 5.33 ControlDesk screen at t=950s of the minibus driving profile HIL simulation

The results from HIL simulation are then compared to the results from software simulation. Despite the small overshoots in HIL simulation, the vehicle velocity, machine rotational speed, and torque are similar in both cases. For the battery, it should be noted that the battery voltage of the simulation depends on the SoC at the moment of the simulation. The initial value in software simulation was adjusted accordingly. The software simulation shows reduction of battery voltage from 78.5 to around 77.7 V. It can be observed that the actual battery recovers more than the model. However, the lowest peak in actual battery is much lower than the model. The error could be from the inaccuracy of the model. The model used in this simulation is a linear model. Temperature effect and non-linearity are not taken into account. This could be important if this large drop results in a voltage lower than the permitted voltage as it might damage the battery cell. This clearly shows the necessity of a HIL simulation. The battery current in the HIL simulation also has higher peak than in the software simulation.

In addition, the results in the full power subsystems are shown in Figure 5.34. Full-scale machine torque is shown in Figure 5.34 (a) while machine speed is shown in Figure 5.34 (b). In addition, the electrical and mechanical powers are shown in Figure 5.34 (c). It can be seen that continuous limits were exceeded during the peak period and the subsystems would be working in transient during that time. The difference between the mechanical and the electrical power is the efficiency of the drive.

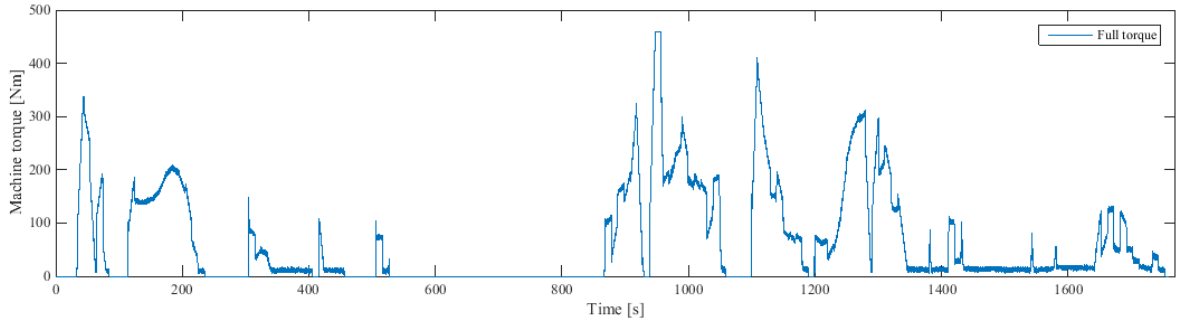

(a)

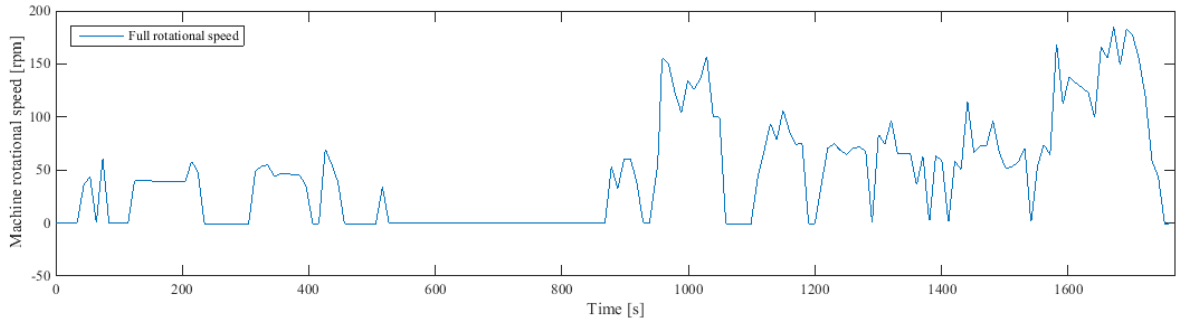

(b)

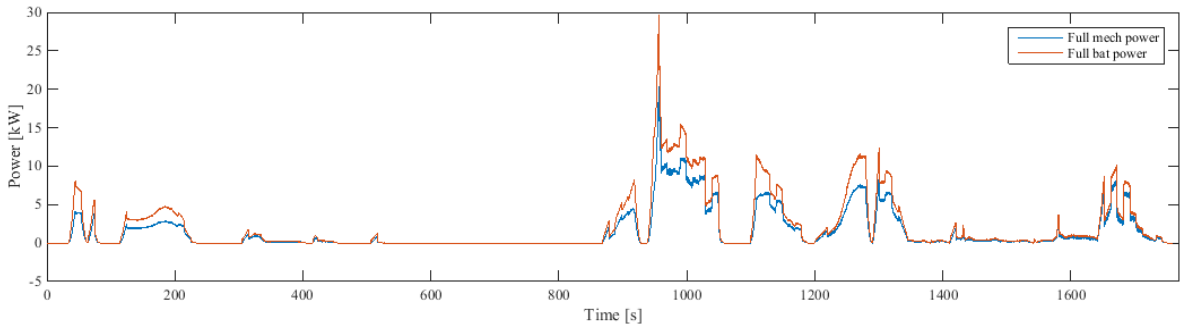

(c)

Figure 5.34 Full-scale (a) machine torque, (b) speed, and (c) electrical and mechanical power from the minibus driving profile HIL simulation

Despite the transient operation which would allow the machine to work with higher limits, it should be noted that the reference was taken with an average of 10 passengers and an average of 75-kg weight was used. However, these are average values. It is possible that at the time of peak torque requirement, the total weight of the vehicle might be less due to less weight of passengers. Therefore, in order to allow more accurate study, a more controlled condition should be applied to acquire the reference profile.

The process of the developing, the setup, and the results of this work are also summarized in a paper titled “Reduced-scale Hardware-In-the-Loop simulation of an Urban Electric MiniBus using Energetic Macroscopic Representation” [31]. This paper has already been accepted to the IEEE Vehicle Power and Propulsion Conference (VPPC) 2017 which will be held in Belfort, France, on December 11th-14th 2017.

Chapter 6 Conclusion and Future work

6.1 Conclusion

This thesis presents a process of developing Hardware-In-the-Loop simulation of an electric minibus powertrain. In the first part, the charging procedure of the test bench was improved. Current measurement issue was solved and additional components were added to the system to allow safe charging environment. Schematic diagram and operating instructions were also established. Then, the electric minibus of Coimbra was modelled and represented using the EMR graphical formalism. After that, the EMR was extended to HIL simulation of such vehicle. dSPACE platform was utilized to allow such simulation. Moreover, several tests were carried out to configure the system to be ready for the emulation. Finally, the reduced-scale P-HIL was carried out on the test bench in ISEC-IPC.

From all the result, it can be seen that there were differences between the software simulation and the HIL simulation. The main difference was due to the friction and physical limitation. Due to complexity of complete modelling and lack of information, several parameters or phenomenon are usually neglected in software simulation. For such reason, HIL can be a potential intermediate step in the design process. It allows obtaining more realistic results. In addition, this result can be used to extract some unknown parameters to improve the software simulation process.

6.2 Discussion and future work

Although the test bench is now able to perform a HIL simulation, optimization of the program can be done to obtain better machine response.

Regarding the electric minibus implementation, the next step would be to verify the results from the test bench with measurements from real electric minibuses of Coimbra. It would also be beneficial to obtain more information about the minibus. Several assumptions were made during this study due to lack of information. Information from the real system can improve this simulation. Once the reduced-scale HIL simulation is well studied, the next step would be to perform a full-scale HIL simulation.

On the other hand, although the detail of the simulation might not be very accurate due to the lack of information, the structure and setup of the test bench is working quite

properly. Therefore, this test bench can be adapted to study different case study and scenario such as different driving behavior and possibility of specified stops for the electric minibus of Coimbra.

6.3 Quality report

Implementation of the test bench in ISEC-IPC to perform a HIL simulation of the electric minibus of Coimbra is explained in this thesis. The thesis was developed with the guidelines provided by the supervisors. The first step in this thesis was to operate the test bench in ISEC-IPC with the previous setup. Then, the problems regarding the charging facilities were solved despite the lack of previous implementation information. The connection between different components and the adaptations were not explicitly stated in any document. Several experiments were performed to find the information which was not provided by the manufacturers. Finally, a full schematic of the system and operation guidelines were developed. These documents will be valuable for future development. For the best interest, they should be kept updated.

After that, the EMR of the electric minibus of Coimbra was developed. This was mainly done in L2EP, University of Lille1 at Lille, France. Static models of the drives were employed. Several assumptions were also made to overcome the issue regarding the parameters. Some issues were noticed with a dynamic model simulation as several variables were not in realistic ranges. Consequently, it was advisable to perform a controlled and detailed experiment to obtain the required parameters in order to allow a more accurate simulation.

An intermediate stay at University of Lille was of valuable interest. It was very beneficial to get firsthand experiences with working HIL test bench and dSPACE platform as well as to learn EMR technique. It is encouraged to continue this cooperation between institutes. Nonetheless, due to shortage of time, not all expected aspects were covered in Lille. The work was carried on in Coimbra with some adaptations required due to compatibility issues. Although the time in Lille was short, its proportion to the entire thesis time was appropriate. Therefore, an extension of the whole thesis period would be helpful in developing the thesis even further.

Regarding the test bench configuration for HIL simulation, the main problem encountered in previous study was the difficulty to develop the control through the CAN network. In order to overcome such problem, in this thesis, it was decided to achieve the measurements from CAN communication and send the references via analog signals. Then, the drives were configured for the HIL simulation. Since the controller was designed to work in real vehicles or industrial drives, there are several configurations which are beneficial for real environment but could become limitations in research environment if it is not configured appropriately. For instance, the speed limit of the drive can prevent the motor from providing required torque. These were configured cautiously.

After both drives were configured, HIL simulations were performed through dSPACE

platform. Several experiments and tuning were required to obtain the final results. Mainly, the difficulties were due to the lack of information and the tuning which is required for any control system. A software simulation is a valuable tool to verify the program before hardware implementation. This step should not be neglected even though the simulation might not be that accurate due to assumptions made during the modelling process.

Although, there were several issues which occurred during the thesis as previously explained, efforts were made to solve all the issues. Finally, satisfying final results were obtained. Moreover, it should be noticed that different knowledge from different subjects throughout the master course (and further) were implemented in order to achieve the final results. This thesis has been beneficial. It has shown an example of applying the theoretical knowledge to achieve experimental results.

Bibliography

[1] D. Maclay, “Simulation gets into the loop,” in *IEE Review*, vol. 43, no. 3, pp. 109-112, May 1997.

[2] A. Bouscayrol, “Hardware-In-the-Loop simulation,” in *Industrial Electronics Handbook, second edition, tome “Control and mechatronics”, Chapter 33*, Chicago, CRC Press, Taylor & Francis group, Mar. 2011.

[3] A. L. Allègre, A. Bouscayrol, J. N. Verhille, P. Delarue, E. Chattot, S. El Fassi, “Reduced-scale power Hardware-In-the-Loop simulation of an innovative subway,” *IEEE transactions on Industrial Electronics*, vol. 57, no. 4, pp. 1175-1185, Apr. 2010.

[4] T. Letrouvé, W. Lhomme, A. Bouscayrol, N. Dollinger, “Control validation of Peugeot 3∞8 Hybrid4 vehicle using a reduced-scale power HIL simulation*", Journal of Electrical Engineering and Technology*, Vol. 8, no. 5, pp. 1227-1233, Sep. 2013.

[5] A. Bouscayrol, J. P. Hautier, and B. Lemaire-Semail, “Graphic Formalisms for the Control of Multi-Physical Energetic Systems,” *Systemic Design Methodologies for Electrical Energy, tome 1, Analysis, Synthesis and Management, Chapter 3, ISTE Willey editions,* October 2012, ISBN: 9781848213883.

[6] R. Kühne, “Electric buses – An energy efficient urban transportation means,” *Energy,* vol. 35, no. 12, pp. 4510-4513, Dec. 2010.

[7] P. Rook, “Controlling software projects”, in *Software Engineering Journal*, vol. 1, no. 1, pp. 7-16, Jan. 1986.

[8] A. Bouscayrol, B. Davat, B. de Fornel, B. François, J. P. Hautier, F. Meibody-Tabar, M. Pietrzak-David, “Multimachine Multiconverter System: application for electromechanical drives,” *European Physics Journal - Applied Physics,* vol. 2, no. 2, pp. 131-147, May 2000.

[9] A. Bouscayrol, “Different types of Hardware-In-the-Loop simulation for electric drives,” *IEEE-ISIE’08*, Cambridge, UK, Jun. 2008.

[10] C. R. Kelber, B. R. R. Reis, R. M. Figueiredo, “Improving Functional Safety in Autonomous Guided Agricultural Self Propelled Machines using Hardware-In-the-Loop (HIL) Systems for Software Validation,” *IEEE-ITSC’16*, Rio de Janeiro, Brazil, Nov. 2016.

[11] P. G. Fuente, “Simulation and Full-Scale Emulation of a Powertrain for Small Electric Vehicle,” M.S. thesis, University of Oviedo, Spain, 2016.

[12] EMR Website. (2017). *Energetic Macroscopic Representation*. [online] Available at: http://www.emrwebsite.org

[13] W. Cowart, V. Pesinova, and S. Saile, “An Assessment of GHG Emissions From The Transportation Sector,” *12th International Emission Inventory Conference*, San Diego, USA, 2003. [Online]. Available: https://www3.epa.gov/ttnchie1/conference/ei12/green/pesinova.pdf.

[14] M. Mahmoud, R. Garnett, M. Ferguson, P. Kanaroglou, “Electric buses: A review of alternative powertrains”, *Renewable and Sustainable Energy Reviews*, Vol. 62, pp. 673-684, Sep. 2016, .

[15] T. Ly, D. Goehlich, L. Heide, “Assessment of the Interaction of Charging System and Battery Technology for the Use in Urban Battery Electric Bus Systems,” *IEEE-VPPC’16*, Hangzhou, 2016.

[16] N. Faria, J. P. Trovão, A. F. Ramos, P. G. Pereirinha. “Comparison of Different Battery Technologies for Electric Minibuses Using Energetic Macroscopic Representation,” *IEEE-VPPC’14*, Coimbra, Portugal, Oct. 2014.

[17] N. Faria, P. G. Pereirinha, J. P. Trovão, “Modelling of an Urban Electric MiniBus using Energetic Macroscopic Representation Graphic Description,” *IEEE-VPPC’15*, Montreal, Canada, Oct. 2015.

[18] 123electric, “User Manual: Battery Management System - 123 BMS,” Rev 1.4, Aug. 2015. [Online]. Available: http://www.123electric.nl.

[19] “lithium & solar power LiFePO4 - Controlling Analog Charger by BMS123,” GWL/Power, 2014. [Online]. Available: http://gwl-power.tumblr.com/tagged/BMS123.

[20] GWL/Power group Technology Solutions, “POW72V35A/BMS Charger Specification” [Online]. Available: https://files.i4wifi.cz/inc/_doc/attach/StoItem/2031/GWL-Power-POW72V35A-BMS_Spec.pdf.

[21] SEVCON, “Gen4 Applications Reference Manual,” Rev 3.3.

[22] P. Lotrakul, “EMR of the Electric minibus of Coimbra,” University of Lille, 2017.

[23] C. Mayet, L. Horrein, A. Bouscayrol, P. Delarue, J. N. Verhille, E. Chattot, “Dynamical and static models of the traction system of an automatic subway,” *IEEE-EPE’13*, Lille, Septermber 2013, pp. 1-10.

[24] P. Delarue, A. Bouscayrol, E. Semail, “Generic control method of multi-leg voltage-source-converters for fast practical implementation,” *IEEE Transaction on Power Electronics*, vol. 18, no. 2, pp. 517-526, Mar. 2003.

[25] W. Lhomme, A. Bouscayrol and P. Barrade, “Simulation of a series hybrid electric vehicle based on Energetic Macroscopic Representation,” *IEEE-ISIE’04*, vol. 2, pp. 1525-1530 May 2004.

[26] Heinzmann, “Product Catalogue: Disc Motors,” Germany, 2012.

[27] dSPACE GmbH, “MicroAutoBox II Hardware Installation and Configuration,” November 2014.

[28] A. Ghaffari, “dSPACE and Real-Time Interface in Simulink,” San Diego State University, December 2012.

[29] “CANopen – The standardized embedded network,” CAN in Automation. [Online]. Available: https://www.can-cia.org/canopen/.

[30] I. G. Units, D. Electronics, D. Automation, “MOVIDRIVE ® MDX60B/61B Drive Inverter. Operating Instructions, 1122 2913/ EN,” Feb. 2004.

[31] P. Lotrakul, P. G. Pereirinha, A. Bouscayrol, “Reduced-scale Hardware-In-the-Loop Simulation of an Urban Electric Minibus using Energetic Macroscopic Representation,” accepted to *IEEE-VPPC’17*, Belfort, France, Dec. 2017.

Appendix A Schematic diagrams and working procedure

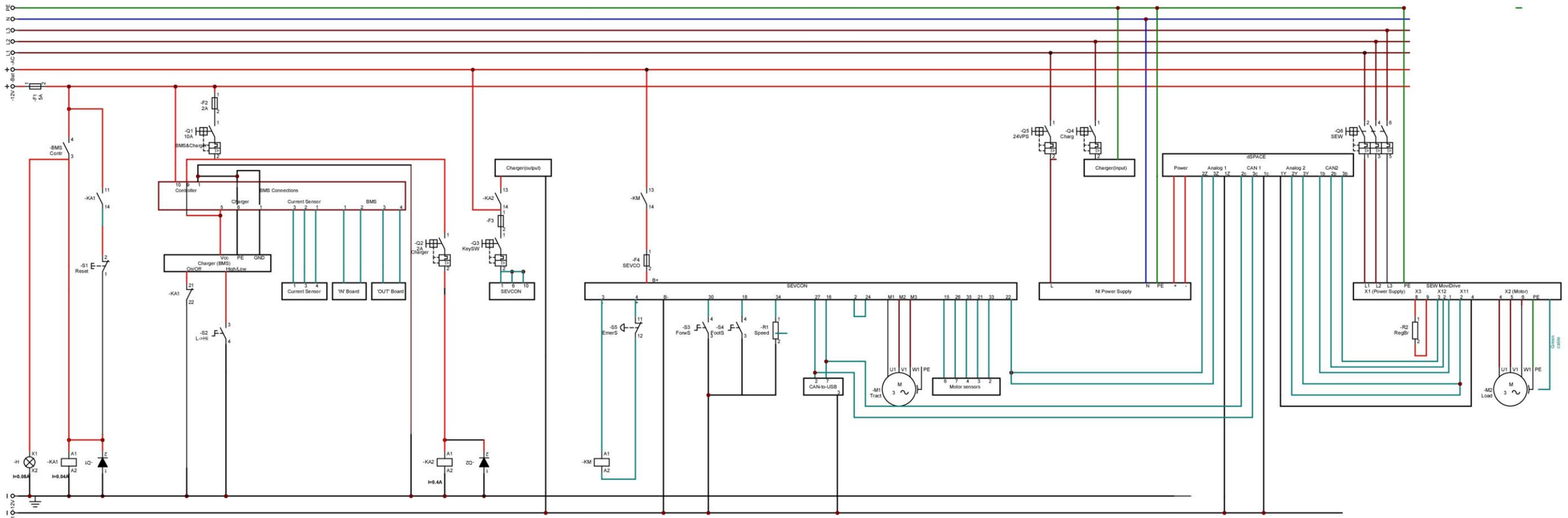

Fig A.1 Developed schematic of the test bench

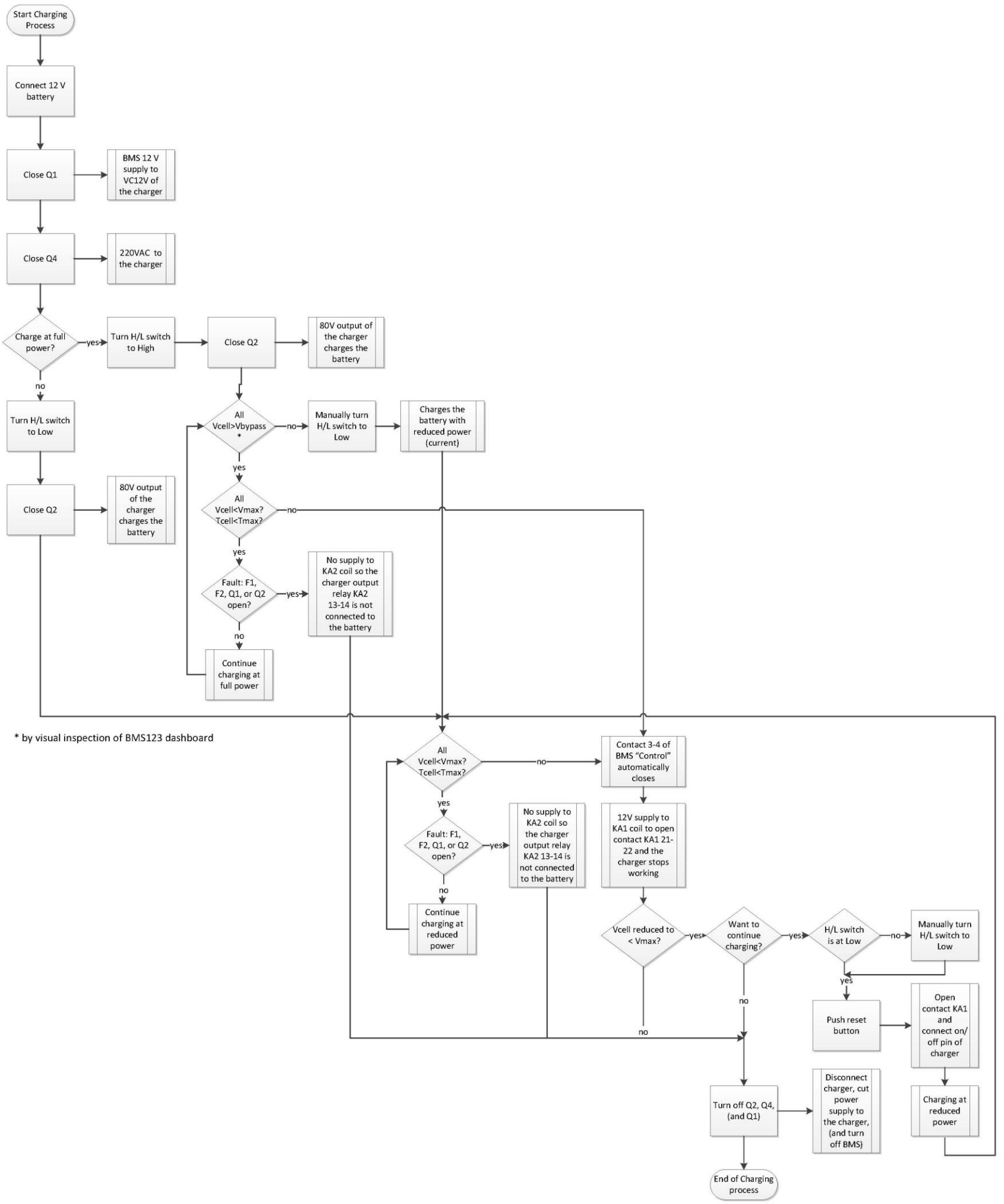

Fig A.2 Charging process guideline

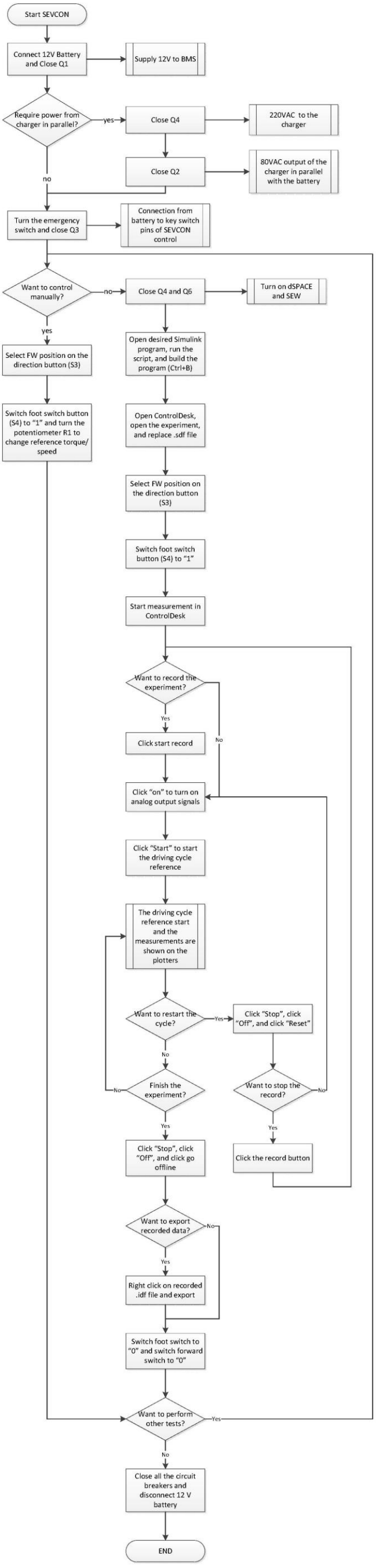

Fig A.3 SEVCON operation and HIL simulation process guideline